

# **Site-Directed Modifications of Myosin**

A DISSERTATION  
SUBMITTED TO THE FACULTY OF THE GRADUATE SCHOOL  
OF THE UNIVERSITY OF MINNESOTA  
BY

Rebecca Jane Moen

IN PARTIAL FULFILLMENT OF THE REQUIREMENTS  
FOR THE DEGREE OF  
DOCTOR OF PHILOSOPHY

David D. Thomas, advisor

June 2013



## Acknowledgements

First, I want to acknowledge my advisor **Dr. David Thomas**. Without his guidance, knowledge, and encouragement this work would not have been possible. You allowed me the creative scientific freedom and independence I desired while providing focused direction and continual support that truly allowed for all of my successes. I look forward to many, many more years of collaboration with you.

Thank you, **Dr. Meg Titus**, for your mentorship and guidance over the last four years. You've instilled in me a fondness for a slime mold called "*Dicty*" and also a love for cellular and molecular biology. I've always admired the way you train young scientists in your lab with a very hands-on approach and teach how to "think" about science, not just "do" science.

I want to extend a special thanks to **Dr. Jennifer Klein**. I am so grateful for all of our conversations about science but above all about balance in life and showing me that we really can have it all.

Thank you **Sarah Blakely** and **Octavian Cornea**, your expertise and assistance has saved me countless hours. I am thankful for your knowledge and friendship. You make the Thomas lab run so smoothly.

**Joe Muretta**, **Ewa Prochniewicz**, and **Piyali Guhathakurta**: thank you for the helpful and enjoyable discussions about everything myosin. This thesis would not be possible without each of your expertise. Thank you **Zach James** and **Jesse McCaffrey** for assistance and insightful conversations about EPR spectroscopy.

Over the past four years I have been fortunate to have outstanding technical support in areas where my knowledge was lacking. **Sinziana Cornea, Evan Smith, and Florentin Nitu**, I am grateful for your assistance.

I also want to thank my committee members: **Dr. Hikeki Aihara, Dr. Deborah Ferrington, Dr. Alex Lange, Dr. Ian Armitage, and Dr. Kylie Walters**. You have provided invaluable instruction in my graduate career and guidance as I progressed through graduate school.

**Douglas and Patricia Richards**, you have given me continued support and love over the last 32 years. I would not be the person I am today without you. I feel so fortunate that I was blessed with such amazing parents. Finally, I would like to thank my incredible husband **Jordan Moen** and two beautiful children **Connor and Cora Moen**. You are what make all of this worthwhile.

## Dedication

*To my children, **Connor Jordan and Cora Lee***

*You are my constant source of inspiration. I love you more than words could ever describe.*

## **Abstract**

Myosins are a diverse class of molecular motors responsible for movement in all eukaryotic cells. The conversion of chemical energy from ATP hydrolysis into mechanical force produces movement along an actin filament. The mechanism of movement is involved in muscle contraction as well as various cellular processes including cytokinesis, adhesion, and vesicle transport. All myosins contain three functionally important domains: the catalytic head domain (CD), the light chain or lever arm domain (LCD), and the tail. The catalytic head domain is very similar between all classes of myosins, containing the site of ATP binding and hydrolysis and the actin-binding interface. The tail domain of myosins are highly divergent, containing either coiled-coil domains, individual subdomains, or both, that confer each myosin's specific function and cellular localization.

The biochemical steps of ATP hydrolysis in myosins are accompanied by a sequence of structural transitions. A large-scale conformational change within the myosin molecule occurs where the LCD, functioning as a lever arm, rotates relative to CD. In muscle myosin, this large-scale conformation change is associated with a transition of the actomyosin complex from a state of disordered, weak actin binding to a state of ordered, strong actin binding.

This research focuses on two functionally important domains within the myosin molecule: the catalytic domain and the tail domain. First, the structural transitions that occur within the myosin II catalytic domain during the actomyosin ATPase cycle are investigated using a combination of biochemical and spectroscopic approaches, specifically studying how various chemical modifications (chemical crosslinking, oxidative

modifications including methionine oxidation and glutathionylation) produce functional and structural changes. Chemical crosslinking is used to capture a dynamic intermediate in the myosin ATPase cycle, resembling a weak binding state, which is defective in actomyosin functional interaction and is dynamically disordered when bound to oriented actin. *In vitro* oxidative modification of the myosin catalytic domain, as a model for aging and oxidative stress in muscle shows chemical, functional, and structural perturbations are predominantly caused by a specific methionine residue in the actomyosin binding interface. These combined results illustrate a crucial role in proper actin binding cleft structural dynamics in myosin function. Modification of dynamics in this region, either by crosslinking or oxidation at critical residues in cleft, affect muscle function by interfering with the critical structural transitions necessary for actomyosin functional interaction. The focus then shifts to the tail domain of myosin VII, again using biochemical and spectroscopic approaches to elucidate the functional and structural properties of a myosin tail subdomain, the MyTH/FERM domain.

# Table of Contents

ACKNOWLEDGEMENTS.....	i
DEDICATION.....	iii
ABSTRACT.....	iv
TABLE OF CONTENTS.....	vi
LIST OF TABLES.....	viii
LIST OF FIGURES.....	ix
LIST OF EQUATIONS.....	x
ABBREVIATIONS.....	xi
<b>CHAPTER 1: INTRODUCTION TO MYOSIN &amp; MUSCLE CONTRACTION.....</b>	<b>1</b>
1.1 THE MOLECULAR MOTOR MYOSIN.....	1
1.2 MYOSIN IN SKELETAL MUSCLE CONTRACTION.....	3
1.3 ACTIN-BINDING INTERFACE OF MYOSIN CATALYTIC DOMAIN.....	9
1.4 COVALENT MODIFICATIONS IN THE MYOSIN CATALYTIC DOMAIN.....	10
1.5 METHIONINE OXIDATION IN MYOSIN WITH IMPLICATIONS FOR AGING AND DISEASE.....	12
1.6 MOTIVATION FOR RESEARCH.....	15
<b>CHAPTER 2: CONFORMATIONALLY TRAPPING THE ACTIN-BINDING CLEFT OF MYOSIN WITH A BIFUNCTIONAL SPIN LABEL.....</b>	<b>19</b>
2.1 CHAPTER SUMMARY.....	20
2.2 INTRODUCTION.....	21
2.3 METHODS.....	23
2.4 RESULTS.....	28
2.5 DISCUSSION.....	37
2.6 CONCLUSION.....	42
<b>CHAPTER 3: STRUCTURAL AND FUNCTIONAL IMPACT OF SITE-DIRECTED METHIONINE OXIDATION IN MYOSIN.....</b>	<b>43</b>
3.1 CHAPTER SUMMARY.....	44
3.2 INTRODUCTION.....	45
3.3 METHODS.....	48
3.4 RESULTS.....	53
3.5 DISCUSSION.....	65
3.6 CONCLUSION.....	69
<b>CHAPTER 4: REDOX SENSITIVE RESIDUES IN THE MYOSIN II ACTIN-BINDING INTERFACE.....</b>	<b>71</b>
4.1 CHAPTER SUMMARY.....	71
4.2 INTRODUCTION.....	72
4.3 METHODS.....	74
4.4 RESULTS.....	76
4.5 DISCUSSION AND FUTURE DIRECTION.....	82
<b>CHAPTER 5: CHARACTERIZATION OF A MYOSIN VII MYTH/FERM DOMAIN.....</b>	<b>85</b>
5.1 CHAPTER SUMMARY.....	86
5.2 INTRODUCTION.....	86



5.3 METHODS .....	88
5.4 RESULTS.....	93
5.5 DISCUSSION.....	98
5.6 CONCLUSION .....	99
<b>CHAPTER 6: FUTURE DIRECTION.....</b>	<b>101</b>
<b>BIBLIOGRAPHY .....</b>	<b>106</b>
<b>APPENDIX .....</b>	<b>119</b>

## List of Tables

**TABLE 1** Summary of DEER-derived distance distributions for IPSL-537 and 401.... 64

## List of Figures

FIGURE 1. Schematic representation of full-length myosin domain architecture.....	2
FIGURE 2. Skeletal muscle structure.....	3
FIGURE 3. Actomyosin ATPase scheme and associated structural transitions.....	5
FIGURE 4. Structure 1FMV of the CD of <i>Dicty</i> Myosin II.....	6
FIGURE 5. EPR spectra of myosin.....	7
FIGURE 6. Reactive oxygen species (ROS) produce chemical modifications in muscle proteins.....	12
FIGURE 7. EPR spectra used to resolve structural states of myosin.....	14
FIGURE 8. Bifunctional spin labeling of 416.583 S1dC.....	29
FIGURE 9. Monofunctional spin labeling of 416.583 S1dC.....	30
FIGURE 10. SDS-PAGE gel shift assay to determine extent of crosslinking.....	31
FIGURE 11. Effects of spin labeling on ATPase activity.....	32
FIGURE 12. BSL weakens interaction of myosin with actin in the absence of ATP.....	33
FIGURE 13. EPR spectra of BSL-S1dC.....	35
FIGURE 14. Model for the coupling of the actomyosin ATPase cycle to force and movement.....	38
FIGURE 15. Location of native methionines in <i>Dictyostelium</i> myosin II.....	54
FIGURE 16. Functional Sensitivity of <i>Dicty</i> myosin II to global methionine oxidation.....	56
FIGURE 17. Functional sensitivity of <i>Dicty</i> myosin II to site-specific methionine oxidation.....	57
FIGURE 18. Location of <i>Dicty</i> myosin II spin-labeling sites.....	59
FIGURE 19. CD spectroscopy and thermal denaturation of peroxide-treated <i>Dicty</i> myosin containing native Met.....	60
FIGURE 20. Effect of oxidation on structural dynamics of actin-binding cleft.....	62
FIGURE 21. Effect of oxidation on structural dynamics of actin-binding cleft near the actomyosin interface.....	63
FIGURE 22. Effect of oxidation on structural dynamics SH1 helix.....	65
FIGURE 23. Location of M394 (orange) near the cardiomyopathy loop.....	69
FIGURE 24. Location and sequence conservation of <i>Dicty</i> residue M394.....	77
FIGURE 25. Reversal of methionine oxidation in <i>Dicty</i> myosin II by Msr.....	78
FIGURE 26. Recovery of myosin II actin-activated ATPase activity with Msr.....	79
FIGURE 27. Modification of <i>Dicty</i> myosin II with glutathione.....	80
FIGURE 28. Actomyosin functional interaction with glutathionylation.....	81
FIGURE 29. Isolation of the N-terminal MyTH/FERM domain of DdM7.....	93
FIGURE 30. Binding of MF1 to actin.....	94
FIGURE 31. Binding of MF1 to tubulin.....	96
FIGURE 32. Structure and stability of MF1.....	97
FIGURE 33. Bifunctional spin label binds rigidly and stereospecifically.....	102
FIGURE 34. Schematic representation of full-length myosin myosin VII.....	105

## List of Equations

Eq. 1. ROTATIONAL CORRELATION TIME .....	27
Eq. 2. MEAN RESIDUE ELLIPTICITY .....	50
Eq. 3. BIPOLAR BROADENING FUNCTION AS A SUM OF GAUSSIANS.....	52
Eq. 4. GAUSSIAN DISTANCE DISTRIBUTION .....	52

## Abbreviations

A, actin  
ADP or D, adenosine diphosphate  
ATP or T, adenosine triphosphate  
BSL, 3,4-bis-(methanethiosulfonyl-methyl)-2,2,5,5-tetramethyl-2,5-dihydro-1h-pyrrol-1-  
yloxy  
CD, myosin catalytic domain  
Cryo-EM, cryo-electron microscopy  
CW-EPR, continuous wave EPR  
Cys, cysteine  
Dicty, *Dictyostelium discoideum*  
DdM7, *Dictyostelium discoideum* myosin VII  
EPR, electron paramagnetic resonance  
FERM, band 4.1, ezrin, radixin, moesin  
GSH, glutathione  
HNE, 4- hydroxy-2-nonenal  
IASL, 4-(2-Iodoacetamido)-2,2,6,6-tetramethyl-1-piperidinyloxy  
IPSL, 3-(2-Iodoacetamido)-2,2,5,5-tetramethyl-1-pyrrolidinyloxy  
L50, Lower 50 kDa domain  
LCD, myosin light chain domain  
M, myosin  
Met, methionine  
MetO, methionine sulfoxide  
MF1, DdM7 MyTH4/FERM domain  
MSL, N-( 1-oxy-2,2,6,6-tetramethyl-4-piperidinyloxy)maleimide.  
Msr, Methionine sulfoxide reductase  
MyTH, myosin talin homology 4  
P or P<sub>i</sub>, inorganic phosphate  
PH, pleckstrin homology  
RONS, reactive oxygen and nitrogen species  
ROS, reactive oxygen species  
S, strong  
S1, subfragment 1 of muscle myosin, proteolytic fragment  
S1dC, subfragment 1 of *Dictyostelium discoideum* myosin II  
SDSL, site-directed spin labeling  
STEPR, saturation transfer EPR  
U50, Upper 50 kDa domain  
W, weak  
W-S, weak-to-strong transition (of myosin)

# Chapter 1: Introduction to Myosin & Muscle Contraction

## 1.1 The Molecular Motor Myosin

Myosins are a superfamily of actin-based motor proteins. Motor proteins rely on the mechanochemical coupling of ATP hydrolysis to force generation or movement. Common characteristics of all motor proteins are the ability to bind and hydrolyze ATP, to move along a track of either actin or microtubules, and to undergo an ATP-dependent conformational change responsible for generation of movement. Myosins are unique in that they are the only motor proteins that bind and move along helical actin filaments. The myosin superfamily consists of at least 24 classes of myosin [1], all which serve fundamental roles in actin-dependent processes. Myosins perform a diverse set of tasks within all eukaryotic cells. Many of these functions are universal and include such processes as cytokinesis, adhesion, and vesicle transport [1]. Other myosins serve roles only in specialized cells, such as in the maintenance of the structural integrity in stereocilia in the inner ear or retinal cells [2-6]. Myosin may be most well known for its role in muscle contraction. This myosin, myosin II, is termed “conventional” myosin as it was the first class of myosins discovered. All other myosins are broadly classified as “unconventional”. Fundamentally, the same mechanisms that are responsible for motion associated with cell movement or transport are the same as those responsible for muscle contraction.

All myosins, whether conventional or unconventional, contain three functional domains: a catalytic domain, a neck region (light chain or ‘lever arm’), and a tail region (FIGURE 1). The catalytic domain has high sequence and structure conservation between

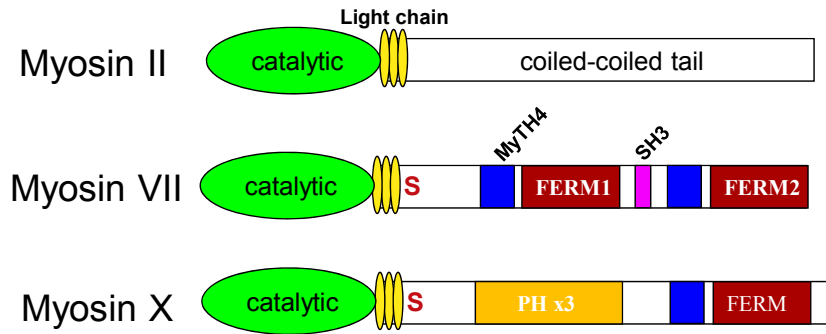


**FIGURE 1. Schematic representation of full-length myosin domain architecture.** The catalytic “head” domain is shown in green, light chain (neck) or ‘level arm’ in yellow, and tail domain in white with specific myosin subdomains highlighted.

all classes of myosins. It contains the ATP binding site as well as the actin- binding interface. The neck region is composed of a long alpha helix of variable length which binds either light chains or calmodulin. Whereas the catalytic heads share a number of conserved elements, the C-terminal tail regions of the various myosin classes are highly divergent with considerable variation in sequence length, domain composition, and organization [7]. The conventional myosin IIs all contain tail regions with predicted alpha-helical coiled-coil domains (FIGURE 1), allowing for dimerization of two myosin molecules and self assembly to form a filament structure. In comparison, the unconventional myosin C-terminal tails contain a variety of subdomains. These subdomains confer each myosin’s individual cellular functions and localization [8]. For example, myosin VII contains two MyTH/FERM domains which are responsible for linking the actin cytoskeleton to microtubules in the plasma membrane [9, 10] (FIGURE 1). Another unconventional myosin, myosin X, has one MyTH/FERM domain in addition to three pleckstrin homology (PH) domains within its tail, suggesting a dual role in binding to microtubules in the plasma membrane but also facilitating cargo transportation by binding phosphoinositides to its PH domains [11, 12] (FIGURE 1).

## 1.2 Myosin in Skeletal Muscle Contraction

Myosin II is the molecular motor that converts chemical energy from ATP hydrolysis into mechanical force to produce muscle contraction. The smallest contractile unit of muscle is the sarcomere, which repeats along the length of the muscle cell, the myofibril. The sarcomere has two main components, thick filaments and thin filaments (FIGURE 2). The thick filament is comprised of myosin, aggregated via its coiled-coil tail region into a bipolar filament. The main component of the thin filament is a helical polymer of globular actin monomers. The thin filament also contains a set of calcium responsive regulatory proteins (tropomyosin and troponins) that regulate muscle

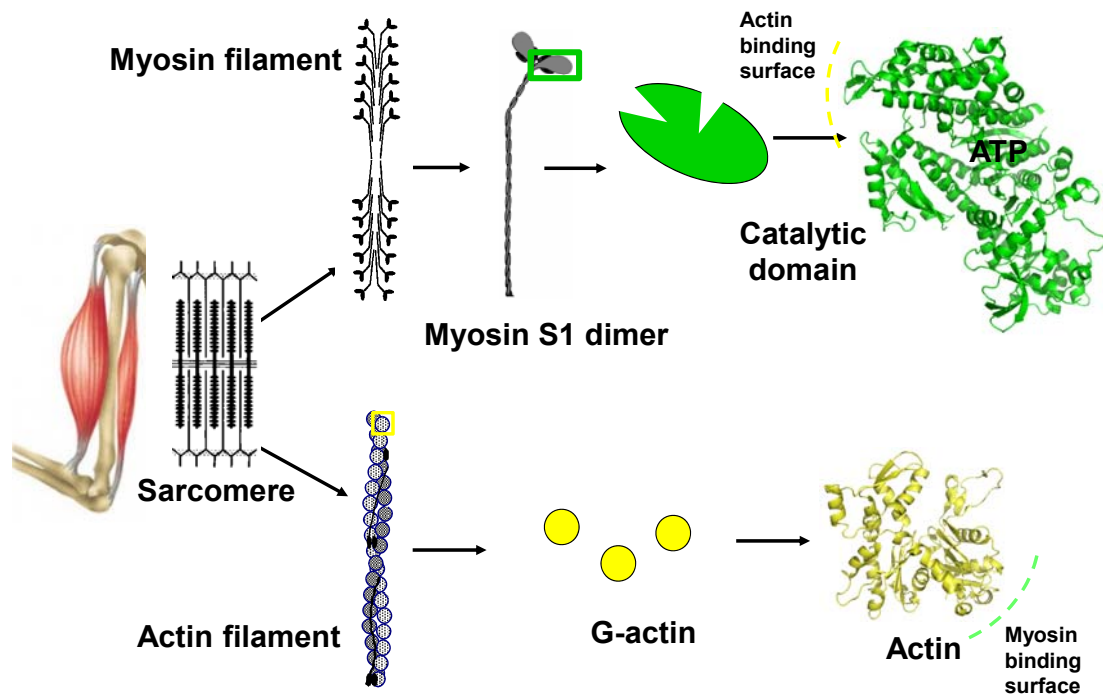


**FIGURE 2. Skeletal muscle structure.** The smallest contractile unit of muscle is the sarcomere, composed of thick and thin filaments. The thick and thin filaments are mainly composed of myosin and actin, respectively. Myosin (green) exists as a dimer. The isolated catalytic “head” domain of myosin is shown (PDB: 1FMV) highlighting the general location of the actin-binding interface and ATP binding pocket. Monomeric actin (PDB: 1ATN) is shown in yellow with the myosin-binding interface highlighted.



contraction by blocking the myosin binding site on actin.

Changes in sarcomere appearance observed by interference microscopy on living muscle fibers captured the sliding motion of the thin filaments relative to the thick filaments, giving rise to the sliding filament theory describing how muscles contract [13, 14]. The interaction of myosin with actin, termed a crossbridge, in the presence of ATP results in sliding of thin filaments past thick filaments shortening the sarcomere. Lymn and Taylor were first to propose the actomyosin ATPase hydrolysis mechanism [15] (FIGURE 3A) which correlates each biochemical state of ATP hydrolysis with a crossbridge structural state. This crossbridge cycle includes four steps: (1) ATP binds causing the myosin crossbridge to rapidly dissociate from the actin filament, (2) ATP hydrolysis occurs inducing a change in myosin orientation, (3) the actomyosin crossbridge reforms and (4) products of ATP hydrolysis are released in association with a conformational change in the crossbridge orientation which presumably generates force termed the “powerstroke”. The exact relationship between the Lymn-Taylor kinetic scheme and the structural transitions within the actomyosin crossbridge remain unknown. Crystallographic and spectroscopic research suggests that the conformational change in crossbridge orientation with the powerstroke is mainly isolated to the light chain domain of myosin, which functions as a ‘lever arm’ (reviewed in [16]). This gave rise to the swinging lever arm hypothesis [17]. All myosins, regardless of function, utilize the lever arm mechanism to generate movement.

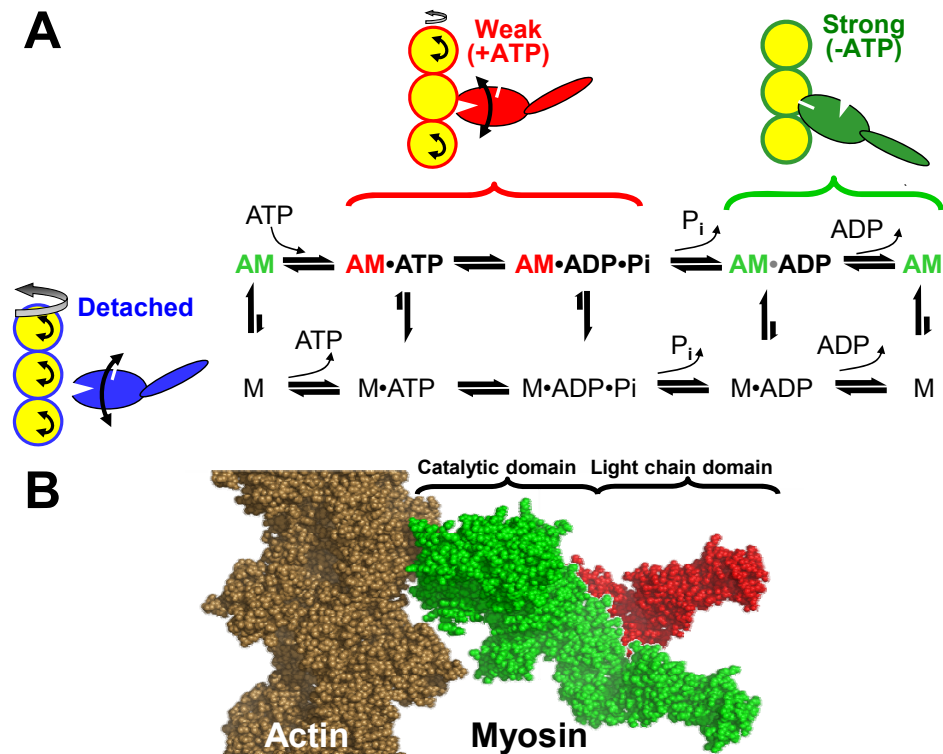


**FIGURE 3. Actomyosin ATPase scheme and associated structural transitions.** A, illustrating proposed coupling of biochemical states to structural states and actin movement (A = actin, M = myosin). Horizontal dimension shows changes in nucleotide bound, which determines the transition from weak (red) to strong (green) binding states. The vertical dimension shows the transition been unbound (detached, blue) and bound actomyosin complex. B, Model of myosin bound to actin in the pre- (red) and post-powerstroke states, highlighting the catalytic ‘head’ and light chain ‘neck’ domains.

As Lyme and Taylor first proposed, the biochemical steps of ATP hydrolysis are accompanied by a sequence of myosin structural transitions. As shown by the David Thomas lab and others, force production involves the coordination of two distinctive steps; a rotation of the LCD and a disorder-to-order transition [16, 18-20] (FIGURE 3). The disorder-to-order transition involves the actomyosin complex converting from a state of disordered, weak actin binding to a state of ordered, strong actin binding (FIGURE 3A). This weak-to-strong (W-S) transition is associated with a large-scale conformational change within the myosin molecule, with the LCD rotating relative to the

CD (FIGURE 3B). The rotation of the LCD, acting as a lever arm, displaces the associated actin filament.

The large-scale structural change of the LCD with respect to the CD is accompanied by smaller-scale structural changes within functionally important subdomains of the myosin CD. These subdomains include the actin-binding cleft, the nucleotide-binding pocket, and the force-generating region (converter, relay helix, SH1 helix) (FIGURE 4A). Both the actin-binding cleft and nucleotide binding pocket are proposed to exist in open and closed conformations [16]. Structural changes within the force generating domain include bending of the relay helix, melting of the SH1 helix, and a coordinated rotation of the converter domain which is directly propagated into the large

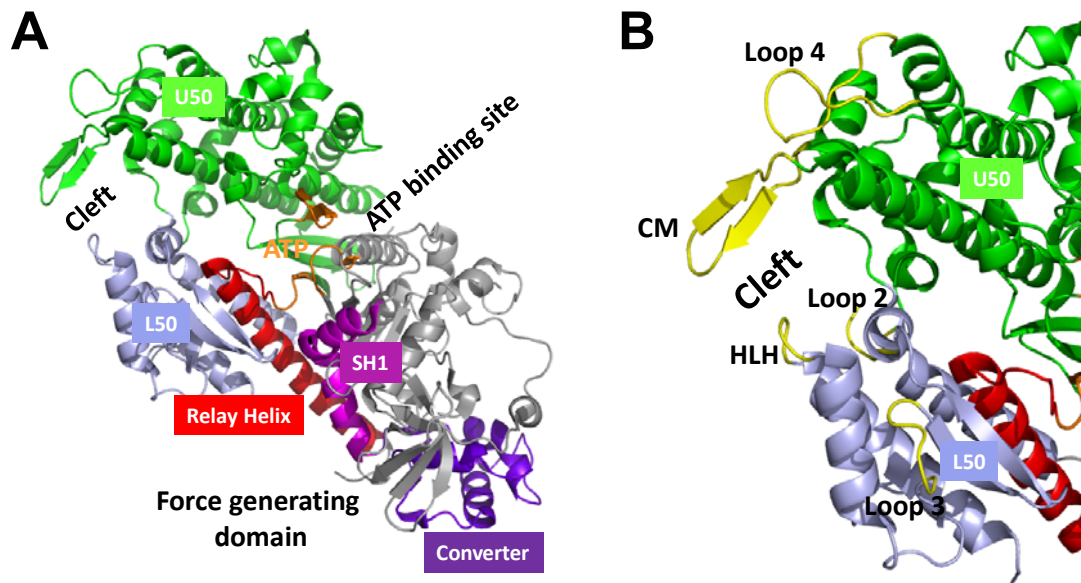


**FIGURE 4. Structure 1FMV of the CD of *Dicty* Myo II.** A, Subdomains highlighted including the ATP binding pocket (orange), actin-binding cleft including the upper and lower 50 kDa domains (U50: green, L50: light blue), and force generating region (relay helix: red, SH1 helix: magenta, and converter: purple). B, Actin-binding loops within the actin-binding cleft of myosin are highlighted in yellow including the cardiomyopathy (CM) loop, loop 2, loop 3, loop 4, and the helix-loop-helix (HLH) motif.

scale movement of the LCD [16]. These subdomains must be structurally coupled so that force generation results from the productive coordination of actin binding and ATP hydrolysis.

The large and smaller scale structural changes that occur within the contractile protein of muscle, specifically myosin and the actomyosin complex, has largely been resolved by the spectroscopic technique electron paramagnetic resonance (EPR) combined with site-directed spin-labeling (SDSL). EPR and SDSL are the ideal tools to study actomyosin structural dynamics as they allow for high-resolution structural detail and dynamics of large macromolecular complexes. This is not feasible by other structural

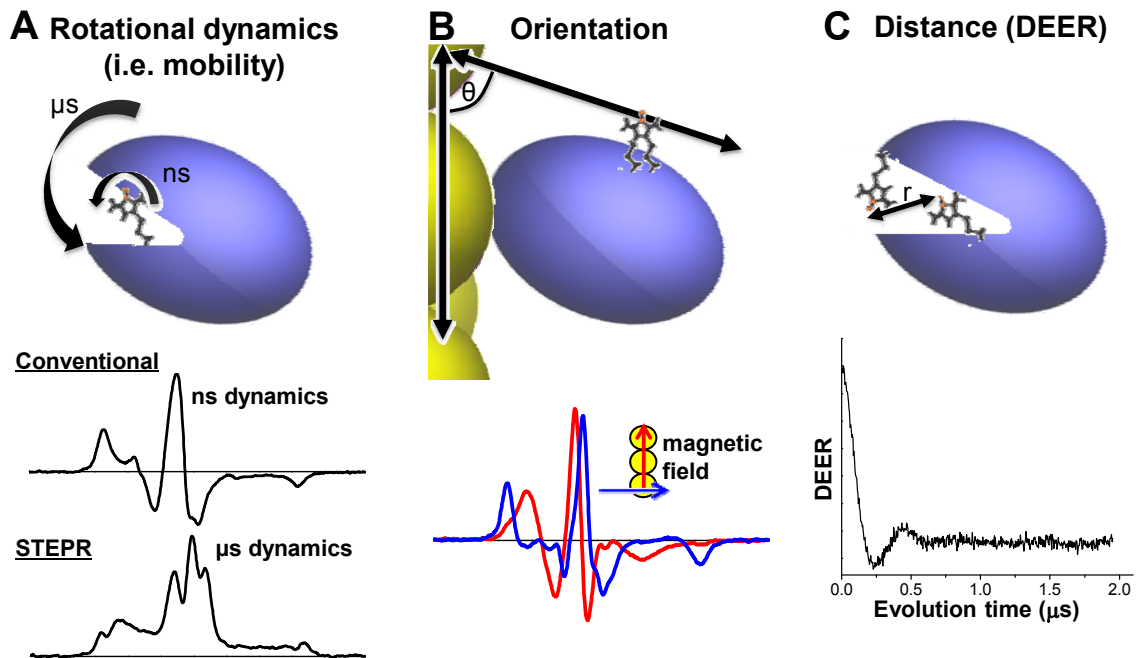


**FIGURE 5. EPR spectra of myosin.** A, conventional ( $V_1$ ) EPR spectrum used for determination of nanosecond rotational motion (top) and saturation transfer EPR (STEPR) spectrum (bottom) used in determination of microsecond rotational motion. B, conventional ( $V_1$ ) EPR of myosin on oriented actin in skinned muscle fibers, with the fiber axis oriented parallel (red) or perpendicular (blue) to the applied magnetic field. C, DEER, used to measure distance  $r$  between two attached spin labels, in the range of 2-6 nm. The oscillation period is proportional to  $r^3$ . In this case  $r = 2.6$  nm.

techniques such as nuclear magnetic resonance (molecular weight size limitation, actomyosin complex is too large) and x-ray crystallography (gives static structural models, actomyosin is dynamic). EPR can be used to study site-specific rotational motion in both the nanosecond (conventional EPR,  $V_1$ ) and microsecond (saturation transfer or STEPR,  $V_2'$ ) time range (FIGURE 5A); orientational order or disorder of myosin relative to the actin filament (FIGURE 5B); and precise distance and dynamics by dipolar electron-electron resonance (DEER) that involves attachment of two spin-probes (FIGURE 5C). EPR is sensitive to rotational dynamics on timescales of picoseconds to milliseconds. Conventional EPR is sensitive to rotational motion in the picosecond to nanosecond range (FIGURE 5A, top spectrum) while STEPR can be used to detect slower motions, in the microsecond to millisecond range (FIGURE 5A, bottom spectrum). EPR is not only sensitive to spin-label mobility but also to orientation with respect to the magnetic field (FIGURE 5B). Muscle fibers can be aligned parallel or perpendicular to the magnetic field, and the resulting EPR spectra report the angle  $\theta$  between the spin label's principle axis and the fiber axis. If a substantial difference is observed between the parallel (red) and perpendicular (blue) spectra, this indicates a highly ordered orientation (FIGURE 5B). A highly disordered orientation would have parallel and perpendicular spectra that are almost identical. EPR can also be used to measure the distance  $r$  between two spin labels (FIGURE 5C). Conventional EPR can be used to measure distances from 0.7 to 2.5 nm, while the pulsed EPR DEER (FIGURE 5C), can be used to measure distances from 1.7 and 6 nm, with 0.1 nm resolution. All of these EPR techniques also have the capability to detect multiple conformational states present in solution at the same time.

### **1.3 Actin-binding interface of myosin catalytic domain**

One of the biologically crucial properties of myosin is its ability to bind actin, forming the actomyosin complex. This interaction is highly specific and essential for all myosins to function. The actin-binding interface consists of structurally conserved loops surrounding the central water-filled actin-binding cleft (FIGURE 4B). The actin-binding cleft of myosin is a solvent-filled cavity that separates the upper 50 kDa (U50) domain from the lower 50 kDa (L50) domain, each of which contributes to the actin-binding interface. No high resolution structural data of the actomyosin complex exists. However, a pseudoatomic cryo-EM model of the actomyosin interface in rigor shows that myosin interacts with two adjacent actin monomers via several surface exposed loops [30]. Regions on myosin involved in actin-binding are the cardiomyopathy (CM) loop, loop 2, loop 3, loop 4, and the helix-loop-helix (HLH) motif (FIGURE 4B). Mutagenesis has shown that the loops within this interface are critical for actomyosin function [21-27].

Crystallographic data has led to the proposal that the actin-binding cleft closes as actomyosin transitions from weak binding to strong binding [20]. Crystal structures of myosin II, the principal isoform of muscle, are consistently observed with an open cleft, but a high-resolution structure of myosin V is proposed to represent the closed cleft state [28]. During the W-S transition, the interface isomerizes from a dynamic, W state, to an ordered S state, rotating the U50 and pushing water from the cleft. How these changes in the actin-binding cleft are coupled to the W-S transition, power stroke and product release is not well understood. In some models, the cleft closes prior to Pi release, while in others, ADP.Pi in the nucleotide pocket prevents cleft closure and the full W-S transition of the interface [29-31]. An intrinsic flexibility of the U50 domain is proposed

to be necessary for myosin to properly transition to the strong binding conformation allowing the myosin cleft to properly transition between “open” and “closed” structural states and produce force [32]. This transition is essential for actin-activation and formation of the strong actomyosin binding state. This U50 flexibility is dependent on biochemical state and is proposed to underlie myosin’s ability to rapidly adopt its strong binding state [33].

Mutations associated with various myopathies are distributed throughout the actomyosin binding interface. Disease-causing point mutations in the myosin catalytic domain have been identified in the cardiomyopathy loop (hence the name) [34-36], loop 3 [37], loop 4 [38], and the HLH motif [39-41]. Myopathies include hypertrophic cardiomyopathy (HCM), dilated cardiomyopathy (DCM), and non-compaction cardiomyopathy. Point mutations with especially severe clinical prognosis or defects in actomyosin functional interaction are found in the CM-loop, for example mutation R403Q [36, 42, 43].

## **1.4 Covalent Modifications in the Myosin Catalytic Domain**

Disease-causing point mutations can alter myosin’s function but the allosteric properties of myosin can also be modified by covalent modification. Covalent modifications can alter a protein’s chemical properties, folding, stability, activity, structure, conformational distribution, cellular localization and consequently, function. Covalent modifications can either inhibit or activate enzymatic activity and are in many cases reversible. Many covalent modifications are involved in complex, regulatory pathways but are also common in disease states.

Myosin is susceptible to a variety of both *in vivo* and *in vitro* covalent modifications leading to perturbation of function and structure. Crosslinking, through either direct disulfide linkage or by use of chemical crosslinking agents, can be used to trap structural states of myosin by linking key subdomains. The effects on function and structural transitions in other subdomains associated with ATP hydrolysis and force generation can then be investigated. To date, crosslinking studies on the myosin catalytic domain focus on sites within the force-generating subdomain [44-48]. Using a cross-linking approach, it was shown that nucleotide binding to myosin induces a flexibility of the SH1 helix, shifting the equilibria among conformational states of the helix [48]. Crosslinking two reactive thiols within the SH1 helix causes defects in ATPase activity and actomyosin functional interaction [44-47]. This crosslinked state is postulated to resemble a myosin with ATP bound (i.e. in the weak state). However, more recent evidence suggests this trapped state is at the threshold of force generation, intermediate between weak binding and rigor [46, 47]. The L50 kDa domain has also been crosslinked to the converter to test intra-myosin inter-subdomain changes associated with the actin-activated ATPase cycle [49].

Covalent modifications induced by oxidative processes have also been studied in myosin. Studies on *in vivo* oxidative modifications of myosin focused on a variety of selected markers including carbonylation [50, 51], glycation [52, 53], formation of HNE adducts [54], oxidation of cysteines [55], and glutathionylation [56]. In most cases, these oxidative modifications adversely affect actomyosin function, decreasing ATPase activity and ability to produce force. Interestingly, low levels of glutathionylation in the myosin



motor domain potentiate function [56]. In most cases, studies that identify site-specific oxidative modifications are lacking.

## 1.5 Methionine Oxidation in Myosin with implications for Aging and Disease

The age-related deterioration of muscle function is characterized by a decrease in contractile force, progressive loss of muscle mass, and slowing of muscle movement. Impaired force with aging is due not only to muscle atrophy, but also to molecular defects involving both contractile and regulatory proteins [57, 58]. Site-specific modifications to amino acid side chains within muscle proteins can be attributed to the action of reactive oxygen species (ROS), produced in muscle by numerous physiological and pathophysiological conditions. ROS in muscle is thought to impair force by two different mechanisms: (1) ROS activity can act via redox signaling mechanisms to alter muscle gene

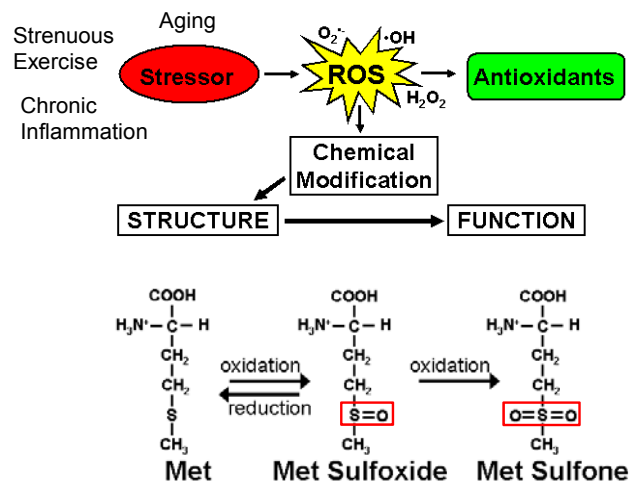


**FIGURE 6. Reactive oxygen species (ROS) produce chemical modifications in muscle proteins, specifically conversion of methionine (Met) to methionine sulfoxide (MetO) or methionine sulfone (MetO<sub>2</sub>), leading to changes in both structure and function.**

expression, causing contractile protein loss resulting in muscle atrophy and (2) ROS can act via post-translational mechanisms to modify side chains of contractile proteins, causing contractile dysfunction that decreases specific force [59]. The sulfur-containing amino acids, cysteine (Cys) and methionine (Met), are the prime cellular targets of ROS [60]. Methionine is oxidized to methionine sulfoxide (MetO) which involves the addition of an oxygen on the sulfur atom present in the side chain of Met (FIGURE 6). This oxidation reaction is reversible by the thioredoxin-dependent antioxidant enzyme methionine sulfoxide reductase (Msr). The reduction of MetO back to Met requires the action of two reductases (MsrA and MsrB) as they reduce of the S- and R-stereoisomers of MetO respectively [60]. Under strong oxidizing conditions, MetO can be further oxidized to methionine sulfone (MetO<sub>2</sub>), a reaction that is irreversible (FIGURE 6).

The defect in force generation associated with aging can be traced to molecular defects within the contractile protein myosin [61-67]. Myosin isolated from aged rats shows a decrease in ability to produce force [65]. EPR reveals that this decrease in force can be attributed to age-related structural changes within myosin. No changes in the EPR spectra were observed when actomyosin was under rigor (all myosin heads strongly bound) or relaxation (all myosin heads weakly bound) conditions, but differences were observed in contraction (combination of strongly and weakly bound myosin heads), suggesting a perturbation in the W-S structural transition of actomyosin crucial for force generation as well as an age-dependent change in contraction (FIGURE 7B). To test the effects of ROS on muscle fibers as a model for aging, skinned muscle fibers from rabbit were treated with hydrogen peroxide [66]. The functional and structural changes in myosin associated with hydrogen peroxide treatment were similar to changes observed for myosin extracted

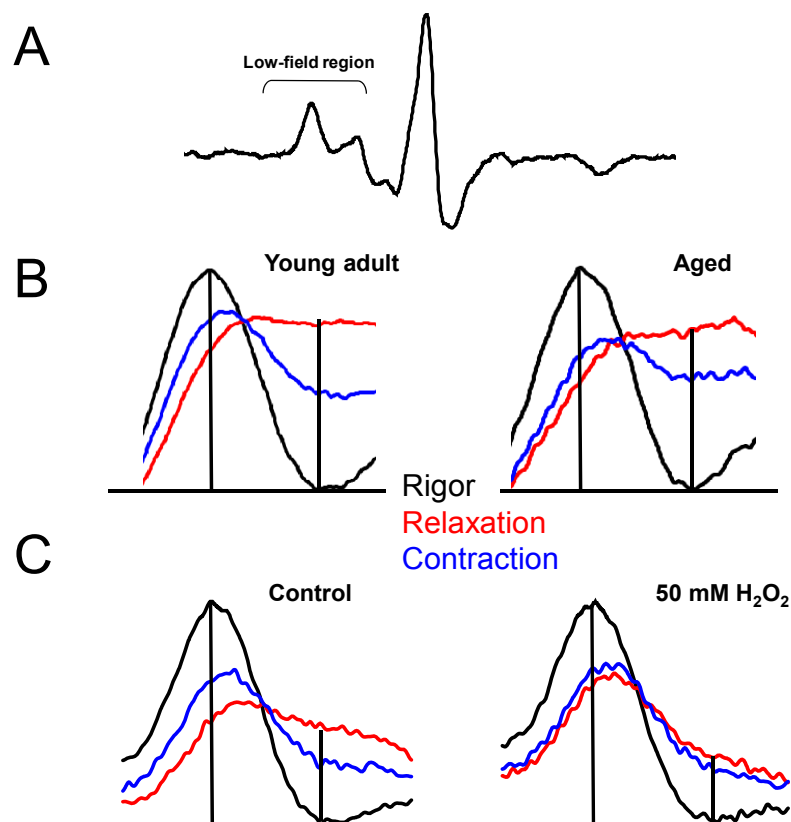


**FIGURE 7. EPR spectra used to resolve structural states of myosin.** A, Representative EPR spectra of IASL found to myosin at Cys-707 (SH1), the low field region is indicated. B, Low field portion of EPR spectra with labeling site as in (A) for muscle fibers extracted from young or aged rats [65]. C, Low field portion of EPR spectra with labeling site as in (A) for muscle fibers extracted from rabbits either untreated (control) or treated with 50 mM hydrogen peroxide [66]. In both B and C, spectra were acquired in rigor (black), relaxation (red), and contraction (blue).

from aged rats (FIGURE 7C). Interestingly, proteomics analysis revealed that these functional and structural changes are due primarily to oxidation of multiple Met residues in myosin heavy chain [66].

The importance of methionine oxidation and its specific reduction by methionine sulfoxide reductase (Msr) in aging is well established (reviewed in [68]) (FIGURE 6). There is an age-related increase in the oxidation of Met residues in calmodulin (CaM) isolated from rat brain, which leads to a loss in ability of CaM to regulate plasma

membrane calcium ATPase [69, 70]. Mutations leading to a loss of Msr activity in worm and mouse models lead to an increase in the number of methionines oxidized to methionine sulfoxide (MetO) but also a decrease in life span [71, 72]. The body wall muscle cells of a *C. elegans* Msr knockout show sarcomeric disorganization [71], a characteristic previously described as a sign of aging in worms [73]. In addition, this worm mutant shows increased presence of protein MetO, locomotion defects, and decreased lifespan providing a link between oxidative damage/repair of Met and muscle tissue aging.

Although oxidation in muscle can be detrimental, ROS production in muscle fibers can be increased not only due to pathophysiological conditions including aging and chronic inflammation but also a variety of normal physiological conditions such as strenuous exercise [59]. Redox signaling mediates many adaptations in muscle, stimulating responses to metabolic, mechanical and functional demands such as exercise, hormonal fluctuations and development. Methionine and cysteine redox sensors have been identified for proteins involved in calcium regulation [74-81], but few such sensors have been characterized for contractile proteins [63].

## **1.6 Motivation for Research**

Actomyosin motility is a dynamic energy-transducing process in which actin-activated hydrolysis of ATP by myosin generates force and movement in all eukaryotic cells. There is no mechanism of more fundamental importance to biology and human health. A detailed understanding of this complex system is needed for the rational design of therapies for not only muscle disorders -- muscle weakness in aging [58], heart disease

[82], and muscular dystrophies [83], – but also diseases associated with unconventional myosins such as Usher syndrome [2-4, 6]. The actomyosin interaction in force generation and cellular movement is an intensely studied biophysical process with elusive mechanistic and structural details. In this work, various biochemical and spectroscopic tools are used to study the dynamic processes of the actomyosin interaction and changes induced by covalent modifications.

A highly important component of the actomyosin interaction is the actin-binding cleft of myosin, which is proposed to undergo a conformational change from an “open” to “closed” state with the W-S transition of force generation as well as require an intrinsic flexibility for this to occur. Chapter 2 investigates how restricting the conformational flexibility of the actin-binding cleft affects actomyosin functional interaction and structural dynamics at the actomyosin interface. By chemically crosslinking two engineered cysteines across the actin-binding cleft, the cleft is trapped. Trapping the cleft effects myosin’s ability to bind and hydrolyze ATP and interact with actin as well as induces a dynamic, intermediate weak binding state when attached to oriented actin filaments, providing direct insight into the early steps of actomyosin force generation.

Understanding the molecular mechanism of age-related decline in muscle strength and contractility requires the examination of the chemical modifications and subsequent functional and structural perturbations of myosin. Chapters 3 and 4 aim to bridge the understanding of protein oxidation and muscle dysfunction with molecular-level insights into myosin structural dynamics and actomyosin functional interaction using a three-pronged approach; Met mutagenesis, *in vitro* oxidation (and enzymatic reversal), and

site-directed spectroscopy. The working hypothesis is that muscle dysfunction related to oxidative stress stems from changes in actomyosin structural dynamics that can be traced back to oxidation of specific Met in the myosin heavy chain. Both aging and oxidation of muscle myosin by hydrogen peroxide inhibit the W-S structural transition of actomyosin [65, 66]. One of the most likely causes of the inhibition of the W-S actomyosin transition is a change in actin-binding cleft dynamics, since closure of this cleft is crucial for strong actin binding [84]. It is not clear which methionines, one or many, are responsible for the observed functional and structural changes in myosin. The goal is to delineate site-specific protein structural changes that explain the decline in muscle function with Met oxidation. A key Met residue identified in Chapter 3 is a known site of glutathionylation in beta-cardiac myosin [56]. The site-specific functional effects of glutathionylation in the actin-binding cleft of myosin are investigated in Chapter 4. This work illustrates the ability of myosin to function as a muscle redox sensor, potentially modulating contractile activity through a redox dependent mechanism in response to oxidative stress. Few such sensors have been characterized for contractile proteins [63].

Most of the work presented focuses on the myosin II catalytic domain. Chapter 5 shifts focus from myosin II to the unconventional myosin VII as well as from the catalytic domain to the tail domain. The functional and structural properties of many myosin tail subdomains are unknown. MyTH/FERM domains are present in numerous cytoskeletal signaling and motor proteins and much remains to be learned about their combined structure and function. The structure of MyTH/FERM domains is predicted to be conserved throughout evolution despite a high degree of sequence divergence of these

domains. The N-terminal MyTH/FERM region of *Dictyostelium* myosin VII (M7) has been isolated as a first step toward gaining insight into the function of this domain and its interaction with binding partners.

## Chapter 2: Conformationally Trapping the Actin-Binding Cleft of Myosin with a Bifunctional Spin Label

Reprinted with permission from:

Rebecca J. Moen, David D. Thomas, and Jennifer C. Klein. Conformationally trapping the actin-binding cleft of myosin with a bifunctional spin label. *J Biol Chem.* 2013;288(5):3016-3024.

**Copyright © 2013 The American Society for Biochemistry and Molecular Biology, Inc.**

Contributions of Authors:

Rebecca J. Moen: Designed all experiments. Performed experiments and analyzed data for gel shift assays, ATPase assays, and cosedimentation assays as shown in figures 10, 11, and 12 respectively. Assisted with EPR experiments shown in figures 8, 9, and 13. Made figures 8-12. Wrote the manuscript.

David. D. Thomas: Designed all experiments. Performed STEPR experiments shown in figure 13B. Made figures 13 and 14. Edited other figures and manuscript.

Jennifer C. Klein: Designed all experiments. Designed and performed mutagenesis for myosin mutants. Performed EPR experiments shown in figure 8, 9, and 13 and analyzed associated data. Edited the figures and manuscript.



## 2.1 Chapter Summary

We have trapped the catalytic domain of *Dictyostelium discoideum* (*Dicty*) myosin II in a weak actin-binding conformation by chemically crosslinking two engineered cysteines across the actin-binding cleft, using a bifunctional spin label (BSL). By connecting the lower and upper 50 kDa domains of myosin, the crosslink restricts the conformation of the actin-binding cleft. Crosslinking has no effect on the basal ATPase activity of isolated myosin, but it impairs rigor actin binding and actin-activation of myosin ATPase. EPR spectra of BSL provide insight into actomyosin structural dynamics. BSL is highly immobilized within the actin-binding cleft and is thus exquisitely sensitive to the global orientation and rotational motions of the myosin head. Conventional EPR shows that myosin heads bound to oriented actin filaments are highly disordered with respect to the actin filament axis, in contrast to the nearly crystalline order of myosin heads in rigor. This disorder is similar to that of weakly bound heads induced by ATP, but saturation transfer EPR shows that the disorder of crosslinked myosin is at least 100 times slower. Thus this cleft-crosslinked myosin is remarkably similar, in both actin affinity and rotational dynamics, to SH1-SH2 crosslinked BSL-myosin S1. We conclude that, whether myosin is trapped at the actin-myosin interface or in the force-generating region between the active site and lever arm, the structural state of myosin is intermediate between the weak-binding state preceding phosphate release and the strong-binding state that succeeds it. We propose that it represents the threshold of force generation.

## 2.2 Introduction

Myosin is the molecular motor that converts chemical energy from ATP hydrolysis into mechanical force to produce muscle contraction. The biochemical steps of ATP hydrolysis are accompanied by a sequence of myosin structural transitions. Force generation by myosin is associated with the transition from a state of weak actin binding, characterized by dynamic disorder, to an ordered, strong actin-binding state [16]. The weak-to-strong transition is associated with large-scale rotation of the light-chain domain (LCD) relative to the catalytic domain (CD) [16, 85-88]. The rotation of the LCD, acting as a lever arm, displaces the associated actin filament, generating movement.

The large-scale structural change of the LCD with respect to the CD is accompanied by smaller-scale structural changes within functionally important subdomains of the myosin CD, including the nucleotide-binding pocket, the actin-binding cleft, and the force-generating region (converter, relay helix, SH1 helix). These subdomains must be structurally coupled so that force generation results from the productive coordination of actin binding and ATP hydrolysis. A generalized picture of the force-generating powerstroke includes rotation of the LCD coupled to a closing of the actin-binding cleft, opening of the nucleotide pocket, and ordering of the bound myosin head. However, spectroscopy has revealed that a single biochemical state, as defined by the ligands of myosin, can produce multiple structural states, as revealed by high-resolution spectroscopy in the SH1 and relay helices of the force-generating domain [89-91] and the actin-binding cleft [84].

The actin-binding cleft of myosin is a solvent-filled cavity that separates the upper 50 kDa (U50) domain from the lower 50 kDa (L50) domain, each of which contributes to

the actin-binding interface. Crystallographic data has led to the proposal that the actin-binding cleft closes as actomyosin transitions from weak binding to strong binding [20]. Crystal structures of myosin II, the principal isoform of muscle, are consistently observed with an open cleft, but a high-resolution structure of myosin V is proposed to represent the closed cleft state [28]. Cryo-EM data has indicated that the actin-binding cleft is structurally sensitive to nucleotide and actin binding [32, 92-94].

Spectroscopic measurements on myosin in solution have demonstrated that for isolated sites within the cleft, changes in cleft conformation do occur in response to nucleotide and actin binding. Solvent exposure of the myosin cleft was probed at an engineered tryptophan at position F425W in smooth muscle myosin [95] (equivalent to S416 in *Dicty* myosin II). Weak-binding (M.ATP, M.ADP.P<sub>i</sub>) states were more solvent-accessible than strong-binding (M.ADP) states in the absence of actin, and actin decreased solvent accessibility, suggesting cleft closure. Actin-induced cleft closure was also suggested by EPR-observed changes in the interspin distance between sites 416 and 537 of *Dicty* myosin II [96], and by pyrene excimer fluorescence at these same positions [97]. We used spin labels attached to several pairs of sites across the cleft to show that the actin-binding cleft exists in a conformational equilibrium between open and closed structural states in all biochemical states, with actin and nucleotides shifting the equilibrium toward the closed and open states, respectively [84]. In support of these results, it has been suggested that intrinsic flexibility in the U50 domain of the actin-binding cleft is necessary for myosin to rapidly adopt the strongly-bound conformation preceding force generation [32, 33, 98].

In the present study, we ask how restricting the conformational flexibility of the actin-binding cleft affects actomyosin functional interaction and structural dynamics at the actomyosin interface. We have chemically crosslinked two engineered cysteines across the actin-binding cleft using a bifunctional methanethiosulfonate spin label (BSL) attached to residues 416 and 583 of the *Dicty* catalytic domain. We determined the effects of this crosslinking on myosin and actomyosin ATPase activity, and actin-binding affinity, and we used both conventional and saturation transfer EPR to determine the orientation and rotational dynamics of crosslinked myosin when attached to oriented actin filaments. The results provide direct insight into the early steps of actomyosin force generation.

## 2.3 Methods

*Preparation of proteins and muscle fibers* - Cysteine mutations for spin labeling were introduced into a *Dicty* myosin II gene truncated at residue 762 (S1dC), containing only a single (non-reactive) cysteine at position 655 [84]. These proteins were expressed and purified from *Dicty* orf+ cells [84]. Glycerinated rabbit psoas muscle fiber strips were prepared and stored in a 1:1 (vol:vol) mixture of rigor buffer (120 mM KCl, 25 mM MOPS, 2 mM MgCl<sub>2</sub>, 1 mM EGTA, pH 7.0) and glycerol [66]. Actin used in these experiments was extracted from rabbit skeletal muscle acetone powder and purified as described previously [99]. F-actin in F-buffer (10 mM Tris, 2 mM MgCl<sub>2</sub>, pH 7.5) was stabilized with 1:1 molar equivalent phalloidin.

*Spin-labeling of S1dC* - S1dC was spin-labeled at sites 416 and 583 with the monofunctional label MSL [N-(1-Oxyl-2,2,6,6-tetramethyl-4-piperidiny) maleimide]

(Toronto Research Chemicals, North York, ON) overnight on ice using 20  $\mu$ M myosin and 100  $\mu$ M MSL in labeling buffer (30 mM Tris, 50 mM KCl, 3 mM MgCl<sub>2</sub>, pH 7.5). The unbound spin label was removed by desalting the labeled protein using two 7 kDa cutoff Zeba size-exclusion spin columns (Thermo Fisher Scientific Inc., Rockford, IL). The same S1dC mutant was labeled with BSL [3,4-bis-(methanethiosulfonyl-methyl)-2,2,5,5-tetramethyl-2,5-dihydro-1h-pyrrol-1-yloxy] (Toronto Research Chemicals, North York, ON). A BSL stock solution was prepared in dimethylformamide (DMF). Labeling was carried out at 20  $\mu$ M myosin and 100  $\mu$ M BSL in labeling buffer. The reaction was complete within 5 min, based on EPR observation of spin label immobilization. After 1 hour, unreacted BSL was removed as described above for monofunctional labeling.

*Determining Extent of Crosslinking by SDS-PAGE* - SDS-PAGE was used to separate BSL-crosslinked from uncrosslinked S1dC, based on gel migration rate. S1dC (1  $\mu$ M) in Laemmli sample buffer (Bio Rad, Hercules, CA), with or without 5%  $\beta$ -mercaptoethanol (Sigma-Aldrich, St. Louis, MO), was applied to a 15% Tris-glycine polyacrylamide gel and run at 150V for 4 hours. Crosslinked and non-crosslinked S1dC was quantified by densitometry using Image J [100].

*Myosin ATPase Activity* - Basal myosin ATPase activity was measured as the release of inorganic phosphate [101] at 25° C. High-salt calcium ATPase activity was measured in a solution containing 0.0125 mg/mL myosin, 10 mM CaCl<sub>2</sub>, 600 mM KCl, 5 mM ATP, and 50 mM MOPS (pH 7.5). Actin-activated ATPase activity was measured by detection of ADP generated by the NADH-coupled ATPase assay [102] using 0.5  $\mu$ M

S1dC, 2 mM ATP, and increasing concentrations of phalloidin-stabilized F-actin in 10 mM Tris, 2 mM MgCl<sub>2</sub> (pH 7.5).

*Actomyosin Binding Affinities* - The equilibrium binding of actin and myosin was measured by both cosedimentation and fluorescence quenching of pyrene-actin. In cosedimentation assays, varying concentrations of actin were mixed with 1 μM S1dC in F-buffer followed by centrifugation at 340,000 x g using a TLA100 rotor (Beckman Coulter) at 25° C, to pellet the actomyosin complex. Supernatant and pellet samples were each run on 12% Tris-glycine SDS-PAGE gels that were stained with Coomassie G (Sigma-Aldrich, St. Louis, MO); and band intensity was analyzed by densitometry using Image J [100]. The equilibrium constant for dissociation of S1dC from actin ( $K_d$ ) was determined by fitting with a quadratic binding function with maximal fraction bound constrained to 1. To further assess the weak or strong mode by which S1dC binds to actin, the quenching of pyrene-actin was measured [103]. Actin was labeled at Cys 374 with pyrene iodoacetamide (Invitrogen, Carlsbad, CA) [104], and fluorescence was measured for 1 μM pyrene-actin in F buffer, using a Varian Cary Eclipse fluorometer (Varian Inc., Palo Alto, CA) with excitation and emission at 350 nm and 407 nm, respectively. Quenching was assumed proportional to the fraction of actin protomers with strongly bound myosin [102].

*EPR spectroscopy* - EPR spectra were obtained at X-band (9.5 GHz) with a Bruker (Billerica, MA) E500 spectrometer, using a TE102 (Bruker 4102ST) cavity at a temperature of 4°C. The sweep width was 120 G (1024 points), sweep time was 40s, and the center field value  $H_C$  was set proportionally to the microwave frequency ( $H_C =$

v/2.803 MHz/G, corresponding to a  $g$  value of 2.0027, the value of  $g_z$  for a typical nitroxide) so that all spectra were equivalently aligned.

For EPR experiments on spin-labeled myosin in solution, samples were dialyzed into EPR buffer (10 mM Tris, 2 mM MgCl<sub>2</sub>, pH 7.5), adjusted to a final concentration of 100  $\mu$ M, and placed into a flame-sealed glass capillary (50  $\mu$ L Wiretrol, Drummond Scientific, Broomall, PA). For experiments on actin-bound myosin, skinned muscle fiber strips were dissected into bundles of approximately 0.5 mm diameter. The fibers were then soaked in the 100  $\mu$ M spin-labeled S1dC solution. After at least 2 h of soaking the fibers were washed several times with EPR buffer to remove any unbound S1dC.

Oriented EPR samples were prepared as previously described [46, 47]. S1dC-decorated muscle fiber bundles were blotted to remove excess buffer, cut into 0.5 cm lengths, and aligned perpendicular to the long axis of a quartz tissue flat cell; the fiber axis was manually oriented parallel or perpendicular to the external magnetic field. Spectra of randomly oriented fibers were obtained after mincing the fibers with a razor blade. Some spectra were also obtained with a fiber bundle in a capillary tube oriented either parallel or perpendicular to the magnetic field, using a peristaltic pump to perfuse the fiber such that the buffer was replaced every 30 s [46]. This was useful for removing traces of free spin label that was slowly released. Perfusion of a fiber bundle for one hour did not decrease the EPR signal by more than 5%, indicating that virtually all of the labeled myosin was bound to actin.

Conventional EPR spectra ( $V_I$ ) spectra were recorded at a microwave field amplitude of  $H_1 = 0.14$  G, with modulation frequency  $\nu_m = 100$  kHz (first harmonic),

peak-to-peak modulation amplitude  $H_m = 1$  G, and modulation phase  $\phi_m = 0$  degrees (maximum signal). The  $V_1$  spectrum of a randomly oriented sample was analyzed to determine the rotational correlation time using Eq. 1

$$\tau_R = a[1-(T_{\parallel}'/T_{\parallel})]^b, \quad \text{Eq. 1}$$

where  $a = 0.54$  ns,  $b = -1.36$ ,  $T_{\parallel}'$  is the splitting between the outer extrema, and  $T_{\parallel}$  is the rigid-limit value of  $T_{\parallel}'$  [105]. Spectra of spin-labeled S1dC attached to actin in oriented muscle fibers were analyzed to determine the orientational distribution of the nitroxide spin label relative to the muscle fiber axis, using computational simulation and least-squares minimization, as described previously [46, 106, 107]. STEPR ( $V_2'$ ) spectra were recorded as described previously [108], with  $H_1 = 0.25$  G,  $\nu_m = 50$  kHz,  $H_m = 5$  G, phase-sensitive detection at 100 kHz (second harmonic),  $\phi_m = 90$  degrees, and the filter time constant equal to twice the conversion time. The rotational correlation time was determined from  $V_2'$  spectra by comparison with reference spectra [109].

The extent of spin labeling was quantified by digital analysis of EPR spectra. The double integral of the  $V_1$  spectrum of 100  $\mu$ M S1dC was obtained at low power (1 mW) and compared to that of a sample of known spin label concentration, to obtain the number of spin labels per myosin. For labeling di-Cys myosin, we found precisely two ( $1.95 \pm 0.04$ ) monofunctional MSL labels and one ( $1.03 \pm 0.05$ ) bifunctional BSL label per myosin.



*Molecular Modeling* – Spin labels were modeled on crystal structure 1FMV using Discovery Studio 2.5.5 (Accelrys Software Inc., San Diego, USA) and visualized using the PyMOL Molecular Graphics System, Version 1.5.0.3 (Schrodinger, LLC).

## 2.4 Results

A bifunctional spin label (BSL), with two cysteine-reactive functional groups, was reacted with a double-Cys myosin mutant to form a crosslink containing two mixed (label-protein) disulfide bonds. The mutations S416C and D583C, across the actin-binding cleft from each other (FIGURE 8A), were introduced into a Cys-lite *Dicty* myosin II (S1dC) background suitable for site-directed spectroscopy, as described previously [84]. This approach is feasible because S1dC mutants can be expressed in milligram quantities [84], which is not true for muscle myosin. The EPR spectrum of BSL-S1dC was stable at 4° C for at least one day, but at 25° C, spin label immobilization was partially reversed (less than 5%) on the time scale of hours, presumably because of disulfide exchange to produce an intraprotein disulfide bond and free spin label [110]. The conventional EPR ( $V_1$ ) spectrum (FIGURE 8B) indicates that the label is strongly immobilized on the nanosecond time scale, i.e., that it is rigidly fixed to the protein, as expected for the bifunctional attachment of BSL [16, 46, 47, 111].

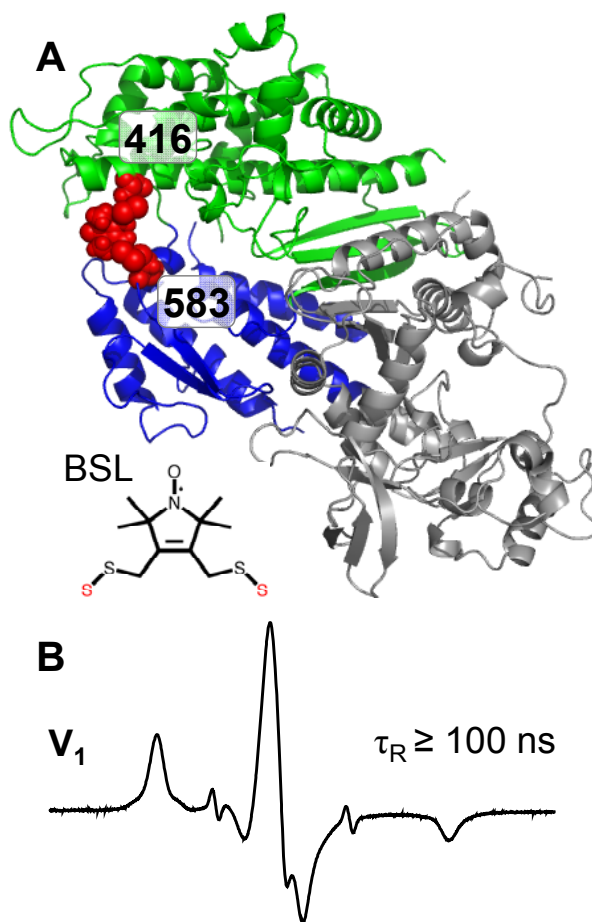


**FIGURE 8. Bifunctional spin labeling.** A, *Dicty* myosin II catalytic domain crosslinked by a bifunctional spin label (BSL), shown in red (space-filling), between engineered cysteine residues 416 and 583 in the U50 (green) and L50 (blue) domains of the actin-binding cleft. BSL was modeled on crystal structure 1FMV using Discovery Studio 2.5.5 and visualized using PyMOL. B, Conventional ( $V_1$ ) EPR spectrum of the labeled protein in solution.

Dipolar EPR measurements between MSL-labeled S416C and D583C (FIGURE 9A&B) were used to determine the distance between these two labeling sites in solution. Fitting the EPR spectrum to a Gaussian distribution shows that the myosin cleft samples two major conformations, in which residues 416 and 583 are separated by approximately 0.8 and 1.2 nm (FIGURE 9C) [84]. The distance between the two sulfur atoms in BSL is approximately 0.9 nm, establishing the feasibility of crosslinking cysteine residues 416 and 583 with BSL.

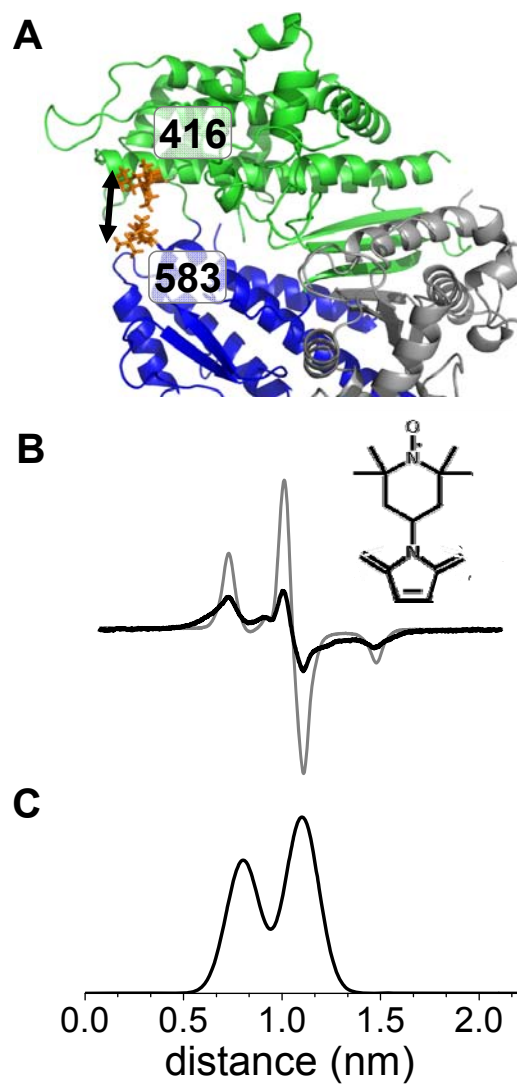


**FIGURE 9. Monofunctional spin labeling.** A, *Dicty* myosin II actin binding cleft with residues 416 and 583 labeled with MSL (highlighted with orange sticks) in the U50 (green) and L50 (blue) domains. MSL was modeled on crystal structure 1FMV as in FIGURE 8. B, Dipolar broadened CW EPR spectra of apo myosin spin-labeled with MSL at residues 416 and 583 (black) with a singly labeled MSL control using the mutant S416C (in gray). C, Distance distribution from fit of data in B.

*Extent of BSL-Crosslinking* - In addition to monitoring BSL immobilization by conventional EPR, the extent of myosin crosslinking by BSL was determined by separating the crosslinked and non-crosslinked myosins by SDS-PAGE under non-reducing conditions (FIGURE 10). The crosslinked myosin migrates more slowly

through a polyacrylamide gel so that the band is shifted to higher apparent molecular weight. When BSL is reacted with myosin at a molar ratio of 0.5 BSL per myosin, two bands are observed (FIGURE 10). The lower band (~88 kDa) represents non-crosslinked myosin, while the upper band (~100 kDa) represents crosslinked myosin. When a 5-fold molar excess of BSL is used, crosslinking is essentially complete, as shown by a single band at 100 kDa. No gel shift is observed for unlabeled or MSL-labeled myosin (FIGURE 10). Since the BSL-crosslink consists of two mixed protein-label disulfide bonds, it can be reversed by treatment with a reducing agent such as  $\beta$ -mercaptoethanol ( $\beta$ ME) or dithiothreitol (DTT). Inclusion of  $\beta$ ME in the gel sample results in reduction of the BSL-crosslink so that the sample migrates at the same rate as the unlabeled or MSL-labeled myosin (FIGURE 10).

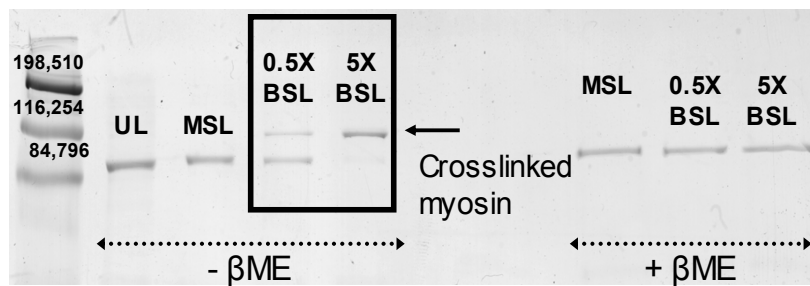


**FIGURE 10. SDS-PAGE gel shift assay** to determine extent of crosslinking of 416.583 S1dC by BSL under non-reducing ( $-\beta$ ME) and reducing ( $+\beta$ ME) conditions. UL: unlabeled. MSL: MSL spin-labeled, BSL: bifunctional spin-labeled, labeled with molar ratios of either 0.5 BSL per myosin (0.5X) or 5 BSL per myosin (5X).

*Myosin ATPase Activity* - In the absence of actin, the basal myosin ATPase activity ( $0.010 \pm 0.002 \text{ s}^{-1}$ ) was not affected by crosslinking ( $0.012 \pm 0.002 \text{ s}^{-1}$ ). However, crosslinking of the myosin cleft with BSL induces a virtually complete loss of actin-activated ATPase activity, in comparison with unlabeled or MSL-labeled myosin (FIGURE 11A&B). Consistent with SDS-PAGE gel-shift data (FIGURE 10), treatment

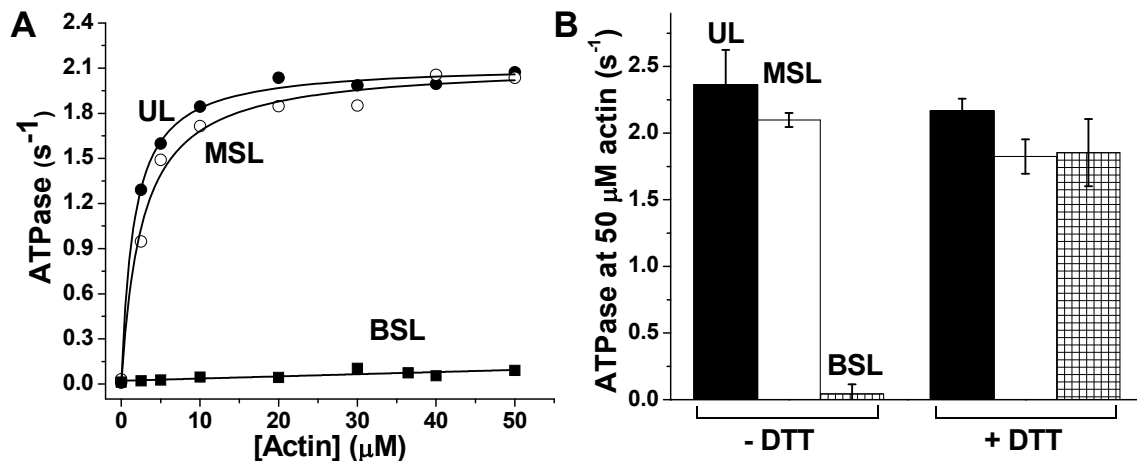


**FIGURE 11. Effects of spin labeling on ATPase activity.** A, actin-activated ATPase activity of 416.583 S1dC unlabeled (UL, ●), labeled with MSL (○), or crosslinked with BSL (■). Data for UL and MSL were fit by  $V = (V_{\max} - V_0) [\text{actin}] / ([\text{actin}] + K_{\text{ATPase}})$ , yielding the following  $V_{\max}$  and  $K_{\text{ATPase}}$  values, respectively: UL  $2.1 \pm 0.1 \text{ s}^{-1}$ ,  $1.6 \pm 0.1 \mu\text{M}$  and MSL-labeled ( $2.1 \pm 0.1 \text{ s}^{-1}$ ,  $2.7 \pm 0.4 \mu\text{M}$ ). These values of  $K_{\text{ATPase}}$  are lower than in some previous reports [112], because (a) ionic strength is lower in our study, and (b) we are using a Cys-lite construct of S1dC that has low  $K_{\text{ATPase}}$  values [84, 113]. BSL-labeled data were fit by a linear function, yielding a second-order rate constant ( $V_{\max}/K_{\text{ATPase}}$ ) of  $1400 \pm 400 \text{ M}^{-1}\text{s}^{-1}$ . The  $K_{\text{ATPase}}$  value must be  $> 10 \mu\text{M}$ . **B:** ATPase activity at  $50 \mu\text{M}$  actin in the absence or presence of 1 mM dithiothreitol (DTT). Data represents mean  $\pm$  S.E.,  $n=3$ .

of BSL-crosslinked myosin with a reducing agent reverses the functional effect of crosslinking, with no labeled myosin (FIGURE 11B).

*Actomyosin Interaction* - Cosedimentation of myosin with actin in the absence of nucleotide (i.e., in rigor) shows that unlabeled and MSL-labeled 416.583 S1dC bind actin strongly, with  $K_d$  values less than  $1 \mu\text{M}$ , but crosslinking the myosin cleft with BSL substantially weakens myosin's actin affinity, yielding a  $K_d$  value of about  $20 \mu\text{M}$  (FIGURE 12A). While this binding is much weaker than in rigor, it is still strong enough to obtain EPR spectra of the actin-bound complex. In EPR studies below, whenever we study EPR of BSL-S1dC in the presence of actin, the actin concentration is in large excess above the  $K_d$  value of  $20 \mu\text{M}$ , ensuring that virtually all BSL-S1dC is bound to

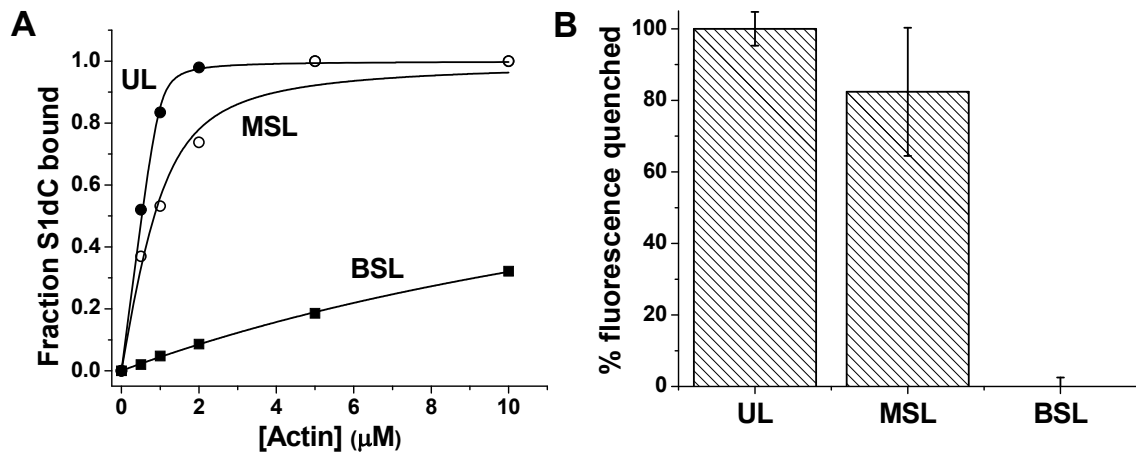


**FIGURE 12. BSL weakens interaction of myosin with actin in the absence of ATP.** A, fraction of myosin S1dC bound to actin from cosedimentation. Data were fit by the quadratic binding function  $y = \frac{([M]_t + [A]_t + K_d) - \sqrt{([M]_t + [A]_t + K_d)^2 - 4[M]_t[A]_t}}{2[A]_t}$  where  $M$ =[myosin] and  $A$ =[actin], yielding  $K_d$  values of  $0.03 \pm 0.01 \mu\text{M}$  (UL),  $0.4 \pm 0.1 \mu\text{M}$  (MSL), and  $20.6 \pm 0.2 \mu\text{M}$  (BSL). B, fluorescence quenching of  $1 \mu\text{M}$  pyrene-actin by  $20 \mu\text{M}$  S1dC. Data represents mean  $\pm$  S.E.,  $n=3$ .

actin. Strong binding of S1dC to actin was measured by fluorescence quenching of pyrene-labeled actin. Strong actin binding is known to quench pyrene fluorescence, whereas weak binding (e.g., in the presence of saturating ATP) has no effect [103]. Unlabeled and MSL-labeled myosin quenched the fluorescence, whereas BSL-crosslinked myosin had virtually no effect (FIGURE 12B), indicating that crosslinked myosin is unable to form a high-affinity (strongly bound) actomyosin complex. Unlabeled 416.583 S1dC quenched pyrene fluorescence to the same extent as rabbit skeletal S1.

*Myosin Rotational Dynamics and Orientation* – Conventional EPR ( $V_1$ ) is sensitive to rotational motion in the range from about 0.01 to 600 ns [16, 114]. The  $V_1$  spectrum of BSL-labeled S1dC in solution has the characteristic lineshape of a strongly immobilized spin label (FIGURE 13A, black), confirming its rigid bifunctional binding to two Cys. Actin binding, causes a small increase in label restriction (FIGURE 13A,

green), increasing the splitting between the outer peaks by  $0.90 \pm 0.05$  G. If, as indicated by further studies below (FIGURE 13B), we assume that actin-bound S1dC is at the rigid limit for conventional EPR (rotational correlation time  $\tau_R > 1$   $\mu$ s),  $\tau_R$  for BSL-S1dC free in solution is  $200 \pm 20$  ns (Eq. 1), corresponding to the expected value at 4° C for a rigid protein the size of S1dC [47, 115]. This result confirms that BSL is rigidly bound to S1dC, but it does not provide much information about the rotational dynamics of BSL-S1dC on actin.

This requires saturation transfer EPR (STEPR,  $V_2'$ ), which is sensitive to rotational correlation times  $\tau_R$  as long as 600  $\mu$ s [16, 114, 116]. Thus STEPR is ideal for measuring global rotational motions of large proteins within macromolecular assemblies, such as actomyosin [16, 114]. Unlike conventional EPR (FIGURE 13A), STEPR is extremely sensitive to the affect of actin binding on the rotational dynamics of BSL-S1dC (FIGURE 13B). Rotational motion of BSL-S1dC on actin is at or near the rigid limit of 600  $\mu$ s for STEPR (FIGURE 13B, green), at least 6000 times slower than S1dC free in solution (FIGURE 13B, black), indicating that any remaining rotational motion is in the millisecond range or slower. The rotational motion of actin-bound BSL-S1dC is at least 60 times slower than previously observed for MSL-S1dC weakly attached to actin in the presence of saturating ATP [117-120] and is virtually identical to that observed for strongly bound MSL-S1dC in rigor [106].

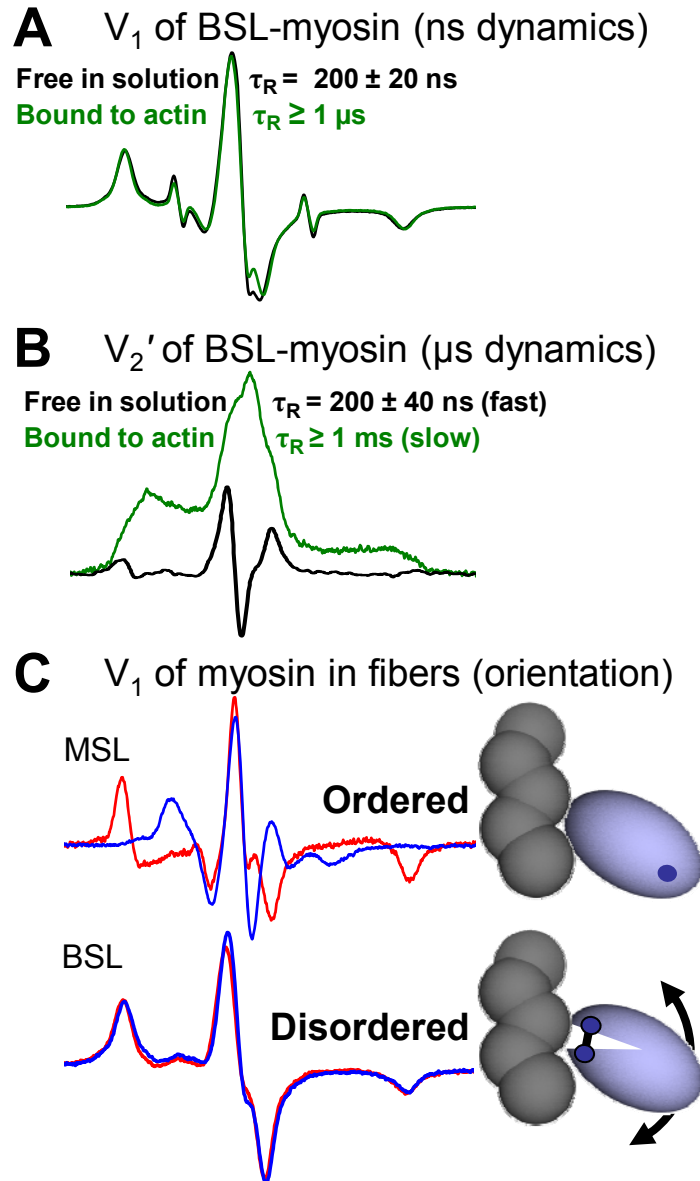


**FIGURE 13. EPR spectra of BSL-S1dC.** A, conventional ( $V_1$ ) EPR spectra (at 4°C) for myosin BSL-crosslinked at positions 416 and 583, free in solution (black) and bound to excess actin in randomly oriented muscle fibers (green). Spectral lineshapes are at or near the rigid limit, indicating strong immobilization of the spin labels on myosin. B, STEPR ( $V_2'$ ) spectra of the same samples as in A, showing that the rotational motion of actin-bound BSL-S1 is at least 5000 times slower than when free in solution [108]. C, conventional ( $V_1$ ) EPR of spin-labeled S1dC on oriented actin in skinned muscle fibers, with the fiber axis oriented parallel (blue) or perpendicular (red) to the applied magnetic field. MSL-myosin (at T688C) is highly ordered orientationally (red and blue spectra quite different) while BSL-labeled myosin is highly disordered (red and blue spectra almost identical, implying at least 90° of angular disorder).



EPR is not only sensitive to spin-label mobility but also to the orientational distribution of a spin-label with respect to the applied magnetic field. In a well-oriented muscle fiber, aligned either parallel or perpendicular to the magnetic field, the EPR spectrum directly reports the angle between the spin-label's principal axis and the fiber axis [106]. The parallel and perpendicular spectra can be used together to determine the degree of orientation of the spin-label relative to the fiber axis. The orientation of BSL- or MSL-labeled myosin bound to actin, with respect to the actin filament axis, was determined from EPR spectra of skinned muscle fibers in the presence of labeled myosin (FIGURE 13C). As shown previously, myosin spin-labeled with MSL at SH1 (T688C) is highly ordered with respect to the filament axis as indicated by the large differences observed between EPR spectra acquired in the parallel and perpendicular orientations (FIGURE 13C, MSL) [121]. In contrast, fibers decorated with BSL-S1dC yield EPR spectra showing little difference between the parallel and perpendicular orientations, indicating nearly random orientation (FIGURE 13B).

The relatively static disorder of myosin on actin, due to the cleft crosslink is in good agreement with that observed for myosin trapped by crosslinking SH1 and SH2 in the force-generating domain of myosin obtained from muscle [46, 47] or *Dicty* [122]. Virtually all of the BSL-myosin in skinned fiber bundles in Fig. 6 must be bound to actin, because the STEPR spectrum is at or near the rigid limit of STEPR, indicating a rotational correlation time  $\tau_R \geq 1$  ms, which is at least 5000 times slower than free myosin in solution [16]. In addition, it is not plausible that the orientational disorder is due to a significant population of unbound myosin, since the  $K_d$  of the cleft-crosslinked

S1dC is 20.6  $\mu\text{M}$  (FIGURE 12), which is at least 18 times less than the concentration of unoccupied actin in a vertebrate muscle fiber [123].

## 2.5 Discussion

We have found that the actin-myosin interaction is impacted profoundly, both functionally and structurally, by conformationally restricting the myosin actin-binding cleft through chemical crosslinking with a bifunctional spin label (BSL). The crosslink forms rapidly and completely between a pair of labeling sites, 416 and 583, in the U50 and L50 domains of the actin-binding cleft. The ATPase activity of isolated myosin is not affected by this crosslink, but actin cannot activate it (FIGURE 11), and myosin's affinity for actin in the absence of ATP is decreased by >20-fold (FIGURE 12B). Even when it binds to actin, this crosslinked myosin loses its ability to quench pyrene-actin fluorescence (FIGURE 12A), consistent with the formation of a weak actomyosin bond. Structurally, crosslinking the cleft induces an actin-bound myosin catalytic domain with a high degree of orientational disorder but very slow rotational motion on the microsecond time scale (FIGURE 13). The disorder is similar to that reported previously for weakly bound heads induced by ATP, but the rotational motion is orders of magnitude slower, similar to that of strongly bound heads in rigor. These results are virtually identical to those obtained with myosin crosslinked between SH1 and SH2 in the force-generating domain [46, 47], indicating that a similar intermediate was trapped. FIGURE 14 illustrates these results in the context of the actomyosin ATPase cycle.

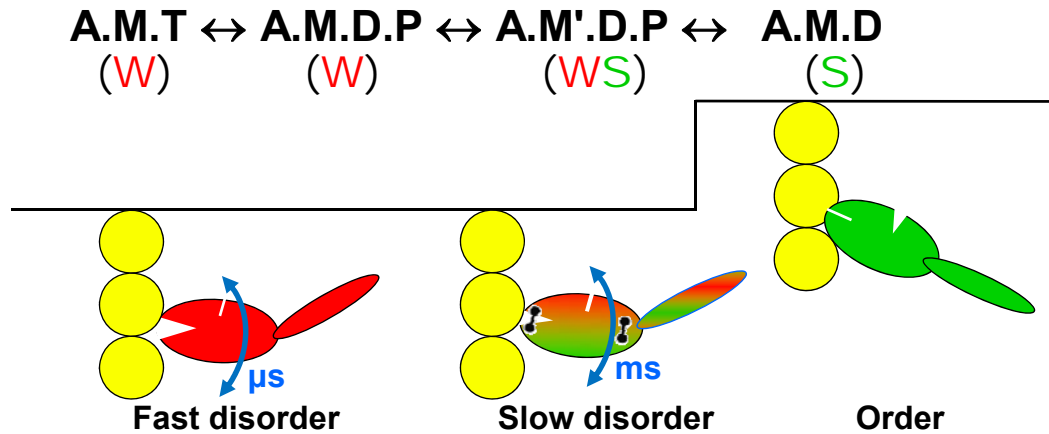


**FIGURE 14. Model for the coupling of the actomyosin ATPase cycle to force and movement.** The actin-binding cleft of myosin transitions from an open structural state having a dynamically ( $\mu s$ ) disordered catalytic domain when weakly bound (W, left) to a closed state having an immobile and ordered CD (S, right). Force production is initiated when the CD enters a short-lived intermediate state (WS, middle) with intermediate affinity (FIGURE 12) and much slower ( $ms$ ) orientational disorder (FIGURE 13). The black linkers shown in the WS state represent two crosslinking sites, across the actin-binding cleft or between SH1 and SH2 in the force-generating domain [46, 47]. Each of these crosslinks traps the elusive intermediate and inhibits the actin-activated ATPase activity.

*Effects of Cleft Crosslinking on Actomyosin Functional Interaction* - During the actomyosin ATPase cycle, myosin transitions from a dynamically disordered, weak actin-binding state (W, FIGURE 14, left) to an ordered, strong actin-binding state (S, FIGURE 14, right). This transition from W to S also involves a shift in the populations of the actin-binding cleft structural states (“open” versus “closed”), with S stabilizing the closed conformation. Extensive experimental analysis has sought to define the biochemical and structural properties of W and S states of the actomyosin complex. The W state appears to be stabilized by hydrophobic interactions between loop 2 of the L50 domain of myosin and actin [32, 94, 124, 125].  $K_d$  for actomyosin weak binding using the *Dicty* myosin II motor domain has been previously reported as  $\sim 60 \mu M$  [126]. In contrast, strong binding

is characterized by  $K_d < 1 \mu\text{M}$ , stabilized by predominantly electrostatic interactions with the U50 domain [24-26, 32, 125]. Generally, mutations within both the weak- and strong-binding interfaces decrease myosin's affinity for actin and reduce actin-activated ATPase activity. Crosslinking the cleft produces an intermediate  $K_d$  of  $20 \mu\text{M}$  (FIGURE 12A), and complete loss of actin-activated myosin ATPase activity. Since 416.583 BSL-labeled S1dC interacts with actin but its ATPase activity is not activated by actin, we hypothesize that the crosslink stabilizes a conformation of the actin-binding interface that can interact with actin at weak-binding contacts while still containing bound  $P_i$ . Together these results indicate that crosslinked myosin is trapped in a weak actin-binding state and suggest that BSL crosslinking the actin-binding cleft severely diminishes the coupling between the actomyosin interface and the myosin active site. Structurally, the trapped state is probably characterized by a partially open actin-binding cleft that preferentially stabilizes a weak-binding interface and a closed nucleotide pocket, preventing  $P_i$  release (FIGURE 14). We have previously shown that the actin-binding cleft exists in a conformational equilibrium between "open" and "closed" structural states in all biochemical states tested, with strong actin binding preferentially stabilizing the closed cleft conformation [84]. We have now demonstrated directly the necessity of conformational flexibility within the actin-binding cleft, allowing the myosin cleft to properly transition between "open" and "closed" structural states, which is essential for actin-activation and transition to the strong actomyosin binding state. Consistent with our data, recent cryo EM data suggests that intrinsic flexibility of the U50 domain is necessary for myosin to properly transition to the strong binding conformation [32]. In addition, simulations of the U50 domain from

various crystal structures reveals that U50 flexibility is dependent on biochemical state and is proposed to underlie myosin's ability to rapidly adopt its strong binding state [33].

*Effects of Cleft Crosslinking on Actomyosin Structural Dynamics* – As illustrated in (FIGURE 14), cleft crosslinking creates an actomyosin complex with hybrid structural and dynamical properties: The orientational disorder of the actin-bound head is great (FIGURE 13C, BSL) - comparable to that induced in the absence of crosslinking by ATP [106, 107, 127-129] and in sharp contrast to the high degree of orientational order observed in the absence of ATP for uncrosslinked myosin bound to actin (FIGURE 13C, MSL) [47, 106, 127, 130]. In contrast, the rotational motion of the crosslinked catalytic domain is very slow, undetectable on the submillisecond time scale (FIGURE 13B, BSL) – comparable to that observed in the absence of ATP for uncrosslinked myosin bound to actin [47, 106, 115, 131], and several orders of magnitude slower than the microsecond dynamics induced by ATP [117-120, 131, 132].

*Comparison with Effects of other Internally Crosslinked Myosins* - Although this is the first study to crosslink the actin-binding cleft of myosin, there have been numerous studies in which a crosslink was introduced between reactive cysteines SH1 and SH2 in the force-generating region of the catalytic domain of myosin, from rabbit skeletal muscle [44-47] or *Dicty* myosin II [122]. In all cases, the SH1-SH2 crosslink greatly reduced actin activation and actomyosin affinity, indicating that myosin was trapped in a weak-binding conformation. In one of these studies, rabbit skeletal myosin II was crosslinked with BSL at SH1 and SH2, yielding a  $K_d$  for actomyosin interaction of 30  $\mu\text{M}$  [47]; similar to the 20  $\mu\text{M}$  value observed here for cleft crosslinking by BSL in *Dicty* myosin II. Crosslinking SH1 and SH2 with BSL produced an actin-bound myosin

catalytic domain with a high degree of orientational disorder and very slow rotational motion ( $\tau_R \geq 1$  ms) [46, 47], just as we found in the present study with a crosslink in the cleft (FIGURE 13). It is remarkable that conformational trapping of myosin at two distant locations, one in the actin-binding cleft and another in the force-generating region, have strikingly similar effects on actomyosin structure, dynamics, affinity, and function. This result strongly suggests that crosslinking the actin-binding cleft, like crosslinking SH1 and SH2, can trap myosin in an intermediate state between weak binding and rigor; i.e., early in force generation (FIGURE 14). In the absence of crosslinking, this state is probably stabilized by ATP hydrolysis products (ADP + P<sub>i</sub>) within the nucleotide binding pocket and shares the orientational disorder characteristic of ATP-induced weak binding, but the slow rotational motion of strong binding (FIGURE 14) [47].

*Allosteric Coupling* - The similar effects of crosslinking the actin-binding cleft and SH1-SH2 region of the force-generating domain demonstrate that intrinsic conformational flexibility within the myosin catalytic domain and structural coupling between functionally important subdomains are required for force generation. Continued analysis of the intricate structural and biochemical coupling between myosin subdomains, in space and time, is needed to understand the mechanism of force transduction in actomyosin. Specifically, how tightly coupled is the communication pathway from the actin interface to the nucleotide pocket or to the force-generating domain? There is evidence for coupling between the actin-binding cleft and nucleotide pocket [133-135], as well as between the nucleotide pocket and the force-generating domain [136, 137]. Recent work suggests that there is direct coupling between the actin-binding interface, particularly the myosin activation loop, and the relay helix in the myosin force-generating

domain [138]. We must next ask how conformationally trapping the actin-binding cleft affects the nucleotide-binding pocket structural dynamics, and the orientation of the myosin lever arm.

## **2.6 Conclusion**

We produced a chemically modified *Dicty* myosin II catalytic domain, in which the actin-binding cleft is conformationally trapped by crosslinking the U50 and L50 domains with a bifunctional methanethiosulfonate spin label: Crosslinking produces a myosin catalytic domain that cannot be activated by actin and has weakened actin affinity. When bound to actin in an oriented muscle fiber, this protein is highly disordered with respect to the actin filament axis, and is characterized by very slow rotational motion on the microsecond time scale. Cleft-crosslinked myosin has greater binding affinity and slower motion on actin than that observed for ATP-induced weak-binding states. Thus it resembles the weak-binding state induced by crosslinking reactive cysteines SH1 to SH2 in the force-generating domain, which is proposed to be the structural state that is at the threshold of force generation.

## Chapter 3: Structural and Functional Impact of Site-Directed Methionine Oxidation in Myosin

Reprinted with permission from:

Jennifer C. Klein, Rebecca J. Moen, Evan A. Smith, Margaret A. Titus, and David D. Thomas. Structural and functional impact of site-directed methionine oxidation in myosin. *Biochemistry*. 2011;50(47):10318-10327.

**Copyright © 2011 American Chemical Society**

Contributions of Authors:

Jennifer C. Klein: Designed and performed mutagenesis for myosin mutants. Designed all experiments. Performed ATPase assays and mass spectrometry shown in figures 16 and 17. Performed and analyzed EPR experiments shown in figures 20, 21, and 22. Made figures 15, 18, 20, 21, 22, and 23 and wrote the manuscript.

Rebecca J. Moen: Assisted with experiment design. Performed ATPase assays and mass spectrometry shown in figures 16 and 17 and circular dichroism and thermal denaturation experiments shown in figure 19 and associated data analysis. Made figures 16, 17, and 19. Edited other figures and wrote the manuscript.

Evan A. Smith: Designed and performed mutagenesis for myosin mutants. Expressed and purified myosin mutants. Edited the manuscript.

Margaret A. Titus: Assisted with experiment design. Edited the manuscript.

David. D. Thomas: Designed all experiments. Edited the figures and manuscript.



### 3.1 Chapter Summary

We have examined the structural and functional effects of site-directed methionine oxidation in *Dictyostelium* (*Dicty*) myosin II using mutagenesis, *in vitro* oxidation, and site-directed spin-labeling for electron paramagnetic resonance (EPR). Protein oxidation by reactive oxygen and nitrogen species is critical for normal cellular function, but oxidative stress has been implicated in disease progression and biological aging. Our goal is to bridge understanding of protein oxidation and muscle dysfunction with molecular-level insights into actomyosin interaction. In order to focus on methionine oxidation and to facilitate site-directed spectroscopy, we started with a Cys-lite version of *Dicty* myosin II. For *Dicty* myosin containing native methionines, peroxide-treatment decreased actin-activated myosin ATPase activity, consistent with the decline in actomyosin function previously observed in biologically aged or peroxide-treated muscle. Methionine-to-leucine mutations, used to protect specific sites from oxidation, identified a single methionine that is functionally sensitive to oxidation: M394, near the myosin cardiomyopathy loop in the actin-binding interface. Previously characterized myosin labeling sites for spectroscopy in the force-producing region and actin-binding cleft were examined; spin label mobility and distance measurements in the actin-binding cleft were sensitive to oxidation, but particularly in the presence of actin. Overall secondary structure and thermal stability were unaffected by oxidation. We conclude that the oxidation-induced structural change in myosin includes a redistribution of existing structural states of the actin-binding cleft. These results will be applicable to the many biological and therapeutic contexts in which a detailed understanding of protein oxidation, function and structure relationships are sought.

## 3.2 Introduction

We cannot survive more than minutes without oxygen—nor have we escaped vulnerability to oxidative stress, the natural consequence of aerobic respiration. Disease progression and biological aging are familiar contexts in which the role of “oxidative damage” -- to DNA, lipids, and proteins -- has been recognized, even popularized through the promotion of antioxidant supplements for longevity and disease resistance. Under healthy conditions, too, molecules within cells must sensitively detect and respond to cellular redox state to maintain homeostasis. While irreversible oxidative modifications are potentially damaging, they might also serve as signals for protein repair, degradation and transcriptional regulation [139, 140]. Reversible protein modifications, particularly those involving cysteine and methionine, have been implicated as protein sensors of the cellular environment [60, 141-143]. Yet critical questions remain unanswered: What are the molecular structural principles that govern *how* protein molecules sense, respond, and are eventually damaged by oxidation? Are these principles broadly applicable?

*Redox modulation of muscle function* - Muscle contraction produces reactive oxygen and nitrogen species (RONS) that are countered by an elaborate system of antioxidant enzymes and molecules [63]. Muscle is highly adaptive tissue that must dynamically respond to metabolic, mechanical and functional demands such as exercise, hormonal fluctuations and development; redox signaling mediates many of these adaptations [144]. Disruption of the RONS/antioxidant equilibrium in cardiac muscle contributes to adverse outcomes after myocardial infarction [145] and in models of heart failure [146]. In skeletal muscle, the physiological function of oxidation is complex and

biphasic, with lower levels of RONS potentiating function and higher levels inhibiting [59, 147, 148]. However, elevated production of RONS can lead to the accumulation of oxidatively modified proteins, contributing to a decline of function in biologically aged or diseased muscle [58, 59, 149, 150]. Impaired force with aging is due not only to muscle atrophy, but also to structural and functional defects involving both contractile and regulatory proteins [57, 58, 65, 151]. Knowing the site-specific functional and structural impact of oxidative modifications will aid in developing targeted therapies for oxidative stress-related muscle pathologies.

*Methionine oxidation* - Knowledge of the site and the chemistry of oxidative modifications to proteins, in combination with functional measurements, reveals that amino acid sequences encode not only protein structure and function, but also sensitivity to chemical modification [152]. While cysteine oxidation and reduction is a well-established component of cell signaling, methionine oxidation and specific reduction by methionine sulfoxide reductase is emerging as a novel regulatory mechanism with diverse and far-reaching functional implications [68, 139, 141, 142, 152]. For example, where methionine is part of a hydrophobic kinase recognition sequence, methionine oxidation can prevent phosphorylation by disrupting the kinase binding site, coupling oxidative environment and phosphorylation [153]. Methionine oxidation regulates immune response by attenuating calcineurin function in signal transduction pathways [154, 155]. Methionine and cysteine redox sensors have been identified for proteins involved in calcium regulation [74-81], but few such sensors have been characterized for contractile proteins [63]. In the current study, we have begun to elucidate the principles

that govern how the muscle contractile protein myosin is structurally poised to respond to methionine oxidation.

*Muscle myosin oxidation* - We have previously shown that treating skinned muscle fibers with peroxide ( $H_2O_2$ ) resulted in functional and structural changes in myosin with a pattern similar to changes for myosin extracted from aged rats [55, 58, 66]. Myosin purified from oxidized muscle fibers perturbs structural transitions within the actomyosin complex that are crucial for force generation. Proteomics analysis revealed that myosin functional and structural changes are associated with oxidation of multiple methionine residues in the myosin catalytic domain and essential light chain [66]. It is not clear which methionines, one or many, are responsible for the observed functional and structural changes in skeletal myosin. In the present study, we have directly tested the hypothesis that site-specific methionine oxidation causes functional decline in actomyosin interaction and have identified aspects of myosin internal dynamics and structure that are most sensitive to oxidation.

*Approach* - In order to characterize the functional and structural impact of site-specific methionine oxidation in myosin, we have used Met to Leu mutagenesis to control which myosin methionines are susceptible to oxidation within a Cys-lite *Dictyostelium* (*Dicty*) myosin II (S1dC) background suitable for site-directed spectroscopy. Our approach is possible because S1dC mutants can be expressed in milligram quantities; this is not feasible for skeletal muscle S1. A direct comparison of structural transitions at equivalent sites in the force-generating region of S1dC and skeletal S1 showed that these motors occupy identical structural states, but with altered coupling to biochemical state [90]. Thus S1dC serves as a malleable platform for understanding the chemical and

structural principles that determine how a myosin motor responds to oxidation at selected residues. Our goal was not to mimic physiological conditions of oxidation, but rather to achieve significant functional perturbation while obtaining complete oxidation of the remaining accessible methionines and thus obtaining a chemically well-defined and homogeneous preparation. We varied the concentration of hydrogen peroxide to achieve this goal in a brief (30-min) treatment of purified myosin. We then examined the impact of methionine oxidation on (a) functional sensitivity of myosin ATPase and actin-activated ATPase and (b) structural changes in myosin, measured by site-directed spin labeling and electron paramagnetic resonance (EPR), focusing on sites previously shown to be highly sensitive to key structural transitions in the actomyosin ATPase cycle [84].

### 3.3 Methods

*Protein Preparations, Spin-Labeling and Oxidation* - Cysteine mutations for spin labeling and methionine substitution mutations were introduced into a *Dicty* myosin II gene truncated at residue 762 (S1dC), containing only a single (non-reactive) cysteine at position 655 [84]. Mutations were C49T, C312S, C442S, C470V, C599T, and C678S. These proteins were expressed and purified from *Dictyostelium* orf<sup>+</sup> cells. Spin labeling was carried out overnight on ice using 100  $\mu$ M myosin and 800  $\mu$ M IPSL [3-(2-Iodoacetamido)-2,2,5,5-tetramethyl-1-pyrrolidinyloxy] (Toronto Research Chemicals, North York, Ontario), IASL [4-(2-Iodoacetamido)-2,2,6,6-tetramethyl-1-piperidinyloxy] (Sigma-Aldrich, USA), or MSL [N-(1-Oxyl-2,2,6,6-tetramethyl-4-piperidinyloxy)maleimide] (Toronto Research Chemicals). Spin-labeled sample was reacted with 0 to 500 mM

hydrogen peroxide (purchased as a stabilized 30% solution from Sigma-Aldrich) for thirty minutes on ice. Unreacted label and peroxide were removed by buffer exchange using two sequential Zeba desalting columns (Thermo Fisher Scientific, Rockford, Illinois). Unless otherwise indicated, experiments were carried out at 4°C in EPR buffer (50 mM KCl, 3 mM MgCl<sub>2</sub>, and 10 mM MOPS, pH 7.5). F-actin was prepared from rabbit skeletal muscle [104, 156] and dissolved in F-actin (FA) buffer: 3 mM MgCl<sub>2</sub>, 0.2 mM ATP and 10 mM Tris (pH 7.5).

*Activity Measurements* - ATPase activity was measured as the release of inorganic phosphate [101, 157] at 25° C. High-salt Ca/K ATPase activity was measured in a solution containing 0.0125 mg/mL myosin, 10 mM CaCl<sub>2</sub>, 600 mM KCl, 5 mM ATP, and 50 mM MOPS (pH 7.5). Actin-activated ATPase activity was measured as the increase in activity due to the addition of rabbit skeletal actin (usually 10 μM) to a solution containing 1 μM myosin, 3.5 mM MgCl<sub>2</sub>, 10 mM KCl, and 10 mM MOPS (pH 7.5).

*ESI (electrospray ionization) mass spectrometry (ESI-MS)* - Myosin samples for mass spectrometry were exchanged into 10 mM NH<sub>4</sub>HCO<sub>3</sub> (pH 7.9) using two sequential 0.5 mL Zeba desalting columns. Myosin samples at 2 mg/mL were diluted 1:10 into a solution containing 50:50 acetonitrile:water and 0.1% formic acid. Additional formic acid (10%) was added as needed (1-2 μL) to reach pH < 3. Myosin mass was determined using a QSTAR quadrupole-TOF mass spectrometer (ABI) with an electrospray ionization source. Prior to infusion of the intact myosin solution, a solution of 50:50 acetonitrile:water and 0.1% formic acid (load solution) was infused at 50 μL per minute using an integrated syringe pump. After a stable baseline total ion current (TIC) was established for the load solution, the protein solution (20 μM myosin, pH 3) was

introduced into the solvent stream using a 10  $\mu$ L injection loop installed in the integrated loop injector. After the TIC returned to baseline intensity, four more consecutive loop injections of the protein solution were made for a total of five injections per sample. Data were acquired continuously during load buffer infusion and protein infusions over the range 500 – 2000  $m/z$ . ESI spectra were analyzed with BioAnalyst QS (ABI) software v 1.1.5. The Bayesian Protein Reconstruction tool was used to generate peak lists from the spectra, using a signal-to-noise threshold of 20 for intact myosin. Individual reconstruction error ranged from 0.1 – 0.5 Da.

*Circular Dichroism* - CD spectra were recorded in the far-UV region (200–260 nm) using a JASCO J-815 spectrophotometer with an automated temperature controller. A path length of 10 mm was used, with spectra recorded at 1 nm intervals for 0.25 mg/mL *Dicty* myosin in phosphate buffer (50 mM KCl, 1 mM MgCl<sub>2</sub>, pH 7.0) at 25°C. Baseline scans were obtained using the same acquisition parameters with buffer alone, which were subtracted from the respective CD data scans of *Dicty* myosin. The raw CD signal  $\theta_\lambda$  (millidegrees of ellipticity) was converted to mean residue molar ellipticity  $\theta$  using Eq. 2:

$$\theta = \frac{MRE \times \theta_\lambda}{10 \times C \times \ell} \quad \text{Eq. 2}$$

where MRE = 110, C = protein concentration, and  $\ell$  = path length. Far-UV CD spectra were analyzed using CDPro Analysis Software [158]. Thermal denaturation of *Dicty* myosin was monitored at 222 nm while temperature was increased from 10 to 70°C in

1°C steps, with a 1 min incubation at each step. At the end of each thermal denaturation experiment, the sample was rapidly cooled to 25°C to determine the extent of refolding. Thermal denaturation curves were fit using Origin 8.1 (OriginLab Corp, Northampton, MA).

*CW EPR (Continuous wave EPR): Mobility* - EPR on spin-labeled *Dicty* myosin was carried out as described previously [84]. EPR samples contained 100  $\mu\text{M}$  *Dicty* myosin in EPR buffer. The ADP.V state was formed by addition of 5 mM ADP, followed by 5 mM  $\text{Na}_3\text{VO}_4$ . The actomyosin state was formed by addition of 200  $\mu\text{M}$  F-actin. EPR was performed on deoxygenated samples at 4°C using a Bruker E500 spectrometer (Billerica, MA) at X-band (9.5 GHz), with modulation frequency 100 kHz and modulation amplitude 2 G. Mobility was measured in gas-permeable Teflon tubes (0.6 mm I.D., 20  $\mu\text{L}$  sample volume) sealed with critoseal, placed into the quartz temperature control dewar inside an SHQ cavity (ER4122 ST). Scan width was 120 G and the microwave power of 2 mW produced approximately 40% saturation, with no significant line broadening. Plotted spectra (FIGURE 20, FIGURE 22) were normalized to the double integral. Order parameters were measured from EPR spectra by simulation and fitting with the software NLSL (Nonlinear Least-Squares Analysis of Slow-Motional EPR Spectra) [159-161]. Spectra were simulated for a two-component system, each with its own cone angle ( $\theta_c$ ), correlation time ( $\tau_r$ ) and mole fraction ( $x_i$ ).

*Pulsed EPR: Spin-Spin Distance Measurements* - EPR samples for spin-spin distance measurements were the same as in other EPR experiments (described above), except that the buffer also contained 10% glycerol (v/v), and the 100  $\mu\text{L}$  samples were



flash-frozen using liquid nitrogen in a 5 mm OD quartz NMR tube (Wilmad glass, Buena NJ) and stored at  $-80^{\circ}\text{C}$  until use. Pulsed EPR experiments were performed with a Bruker E580 spectrometer (Billerica, MA) at X-band (9.5 GHz) with a Bruker dielectric ring resonator (MD-5) using a 4-pulse DEER (double electron-electron resonance) protocol [162]. The  $\pi/2$  pulse width was 16 ns, and the ELDOR pulse width was 40-44 ns. The static field was set to the low-field resonance of the nitroxide signal. Temperature was controlled at  $65^{\circ}\text{K}$  during acquisition, which lasted 4–12 h.

Spin-spin distances were determined by fitting the experimental EPR data with simulations assuming a distance distribution function consisting of a sum of Gaussians using Eq. 3 and Eq. 4:

$$\rho(r) = \sum_{i=1}^n x_i g_i(r) \quad \text{Eq. 3}$$

$$g_i(r) = A \frac{1}{\sigma_i \sqrt{2\pi}} e^{-\frac{(r-r_i)^2}{2\sigma_i^2}} \quad \text{Eq. 4}$$

The  $3n-1$  variable parameters in the fit were  $x_i$  (mole fraction),  $r_i$  (center distance), and  $\sigma_i$  (standard deviation), where the full width at half maximum is given by  $w_i = 2\sigma_i \sqrt{\ln 2}$ . The number of components  $n$  in the best fit was defined as the one for which  $n + 1$  produced no further improvement, as defined by the residual plot and the residual sum of squares. The distribution function (Eq. 4) was convoluted with the Pake pattern [163] to simulate the weighted sum of the dipolar broadening function over the distance distribution [164], and this was used to simulate the EPR data, essentially as

described previously for CW EPR [165, 166] and for DEER [167]. CW EPR spectra were fitted using a Monte Carlo search procedure with laboratory-developed software (WACY, Edmund Howard). DEER background correction, distance determination by Tikhonov regularization, and fits based on Gaussian distance distributions were performed using methods provided in the software DEERAnalysis2006.1 [167]. Distances extracted by Tikhonov regularization were consistent with fits based on Gaussian distance distributions. We report the results based on Gaussian distance distributions because they are more useful for discussing models based on discrete conformational states that are common to different biochemical states.

### 3.4 Results

*Methionines in Dictyostelium (Dicty) myosin II subfragment 1 (S1)* - A version of *Dicty* myosin II truncated to contain only the myosin motor domain and devoid of reactive cysteines (“S1dC Cys-lite”[84]) was used as a model system to examine the functional and structural consequences of myosin methionine oxidation. Using *Dicty* myosin as such a model is justified by its high level of structural and functional homology with muscle myosin catalytic domain [168, 169]. *Dicty* myosin contains nine methionines, four of which are strictly conserved among class II myosins: Met 91 in the 25 kDa domain, Met 166 on a loop behind the nucleotide binding pocket, Met 486 at the bend in the relay helix, and Met 642 in the lower 50 kDa domain (FIGURE 15A). Met 394, located at the C-terminus of an  $\alpha$ -helix that transitions into the cardiomyopathy loop in the actin-binding interface, is Cys in cardiac and skeletal myosin and Leu in smooth

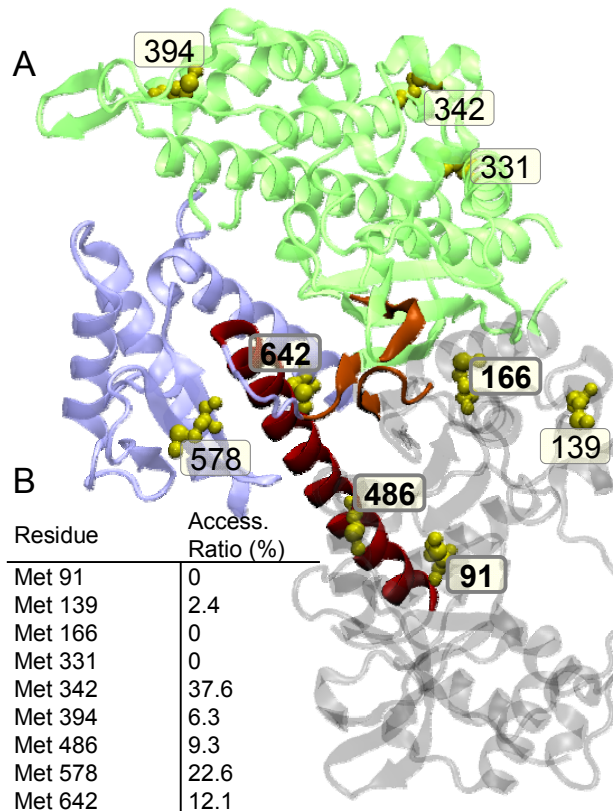


**FIGURE 15. Location of native methionines in *Dictyostelium* myosin II (1FMV).** A, Lower 50 kDa domain (blue); upper 50 kDa domain (green), relay helix (red); nucleotide binding pocket (orange); methionines (yellow spheres). Conserved Met residues are shown **bold**. B, Accessible surface area calculated from the crystal structure 1FMV and reported as a ratio of accessible side-chain surface area to the value calculated for a random coil [170]. VMD (Visual Molecular Dynamics) was used to create renderings of molecular structures [171].

muscle myosin. Met 91, Met 166 and Met 331 are expected to be mostly inaccessible to solvent based on the crystal structure shown in FIGURE 15.

*Functional sensitivity of Dicty myosin II to global methionine oxidation* - The physical properties and biochemical activity of *Dicty* myosin II containing all native methionines and a single spin-labeled (therefore, non-reactive) cysteine were characterized as a function of oxidation by hydrogen peroxide (used as an oxidative agent). Our goal was to produce a sample in which there is substantial functional

perturbation and the accessible methionines were oxidized completely in a brief (30 min) peroxide treatment, producing a homogeneous sample for functional and structural analysis. In an initial series of experiments, the concentration of hydrogen peroxide was varied to achieve this goal as evaluated by mass spectrometry (FIGURE 16, FIGURE 17). It is clear from these data that peroxide concentration on the order of 500 mM is optimal. The change in myosin molecular weight upon treatment of wild-type myosin with 500 mM hydrogen peroxide is 46 Da, equivalent to the addition of 2.9 oxygens (FIGURE 16A), suggesting that at least three methionines are susceptible to oxidation. The mass spectrum for peroxide-treated *Dicty* myosin II is substantially broadened relative to the untreated myosin, indicating the presence of multiple unresolved oxidized states. Treatment with hydrogen peroxide induces a substantial decrease in both the maximum  $Mg^{2+}$  actin-activated ATPase rate in the presence of saturating actin ( $V_{max}$ ) and the actin concentration required for half-maximal activation ( $K_{ATPase}$ ) (FIGURE 16B), consistent with the decline in actomyosin function observed previously for biologically aged or peroxide-treated skeletal myosin [58, 66]. The  $Mg^{2+}$  ATPase activity decreases exponentially with increasing peroxide concentration and is more pronounced in the presence of 10  $\mu M$  F-actin than under basal conditions (0  $\mu M$  F-actin) (FIGURE 16C), indicating that actomyosin interaction is altered with oxidation. High salt  $Ca^{2+}/K^{+}$  myosin ATPase, a non-physiological measure of myosin ATP hydrolysis rate in the absence of actin, also decreases exponentially with increasing peroxide concentration (FIGURE 16D).

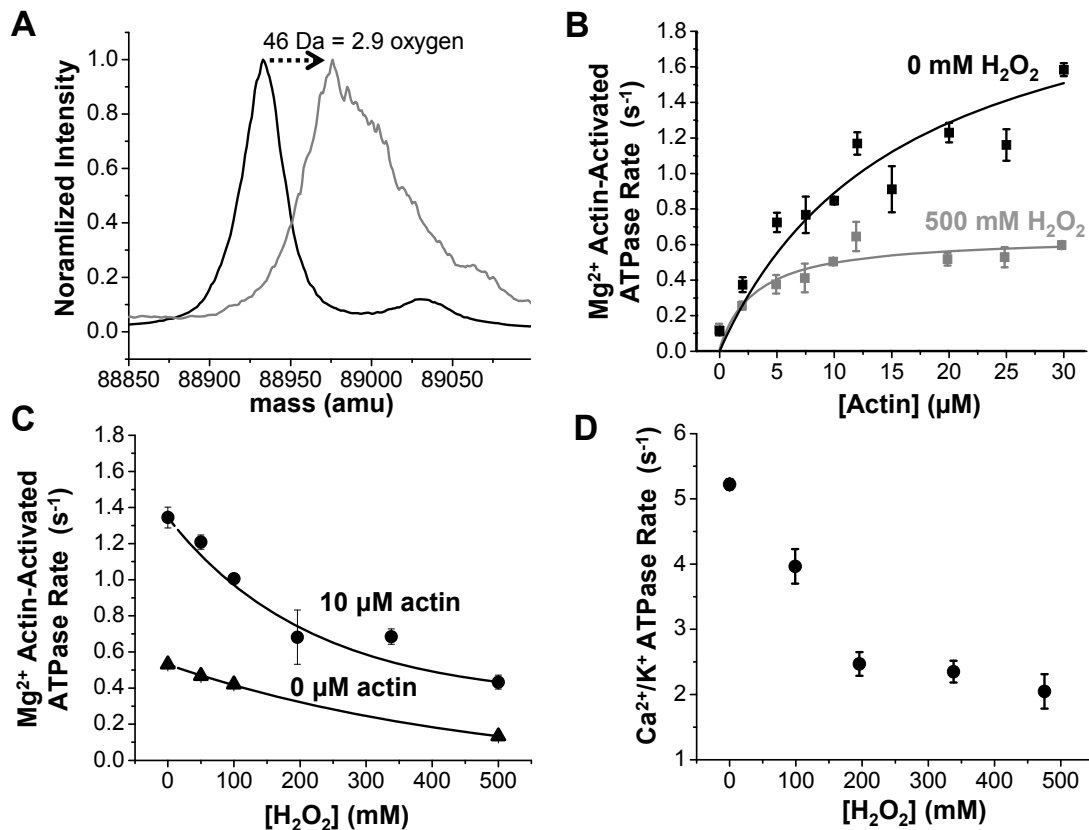


**FIGURE 16. Functional Sensitivity of *Dicty* myosin II to global methionine oxidation.** A, ESI-MS of intact *Dicty* myosin. Deconvoluted mass spectra (normalized to maximum intensity) for 0 mM (black) and 500 mM (gray) peroxide. Peak full width at half maximum is 30 Da for 0 mM and 67 Da for 500 mM. B, Functional assays for the same samples. For 0 mM peroxide,  $V_{\max} = 2.3 \pm 0.5$  and  $K_{\text{ATPase}} = 16 \pm 7$ . For 500 mM peroxide,  $V_{\max} = 0.65 \pm 0.04$  and  $K_{\text{ATPase}} = 3.0 \pm 0.8$ . C, Peroxide dependence of actin-activated ATPase activity in the presence of 10 μM actin (●) and no actin (▲). D, High salt myosin ATPase activity.

*Functional sensitivity of Dicty myosin II to site-specific methionine oxidation* - In order to determine the consequences of methionine oxidation site-specifically, we made methionine substitutions in a *Dicty* myosin II construct devoid of native reactive cysteines. All constructs used for functional measurements contained the T688C mutation in order to introduce a cysteine labeling site for spectroscopy experiments; spin-labeling was carried out prior to peroxide treatment under conditions that assured

complete labeling. Leucine was used to substitute for methionine at sites we desired to protect from oxidation (mutants are described in FIGURE 17C). Leucine is typically considered the most conservative substitute for methionine, and has been shown to produce substantially less structural perturbation than methionine oxidation [76, 172]. Of the M to L mutants tested, only L6 had slightly compromised actin-activated ATPase activity before oxidation (FIGURE 17A). Attempts to express mutants with M to L mutations at 486 and 642 were unsuccessful, possibly because these mutations produce myosins that are unstable or interfere with *Dictyostelium* function.

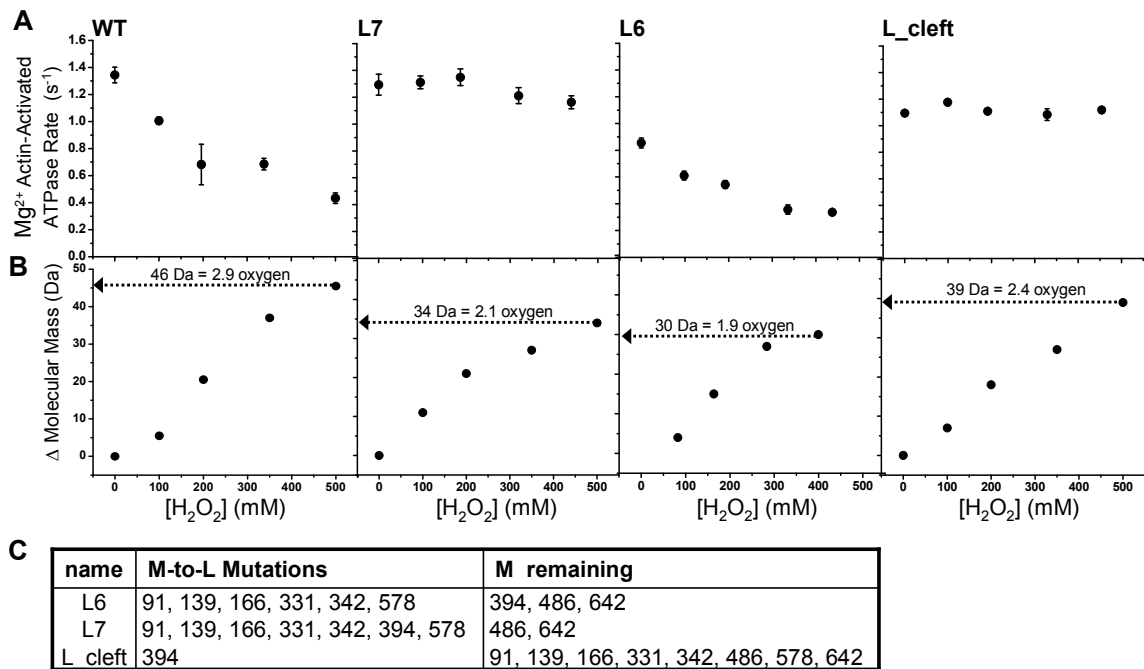


**FIGURE 17. Functional sensitivity of *Dicty* myosin II to site-specific methionine oxidation.** A, ESI-MS of intact *Dicty* myosin. Change in mass with increasing peroxide concentration is reported with respect to the unoxidized, spin-labeled sample. B, Mg<sup>2+</sup> actin-activated myosin ATPase for 10 μM F-actin for wildtype (WT) myosin (T688C spin-labeled) and M-to-L mutants. C. M-to-L mutants are as listed.

Substituting leucine for methionine at all positions except M468 and M642 (L7) protects myosin from the functional decline induced by peroxide-treatment (FIGURE 17 L7). This suggests neither of these two conserved methionines M486, nor M642, are responsible for oxidation-induced functional decline in myosin. In fact, when M394 is re-introduced (L6), functional sensitivity to oxidation is restored (FIGURE 17 L6), indicating that M394 is a functionally sensitive target of oxidation. It is quite surprising that none of the conserved myosin methionines (M91, M166, M486, M642) were *functionally* sensitive to oxidation. Of the non-conserved methionines, M394 was a strong candidate for the site of oxidatively sensitive function because of its proximity to the cardiomyopathy loop in the actin-binding interface. The M394L point mutation is sufficient to rescue the oxidation-induced functional decline in myosin (FIGURE 17 L\_Cleft).

The decline in myosin actin-activation parallels an increase in myosin molecular weight (FIGURE 17). The mass spectrum of unoxidized myosin appears as a broad peak with full width at half maximum equal to 30 Da (FIGURE 16A), consistent with width predicted for the isotopic envelope of a 89 K protein [173]. Full resolution of singly oxidized states is not possible because of the intrinsic peak broadening due to myosin's isotopic envelope. For 500 mM peroxide, myosin containing native Met, the peak maximum increases 46 Da, indicating that, on average, each myosin has an additional 2.9 oxygens (peak width), suggesting at least three of myosin's nine methionines are susceptible to oxidation, but possibly more. The shift in mass is slightly less when leucine replaced methionine at 394 (L\_Cleft); each myosin has an additional 2.4 oxygens after full oxidation, indicating that M394 is at least partially susceptible to oxidation. The

mass of L7 shifts 34 Da, suggesting that the two remaining methionines (M486 and M642) are both highly susceptible to oxidation. The mass of L6 shifts, on average, 30 Da indicating that on average only two of the three methionines present (M394, M486 and M642) are oxidized. The increase in average mass should therefore be interpreted with the understanding that peroxide-treatment results in a distribution of oxidized states. We cannot rule out the possibility that some methionines are oxidized before they are treated, nor can we rule out the unlikely possibility of oxidation of residues other than methionines.

*Structural consequences of methionine oxidation in Dicty myosin II* - Circular dichroism (CD) spectroscopy and site-directed spin labeling in combination with electron paramagnetic resonance (EPR) were used to examine myosin's structural sensitivity to

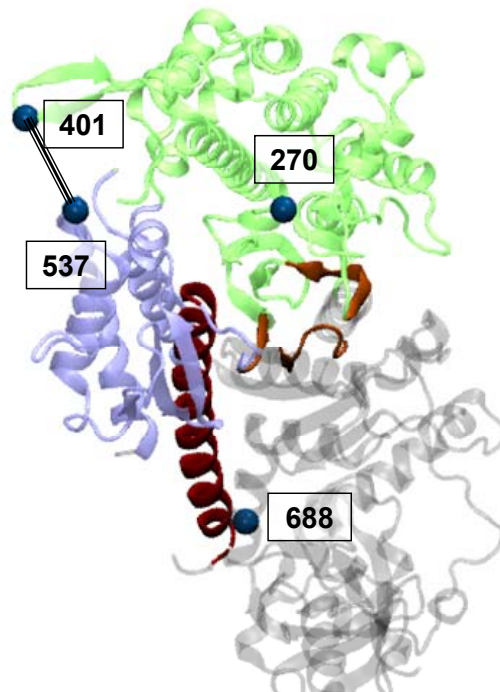


**FIGURE 18. Location of *Dicty* myosin II spin-labeling sites.** Myosin domains colored as in FIGURE 15.



methionine oxidation. Global effects on myosin secondary structure and structural stability were examined using far-UV CD and thermal denaturation. EPR experiments focused on regions that undergo conformational changes related to myosin ATPase activity and actomyosin interaction using previously characterized labeling sites in the actin-binding interface, actin-binding cleft and force-generating region of myosin (FIGURE 18) [84, 90].

*Secondary structure and thermal stability of native and oxidatively modified Dicty myosin II* - CD spectroscopy was used to assess changes in myosin secondary structure as a result of oxidative modification. No spectral differences were detected in the far-UV

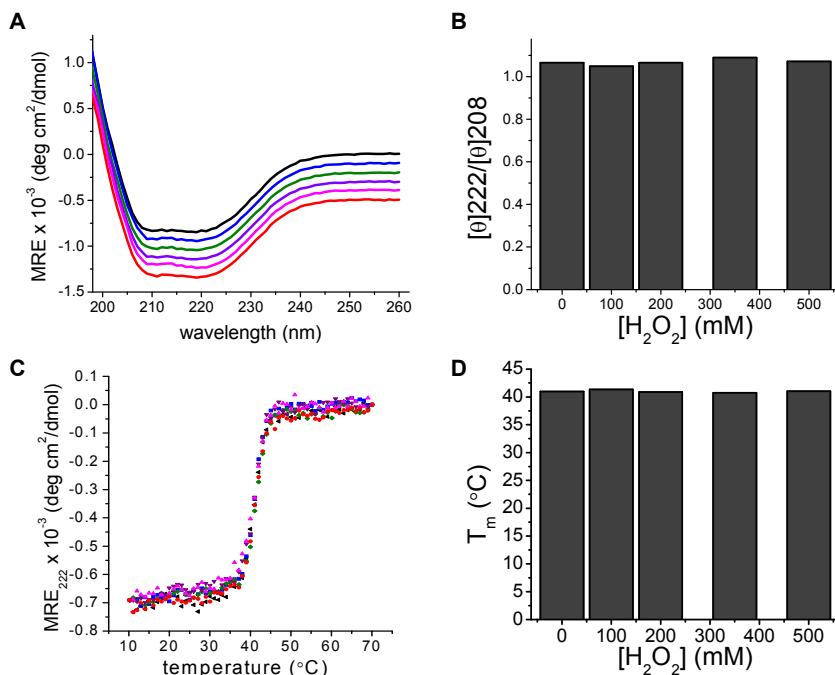


**FIGURE 19. CD spectroscopy and thermal denaturation of peroxide-treated *Dicty* myosin containing native Met.** A, Far UV spectra of myosin with no spin-label (black) and treatment with 0 (blue), 100 (green), 200 (purple), 350 (magenta), and 500 (red) mM  $\text{H}_2\text{O}_2$ , respectively. B, Ratio of molar ellipticity at 222 nm and 208 nm as a function of  $[\text{H}_2\text{O}_2]$ . C, Thermal denaturation curves of myosin. Samples same as part A. D, Transition midpoints derived from thermal denaturation curves as a function of  $[\text{H}_2\text{O}_2]$ .

range (200-260 nm) at any peroxide concentration, suggesting that oxidation does not affect the relative amounts of  $\alpha$  helix,  $\beta$  sheet, and random coil (FIGURE 19A). Thermal denaturation was monitored at 222 nm by CD spectroscopy. All myosins exhibited similar transition midpoints ( $T_m$ ) of  $\sim 41^\circ\text{C}$  (FIGURE 19D), consistent with reported values for myosin motor domains [174]. All samples exhibited highly cooperative unfolding, demonstrated by the sharpness of the unfolding transition, indicating that each myosin forms a well-folded structure (FIGURE 19C).

*Oxidation-induced changes in myosin's actin-binding cleft* - Labeling sites within the myosin actin-binding cleft and the actomyosin interface were used to probe the structural dynamics of myosin alone and in complex with actin. F270C is located in the corner of the actin binding cleft, near switch I of the nucleotide binding site (FIGURE 18). When F270C is labeled with maleimide spin label (MSL), the spin label motion, characterized by a rotational correlation time and cone angle of allowed motion, is sensitive to actin-binding. In the apo and strongly actin-bound biochemical states, two motional components whose relative populations shift in response to actin binding are resolved (FIGURE 20). Global fitting of spectra reveals that the faster component (FIGURE 20, innermost arrow) moves isotropically with a rotational correlation time of  $3.7 \times 10^{-9} \text{ s}^{-1}$ . The slower component (FIGURE 20, outermost arrow) has a rotational correlation time of  $7.9 \times 10^{-9} \text{ s}^{-1}$  and is restricted to a cone angle of  $40^\circ$ . In the apo state, the faster component dominates the spectrum with a mole fraction ( $x_{\text{fast}}$ ) equal to 0.9 and when myosin is strongly bound to actin, the slow component dominates ( $x_{\text{fast}} = 0.4$ ). Oxidation with 500 mM peroxide shifts the equilibrium toward the slower component for

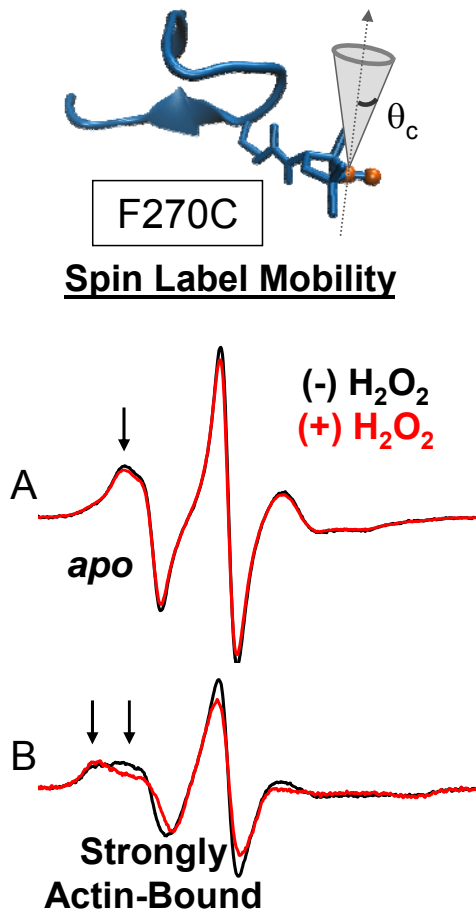


**FIGURE 20. Effect of oxidation on structural dynamics of actin-binding cleft.** CW EPR spectra for MSL-F270C in the apo (A) and strongly actin-bound (B) states.

both the actomyosin complex ( $x_{\text{fast}} = 0.2$ ) and to a lesser extent, for apo myosin ( $x_{\text{fast}} = 0.8$ ).

Distances across the actin-binding cleft from N537C on the lower 50 kDa domain to G401C in the upper 50 kDa domain were measured by double electron-electron resonance (DEER) after spin labeling both sites with IPSL spin label. DEER is a pulsed EPR technique well-suited for measuring distances in the 2-6 nm range [167]. N537C and G401C are located within the actomyosin interface (FIGURE 18) and are sensitive to conformational changes in the actin-binding cleft at key points in force generation.

Notably, the actin-binding cleft populates two distinct conformations when strongly bound to actin, the shorter distance corresponding to an ‘open’ cleft and longer distance corresponding to a ‘closed’ cleft [84].

While the effects of methionine oxidation are subtle in the apo DEER decay, they are pronounced in the decay for the strongly actin-bound complex (FIGURE 21). By visual inspection, the decay for the oxidized actomyosin sample (red) is initially more rapid than for the unoxidized sample (black) (FIGURE 21A); this indicates a shift toward

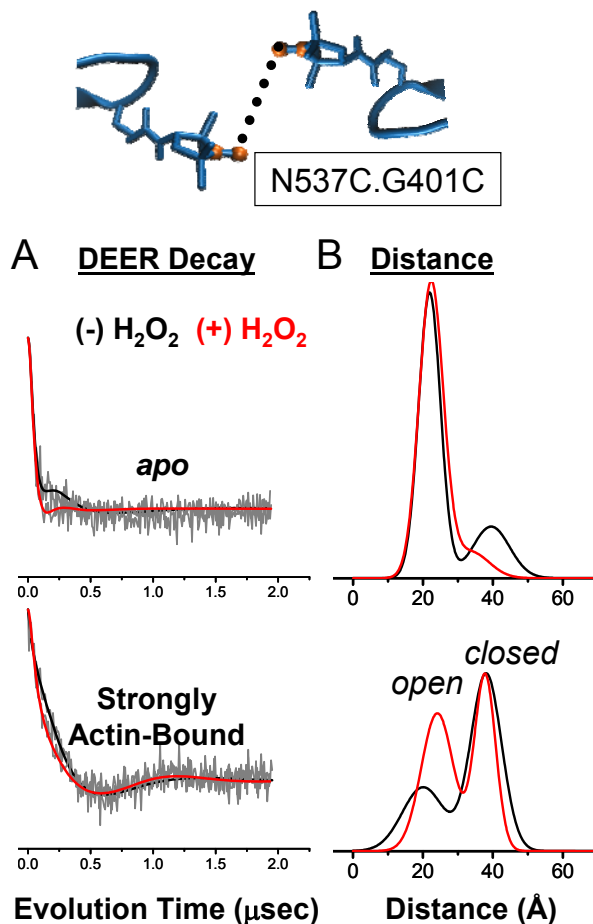


**FIGURE 21. Effect of oxidation on structural dynamics of actin-binding cleft near the actomyosin interface. DEER decay (A) and distance and distribution (B) for spin labels at G401C and N537C in the apo and strongly actin-bound states.**

**TABLE 1** Summary of DEER-derived distance distributions for IPSL-537 and 401.

DEER Sample	$x_1$	$r_1$	$w_1$	$x_2$	$r_2$	$w_2$
537/401 apo, (-) H <sub>2</sub> O <sub>2</sub>	0.781	2.13	1.72	0.219	4.02	2.03
537/401 apo, (+)H <sub>2</sub> O <sub>2</sub>	0.815	2.20	1.20	0.186	2.96	2.30
537/401 actin-bound, (-)H <sub>2</sub> O <sub>2</sub>	0.396	1.84	2.01	0.604	3.81	1.21
537/401 actin-bound, (+)H <sub>2</sub> O <sub>2</sub>	0.545	2.34	1.58	0.455	3.77	1.04
Simulated spectra were fit to experimental spectra as described in Experimental Procedures. Fitting parameters for i=1, 2, or 3 Gaussian distance distributions are defined as follows: $r_i$ is the center distance in nm, $w_i$ is the full width half-maximum in nm, and $x_i$ is the mole fraction. Uncertainties were estimated from SD of repeated experiments (n = 3-5). For distances 1.6 to 3.0 nm, fractional uncertainties in r and w were approximately 12%.						

shorter distances. The resulting distance distributions show how oxidation enhanced the stability of the conformation that corresponds to the shorter distance from 40% to 55% (TABLE 1). The DEER decay for the oxidized sample had slightly more distinct oscillations, indicating more narrow distance distributions. Oxidation restricted small scale conformational sampling in both the open and closed cleft conformations, and significantly stabilized the open cleft conformation.

*No oxidation-induced changes in myosin dynamics in the force-generating region*

- Spin label mobility was measured at the T688C site in the myosin SH1 helix, a well-characterized labeling site that is sensitive to nucleotide binding and hydrolysis [90]. Oxidation does not alter spin label mobility for any biochemical states tested, including the strongly actin-bound state (FIGURE 22).

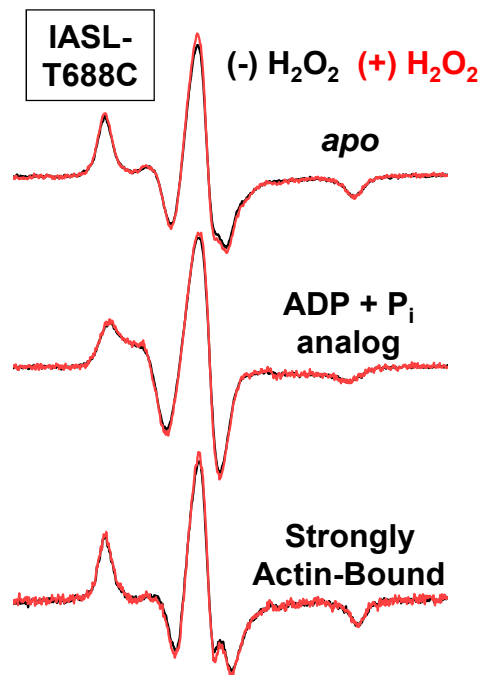


**FIGURE 22. Effect of oxidation on structural dynamics of SH1 helix.** CW-EPR spectra for peroxide treated (500 mM, red) and untreated (black) *Dicty* myosin II spin-labeled with IASL at positions T688C (SH1 helix).

### 3.5 Discussion

*Functional consequences of methionine oxidation in myosin* - Oxidation of *Dicty* myosin containing all nine native methionines is associated with a decrease in myosin ATPase, and a decline in actomyosin interaction (FIGURE 16B, C, D). At least three of myosin's nine methionines are susceptible to oxidation under the conditions tested (FIGURE 16A). Methionine to leucine substitutions, in combination with oxidation, made it possible to determine which sites are functionally sensitive to oxidation. Leucine substitutions, even at seven of the nine myosin methionines, caused only slight functional

change in myosin, a result consistent with what other groups have reported for Leu to Met substitutions [76]. We identified at least three myosin methionines that are at least partially susceptible to oxidation by peroxide: M486, M642 and M394. The M394L point mutation is sufficient to prevent oxidation-induced functional decline in myosin ATPase activity and actomyosin interaction (FIGURE 17).

Prochniewicz et al. found that peroxide treatment of permeabilized muscle fibers is associated with myosin methionine oxidation and a decline in actomyosin interaction [66]. We find that M394 in *Dicty* myosin II, equivalent to C402 in skeletal myosin, is most functionally sensitive to oxidation. Cysteine oxidation was not detected in myosin purified from peroxide-treated muscle fibers, but was detected in myosin purified from aged rats [55, 58, 66]. At least 9 of 22 methionines in the skeletal myosin catalytic domain are susceptible to oxidation (4 of these 9 methionines are oxidized *before* peroxide treatment). Of the three oxidizable methionines in S1dC (M394, M486 and M642), only M486 corresponds to an oxidizable Met in skeletal myosin (M496). M486 is located at the bend in the relay helix, a major path of communication between the nucleotide-binding site and the force-generating domain. Although we did not detect oxidation-induced structural changes at the nearby SH1 helix, a detailed examination of relay helix dynamics structural is warranted.

Skeletal myosin contains nearly double the number of methionines as *Dicty* myosin S1, so it is likely that some of the peroxide-induced loss of function in skeletal myosin [66] is due to methionines that are not present in S1dC. A next step might include introducing novel methionines into *Dicty* myosin at locations equivalent to

skeletal myosin to determine the functional and structural impact of methionines that are unique to skeletal myosin.

Cysteine 400 in cardiac myosin, equivalent to M394 in *Dicty* myosin, is one of at least two cysteines in the myosin heavy chain susceptible to glutathionylation and associated with a decline in myosin ATPase [56]. Glutathionylation is a reversible oxidative modification that could act to modulate actomyosin function during episodes of oxidative stress [175, 176]. During episodes of oxidative stress, when the ratio of oxidized glutathione (glutathione disulfide) to glutathione is high, susceptible Cys are likely to be glutathionylated, while normal cellular conditions promote reduced Cys. It is reasonable to suggest that M394 in *Dicty* myosin II and C400 in cardiac myosin have evolved as redox sensors that act to modulate actomyosin interaction in response to oxidative stress. It remains unknown whether oxidation at M394 is reversible by methionine sulfoxide reductase, as reversibility would strengthen the argument that M394 is a redox sensor.

*Structural consequences of methionine oxidation in myosin* - Overall myosin secondary structure and thermal stability were unaffected by oxidation (FIGURE 19). Changes in myosin structural dynamics due to oxidation were examined for two major locations: the actin-binding cleft and the force-generating region (FIGURE 18). Spectroscopic methods and spin-labeling sites sensitive to key conformational changes have been previously established for these regions [84, 90]. IASL spin label mobility at T688C in the SH1 helix in the force-generating domain was insensitive to oxidation in every biochemical state tested, including when actin was present (FIGURE 22). It is surprising that no sensitivity toward oxidation is observed for the nearby SH1 helix since



we have shown that M486, situated in the bend of the relay helix, is susceptible to oxidation. It remains to be known whether relay helix dynamics are sensitive to oxidation. For the actin-binding cleft, myosin structural dynamics was sensitive to oxidation, but mainly in the presence of actin. Both spin label mobility inside the cleft and distances measured across the cleft in the actin-binding interface resolved two distinct components that probably correspond to two different structural states (FIGURE 20, FIGURE 21). Oxidation shifted the equilibrium between states, indicating that the functional effects of oxidation are due not to the stabilization of a new structural state of myosin, but through a change in the distribution of existing structural states.

M394 is located in the actin-binding interface, so it is reasonable to expect that oxidation to methionine sulfoxide at this location is responsible for the changes observed in cleft structural dynamics observed in the presence of actin. M394 is the last residue of an  $\alpha$ -helix bordering the cardiomyopathy loop (FIGURE 23). Although methionine is well-suited for helical structure, methionine sulfoxide can destabilize helices [141]. We hypothesize that oxidation of M394 destabilizes the end of the helix, effectively lengthening the cardiomyopathy loop, altering the interaction of the upper 50 kDa domain with actin, and therefore changing the distribution of cleft structural states in the presence of actin. It is likely that it is this change in actomyosin structural dynamics that underlies the functional decline in actomyosin interaction observed with peroxide treatment.

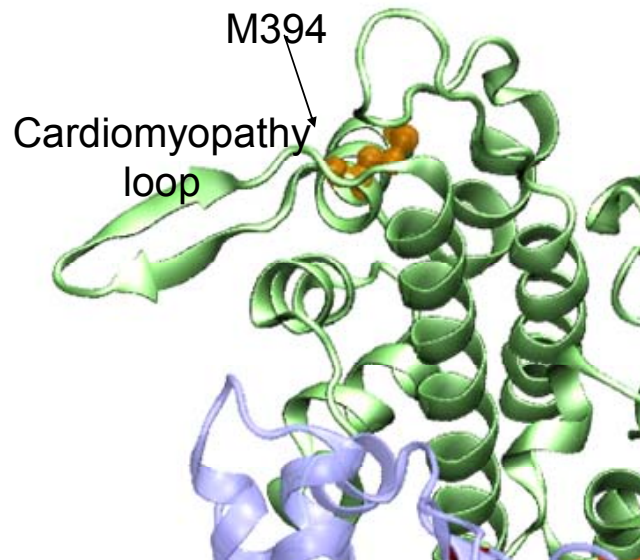


**FIGURE 23: Location of M394 (orange) near the cardiomyopathy loop in the myosin actin-binding interface.**

### 3.6 Conclusion

Site-directed mutagenesis was used to control Met and Cys susceptibility to oxidation by peroxide in order to determine the functional and structural impact of site-specific Met oxidation in myosin. At least three Mets, including two conserved (M486 and M642) and one nonconserved (M394), are susceptible to oxidation. Oxidation is associated with a steep decline in myosin ATPase and actin-activation; the M394L mutation fully blocks this functional sensitivity. Structural dynamics in the actin-binding cleft, both near the nucleotide pocket and in the actomyosin interface, are sensitive to oxidation in the presence of actin. The overall oxidation-induced structural impact includes reduced sampling of conformational space and a large redistribution of existing structural states of the actin-binding cleft. While this work on *Dicty* myosin does not

provide direct insight into oxidative modifications in muscle, it contributes broadly to our understanding of how myosin senses and responds to oxidative stress. Knowledge of the functional and structural impact of site-specific methionine oxidation will be an important factor in the development of targeted therapies for degenerative muscle diseases.

## Chapter 4: Redox Sensitive residues in the Myosin II Actin-Binding Interface

### 4.1 Chapter Summary

We have examined the reversibility of oxidative modification in *Dictyostelium discoideum* (*Dicty*) myosin II. Regulation by oxidation-reduction reactions, termed redox regulation, has emerged as a crucial modulator of protein function. We have previously identified a single methionine residue in *Dicty* myosin II that is sensitive to oxidation and affects function, M394, near the myosin cardiomyopathy loop in the actin-binding interface [113]. We now show that oxidation of this Met is reversible by the antioxidant enzyme methionine sulfoxide reductase (Msr), restoring actin-activated ATPase activity and actomyosin interaction. Sequence alignment reveals that M394 of *Dicty* myosin II is a cysteine residue in all human isoforms of skeletal and cardiac myosin. Using *Dicty* myosin II as a model for site-specific redox sensitivity of this Cys residue, the M394C mutant can be oxidatively modified *in vitro*. Glutathionylation at this site causes a decrease in actin-activated ATPase activity and actin-binding affinity, similar to the effects observed for methionine oxidation in *Dicty* myosin suggesting a defect in the weak-to-strong transition of the actomyosin complex crucial for force production. This work illustrates the ability of myosin to function as a muscle redox sensor, potentially modulating contractile activity through a redox dependent mechanism in response to oxidative stress.

## 4.2 Introduction

Under healthy conditions molecules within cells must sensitively detect and respond to cellular redox state to maintain homeostasis. Reactive oxygen species (ROS) are a family of oxygen-derived molecules that are highly reactive causing protein or DNA damage or activating signal transduction pathways that are essential in disease initiation or progression [78]. Many physiological and pathological conditions are associated with the accumulation of ROS. ROS are countered by an elaborate system of antioxidant enzymes and molecules [63]. An imbalance in the amount of ROS and combating antioxidants is generally termed oxidative stress. The most sensitive and selective targets of ROS and antioxidants in the cell are the sulfur containing amino acids, methionine (Met) and cysteine (Cys).

The rapid rate of sulfur oxidation in combination with its reversibility makes Met and Cys ideal candidates for functional redox-switches in proteins. Met residues are susceptible redox targets of signaling ROS. An oxidized methionine, methionine sulfoxide (MetO), can be reduced to Met by the thioredoxin-dependent enzyme methionine sulfoxide reductase (Msr). The other main redox target of ROS are cysteine thiols in proteins, the oxidation of which may result in reversible intra- or intermolecular disulfide formation or other thiol modifications. One such modification is glutathionylation, which can covalently modify a Cys by attachment of a glutathione (GSH) tripeptide. During episodes of oxidative stress, when the ratio of oxidized glutathione (glutathione disulfide) to glutathione is high, susceptible Cys are glutathionylated.

Several proteins have been identified that use sulfhydryl-based redox switches to control their activity, with either potentiation or inhibition of function. Oxidation of a specific Met residue in the regulatory domain of Calmodulin kinase II (CaMKII) directly activates its activity, even in the absence of its normal activators [77]. Filamentous actin assembly has been shown to be under direct redox regulation [177]. Oxidation of one Met residue in the D-loop of actin decreases polymerization and severs the actin filament, causing cytoskeleton collapse. Two different protein kinases, PKGIa and PKA, are under direct regulation by oxidation [178]. Each is activated by forming an intersubunit disulfide bond between adjacent side chains to form a homodimer complex, activating the kinase activity in the absence of its normal activator molecules. The activities of protein kinase C and cAMP-dependent protein kinase are inhibited by glutathionylation of one surface exposed cysteine residue [179, 180].

Reversible oxidative modifications are emerging as novel regulatory mechanisms to combat oxidative stress in muscle [68, 139, 141, 142, 152]. The body wall muscle cells of a *C. elegans* MsrA knockout show sarcomeric disorganization [71], a characteristic previously described as a sign of aging in worms [73]. In addition, this worm mutant shows increased presence of protein MetO, locomotion defects, and decreased lifespan providing a link between oxidative damage/repair of Met and muscle tissue aging [71]. Numerous muscle proteins of the contractile apparatus have been identified as targets of protein oxidation and glutathionylation including both myosin and actin [55, 56, 66, 67, 176]. However, the identification of specific redox sites within contractile proteins and associated site-specific functional perturbations is limited.

We have previously identified that site-specific methionine oxidation in the *Dicty* myosin II catalytic domain causes a functional decline in actomyosin interaction. The decline is associated with changes in myosin internal dynamics and structure, specifically in the actin-binding cleft [113]. Of the nine Met residues located in the *Dicty* myosin II catalytic domain, at least three are susceptible to in vitro hydrogen peroxide induced oxidation; M394, M486 and M642. However, oxidation of M394 alone appears to be responsible for the decline in myosin ATPase and actin-activation [113]. The functional importance of this residue is not surprising based on its location in the actin-binding interface of myosin, directly N-terminal to the cardiomyopathy loop. Site-directed mutagenesis was used to control methionine and cysteine residue susceptibility to oxidation in order to determine redox sensitive residues in *Dicty* myosin II. The hydrogen peroxide-induced methionine sulfoxide at residue 394 can be reduced to methionine by Msr, rescuing the defect in actomyosin functional interaction. Mutation of M394 to a cysteine, to model potential effects of oxidative modification at this residue in human myosin heavy chain (MHC), reveals that a cysteine at this location is also redox sensitive in that it can be glutathionylated. These results indicate that myosin is an oxidatively labile protein whose level of activity may be regulated by the redox status of selective sulfhydryl groups.

### **4.3 Methods**

*Protein Preparations* - Mutagenesis of *Dicty* myosin II gene truncated at residue 762 (S1dC), containing only a single (non-reactive) cysteine at position 655, was done

using QuikChange II XL Site-directed mutagenesis kit (Invitrogen). All constructs used for functional measurements contain a T688C mutation (needed for sufficient protein expression in *D. discoideum*) which is spin-labeled with IASL [4-(2-Iodoacetamido)-2,2,6,6-tetramethyl-1-piperidinyloxy] (Sigma-Aldrich, USA) to protect from oxidative modification, except the M394C mutant. These proteins were expressed and purified from *Dictyostelium* orf+ cells. F-actin was prepared from rabbit skeletal muscle as previously described [104, 181]. Human methionine sulfoxide reductase A protein was obtained from AbcamBiochemicals (Cambridge, England).

*Oxidation and Glutathionylation of Myosin* - In vitro oxidative modification of Met residues in myosin was accomplished by treatment with 500 mM hydrogen peroxide (purchased as a stabilized 30% solution from Sigma-Aldrich) for 30 minutes on ice. Glutathionylation of the M394C mutant myosin was accomplished by treatment with 10 mM GSH plus 10 mM diamide for 1 hour on ice, unless otherwise noted. Hydrogen peroxide, GSH, and diamide were removed by buffer exchange using two sequential Zeba desalting columns (Thermo Fisher Scientific, Rockford, Illinois).

*Electrospray ionization mass spectrometry (ESI-MS)* - Myosin samples for mass spectrometry were prepared as previously described [113]. Briefly, myosin was exchanged into 10 mM  $\text{NH}_4\text{HCO}_3$  (pH 7.9) using two sequential 0.5 mL Zeba desalting columns, diluted 1:10 into a solution containing 50:50 acetonitrile:water and 0.1% formic acid, pH to 3 with additional formic acid (10%). Myosin mass was determined using a QSTAR quadrupole-TOF mass spectrometer (ABI) with an electrospray ionization source. 20  $\mu\text{M}$  myosin was introduced into the solvent stream using a 10  $\mu\text{L}$  injection loop installed in the integrated loop injector with a total of five injections per sample.



Data were acquired continuously over the range 500 – 2000 m/z. ESI spectra were analyzed with BioAnalyst QS (ABI) software v 1.1.5.

*Enzymatic Assays* - To investigate the repair of MetO in myosin by MsrA, 20  $\mu$ M myosin was incubated for varying times at 25°C with 4  $\mu$ M Msr A in 10 mM Tris (pH 7.5) and 1 mM DTT. Actin-activated ATPase activity was measured by detection of ADP generated by the NADH-coupled ATPase assay [102] using 1  $\mu$ M S1dC, 2 mM ATP, and increasing concentrations of phalloidin-stabilized F-actin in 10 mM Tris, 2 mM MgCl<sub>2</sub> (pH 7.5).

*Actomyosin Binding Affinities* - The equilibrium binding of actin and myosin was measured by cosedimentation. In cosedimentation assays, varying concentrations of actin were mixed with 1  $\mu$ M S1dC in F-buffer followed by centrifugation at 340,000 x g using a TLA100 rotor (Beckman Coulter) at 25° C, to pellet the actomyosin complex. Supernatant and pellet samples were each run on 12% Tris-glycine SDS-PAGE gels that were stained with Coomassie G (Sigma-Aldrich, St. Louis, MO); and band intensity was analyzed by densitometry using Image J [100]. The equilibrium constant for dissociation of S1dC from actin ( $K_d$ ) was determined by fitting with a quadratic binding function with maximal fraction bound constrained to 1.

## 4.4 Results

A version of *Dicty* myosin II truncated to contain only the myosin catalytic domain and devoid of reactive cysteines is used as a model system to examine the functional consequences of reversible oxidative modifications in myosin. Using *Dicty*

myosin as such a model is justified by its high level of structural and functional homology with muscle myosin catalytic domain [168, 169]. The *Dicty* myosin catalytic domain contains nine methionines, three of which are susceptible to *in vitro* oxidative modification [113]. Oxidation of Met 394, which is located at the C-terminus of an alpha-helix that transitions into the cardiomyopathy loop in the actin-binding interface (FIGURE 24A), appears to be responsible for the functional and structural perturbations observed with *in vitro* oxidation. M394 is conserved as a sulfur-containing amino acid side chain, as it is a cysteine residue in all isoforms of human cardiac and skeletal myosin (FIGURE 24B).

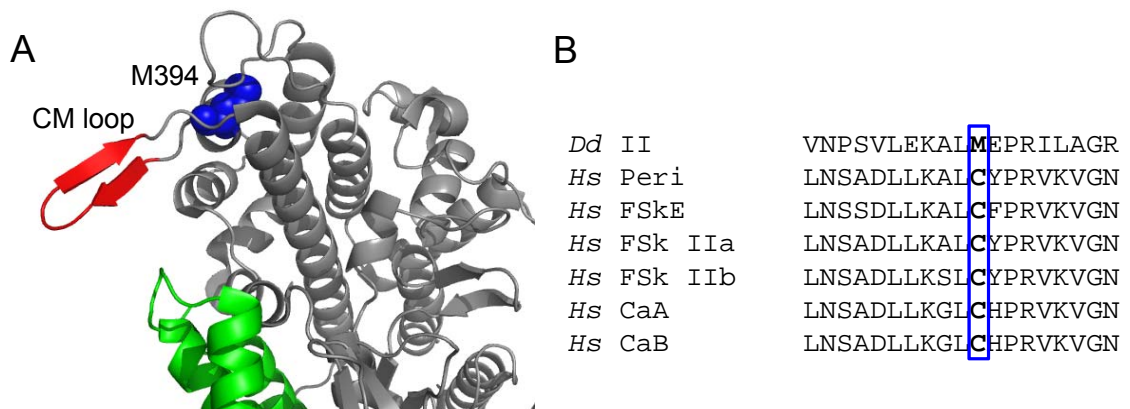


**FIGURE 24. A, Location of M394** (blue) N-terminal to the cardiomyopathy (CM) loop (red) in the myosin actin-binding interface. Upper 50 kDa domain of myosin catalytic domain shown in gray, lower 50 kDa domain when in green. B, Sequence alignment of *Dictyostelium discoideum* (*Dd*) myosin II M394 residue with *Homo sapien* (*Hs*) skeletal and cardiac muscle myosin II isoforms (Peri=perinatal, FSkE=fast skeletal embryonic, FSk=fast skeletal, and Ca=cardiac).

*Reversibility of oxidation at Met 394 by Methionine Sulfoxide Reductase* - To identify the ability of methionine sulfoxide reductase (Msr) to repair individual methionine sulfoxides (MetO) in the myosin catalytic domain, we have used *in vitro* conditions to generate a homogeneous population of oxidatively modified myosin in

which three of nine Mets are oxidized to their corresponding MetO. Prior to oxidative modification, the *Dicty* myosin II catalytic domain exhibits one major peak with a molecular mass of 88930.0 (FIGURE 25A, corresponding to native S1dC expressed in *D. discoideum*). The conditions used for *in vitro* oxidative modification of myosin result in an increase in mass of 49 Da, corresponding to the addition of three oxygens (FIGURE 25A) as we have previously shown [113]. Upon treatment of this oxidized myosin with MsrA, the molecular mass of S1dC decreases by 16 Da, suggesting the reversal of one MetO back to Met (FIGURE 25A). Treatment of native (unoxidized) S1dC with MsrA shows no shift in molecular mass (FIGURE 25A). No additional MetO repair is observed following incubation of myosin with MsrA for longer periods of time.

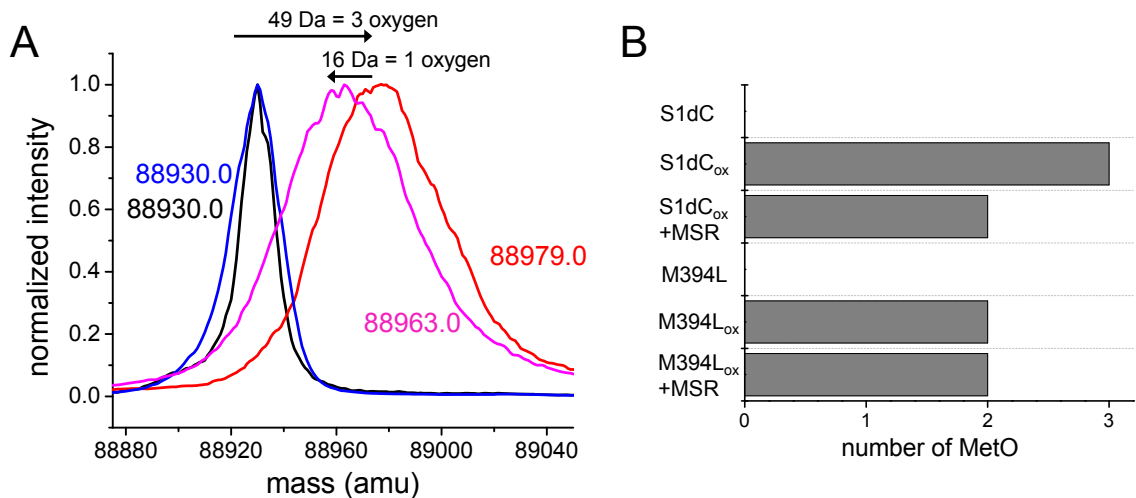


**FIGURE 25. Mass spec illustrating reversal of methionine oxidation in *Dicty* myosin II by methionine sulfoxide reductase.** A, ESI-MS of intact *Dicty* myosin. Deconvoluted mass spectra (normalized to maximum intensity) for 0 mM (black) then treated with MsrA (blue) and 500 mM H<sub>2</sub>O<sub>2</sub> (red) treated with MsrA (magenta). B, Number of MetO calculated from ESI-MS mass shifts for sample in A (T688C S1dC) and M394L mutant.

To determine if M394 was the MetO reversed to Met by Msr, leucine was used to substitute for methionine at M394 to protect from oxidation. Leucine is typically considered the most conservative substitute for methionine, and has been shown to produce substantially less structural perturbation than methionine oxidation [76, 172]. Oxidation of the M394L mutant with H<sub>2</sub>O<sub>2</sub> caused a shift of 32 Da, corresponding to the formation of two MetOs (FIGURE 25B). Treatment of oxidized M394L with MsrA produced a myosin with the same mass of H<sub>2</sub>O<sub>2</sub>-treated M394L, suggesting the oxidation of M486 and M642 are not reversible. These results, combined with the results of methionine sulfoxide reversal on globally oxidized *Dicty* myosin II, suggest M394 is the only Met that after oxidation to MetO, can be reduced back to Met by Msr.

*Reduction of methionine sulfoxide in myosin rescues actin-activated ATPase activity* - We have previously shown that treatment of S1dC with 500 mM hydrogen

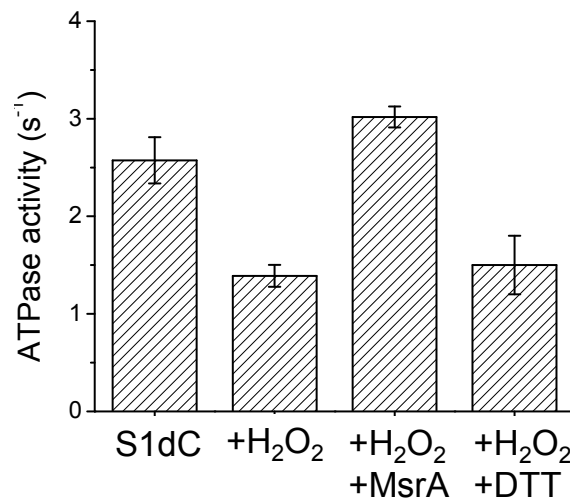


**FIGURE 26. Recovery of myosin II actin-activated ATPase activity** at saturating actin (50 uM) upon repair of methionine sulfoxides with MsrA. S1dC was oxidized with 500 mM H<sub>2</sub>O<sub>2</sub> on ice for 30 minutes. Oxidized S1dC was then treated with either 4 uM MsrA+ 1 mM DDT or 1 mM DTT alone for 30 minutes at 25°C (n=3).

peroxide induces a 2-fold decrease in maximum actin-activated ATPase rate ( $V_{\max}$ ) in the presence of saturating actin [113]. This same decrease in activity is observed (FIGURE 26). Treatment of S1dC with MsrA completely rescues the oxidation-induced decrease in actin-activated ATPase activity (FIGURE 26). Treatment with DTT alone did not rescue the oxidation induced defect in actin-activated ATPase activity (FIGURE 26).

*Cysteine at M394 can be glutathionylated* - To determine the ability of a cysteine at position 394 in S1dC to be glutathionylated *in vitro*, we again have used ESI-MS to measure the molecular mass of myosin. Prior to modification, the M394C mutant S1dC exhibits one major peak with a molecular mass of 88695.0 (FIGURE 27). Note the difference from the molecular mass in FIGURE 25A due to the absence of spin-label. Treatment with GSH and diamide produced a shift in molecular mass of ~305 Da, corresponding to the addition of 1 glutathione (FIGURE 27).

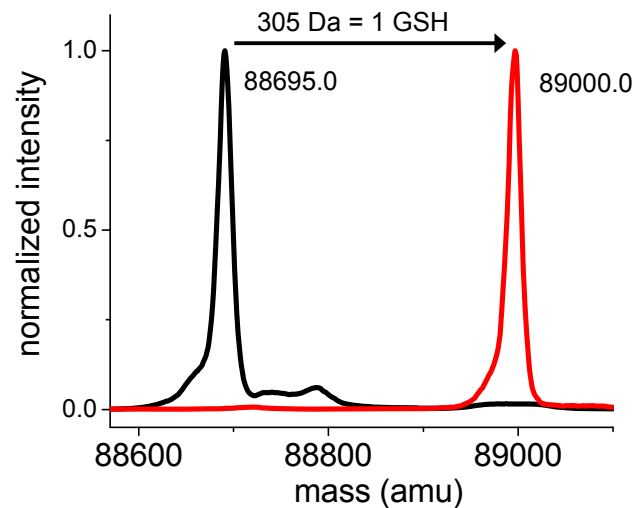


**FIGURE 27. Mass spec illustrating modification of *Dicty* myosin II mutant M394C (black) by treatment with 10 mM GSH and diamide (red).**

*Glutathionylation of M394C S1dC effects actomyosin functional interaction* - To determine the functional effects of oxidative modification of a cysteine residue at position 394 of S1dC, actin-activated ATPase activity was assessed in the presence of various oxidizing and reducing agents, including H<sub>2</sub>O<sub>2</sub>, DTT, glutathione, and diamide. Treatment of M394C S1dC with 500 mM H<sub>2</sub>O<sub>2</sub> causes a modest decrease in actin-

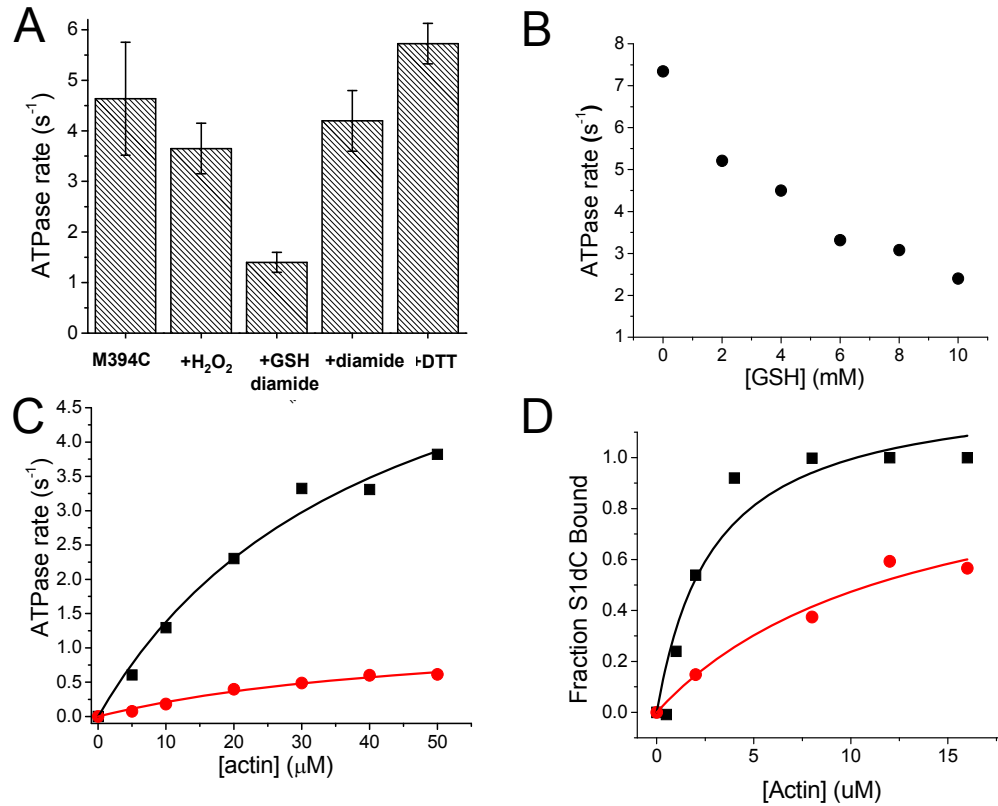


**FIGURE 28. Actomyosin functional interaction with glutathionylation.** A, ATPase activity of M394C in the presence of 50  $\mu$ M actin upon modification by various oxidizing and reducing agents ( $n=3$ ). B, ATPase activity of M394C S1dC in the presence of 50  $\mu$ M actin after treatment with increasing concentrations of GSH. C, ATPase activity of untreated M394C (black) and M394C treated with 10 mM GSH plus diamide (red). D, Fraction of M394C myosin S1dC bound to actin from cosedimentation. Data were fit by the quadratic binding function  $y = \{([M]_t + [A]_t + K_d) - (([M]_t + [A]_t + K_d)^2 - 4[M]_t[A]_t)^{1/2} / 2[A]_t\}$  where  $M=[\text{myosin}]$  and  $A=[\text{actin}]$ , yielding  $K_d$  values of  $2.9 \pm 1.2$   $\mu$ M for untreated M394C (black) and  $13.0 \pm 4.2$   $\mu$ M for M394C S1dC treated with 10 mM GSH (red).

activated ATPase under saturating actin conditions (FIGURE 28A). Glutathionylation of myosin with glutathione plus diamide produces a nearly 5-fold decrease in actin-activated ATPase activity and an increase in the concentration of actin needed for half maximal activation (FIGURE 28A,B,C). Untreated M394C has a  $V_{\max}$  of  $7.0 \pm 1.1 \text{ s}^{-1}$  and a  $K_{\text{ATPase}}$  of  $41.0 \pm 11.8 \text{ }\mu\text{M}$  while glutathionylated M394C has a  $V_{\max}$  of  $1.3 \pm 0.3 \text{ s}^{-1}$  and a  $K_{\text{ATPase}}$  of  $52.7 \pm 17.5 \text{ }\mu\text{M}$  (FIGURE 28C). Treatment of M394C with DTT or diamide alone produces no change in ATPase activity from untreated (FIGURE 28A).

Cosedimentation of myosin with actin in the absence of nucleotide (i.e., in rigor) shows that glutathionylation effects the ability of myosin to strongly bind actin. The  $K_d$  for untreated M394C S1dC is  $2.9 \pm 1.2 \text{ }\mu\text{M}$ , with glutathionylation yielding a  $K_d$  value of about  $13.0 \pm 4.2 \text{ }\mu\text{M}$  (FIGURE 28D).

## 4.5 Discussion and Future Direction

We have previously identified at least three *Dicty* myosin II methionines that are at least partially susceptible to oxidation by peroxide: M486, M642 and M394, with M394 being responsible for the oxidation-induced functional decline in myosin actin-activated ATPase activity and actomyosin interaction [113]. We now show that the oxidation of M394 is reversible by Msr and that the reduction of this MetO completely rescues the decline in ATPase activity. Mutation of this residue to a Cys, mimicking the residue present in all human isoforms of skeletal and cardiac myosin, shows that the Cys can also be oxidatively modified by glutathione decreasing actomyosin functional interaction.

Methionine sulfoxide reductase most readily reverses oxidized methionines that are solvent-exposed and located in regions of proteins composed of predominantly random-coil. It is therefore not surprising that only oxidation of M394, but not M486 and M642, is reversible. M394 is predicted to be solvent exposed when myosin is not bound to actin, and exists at the extreme end of an alpha-helix, transitioning into a random coil of the CM-loop (FIGURE 24A). As oxidation of methionine residues can cause helical destabilization, the hypothesis remains that oxidation of M394 destabilizes the adjacent helix, changing the structural dynamics of the entire CM-loop and hence interaction with actin. Although both M486 and M642 are also predicted to be solvent exposed (FIGURE 15), they exist in highly structured regions of S1dC, in the force-generating domain.

Glutathionylation is a reversible oxidative modification that plays a key role in redox regulation of proteins and signal transduction. In cardiac myosin, three Cys within the myosin heavy chain are susceptible to glutathionylation and associated with a decline in myosin ATPase activity at high levels of GSSG [56]. Two of these Cys residues, Cys 400 and Cys 695, are located within the myosin catalytic domain. Cys400 is equivalent to M394 in *Dicty* myosin, located in the actin-binding cleft adjacent to the CM-loop, while Cys695 is the reactive cysteine SH2 in the force-generating domain of myosin. The M394C S1dC mutant can be modified by glutathione *in vitro*. This modification causes a decrease in actin-activated ATPase activity and actomyosin interaction (FIGURE 28). Although unclear at this point, glutathionylation may have a dual role in protecting myosin against irreversible protein thiol oxidation at Cys residues in crucial subdomains of myosin such as the actin-binding cleft and modulating myosin's function. It is plausible that the location and presence of the sulfhydryl containing amino acid side



chain at position M394 in *Dicty* is evolutionarily conserved to allow for redox sensitivity that can modulate actomyosin interaction in response to varying situations of oxidative stress.

The glutathionylation of myosin causes a 5-fold decrease in actin-activated ATPase activity but it remains unknown if this represents a reversible mechanism for the protection of cysteine thiols against irreversible oxidation. The reversibility of this modification can be assessed by addition of DTT or glutathione reductase. In addition, the ability of M394C to be oxidized *in vitro* is unknown. If glutathionylation protects this specific Cys residue from irreversible oxidative modification, it should be oxidized to a sulfenic acid, or possibly the more highly oxidized sulfinic or sulfonic acid species that typically are more disruptive to protein structure and function, by treatment with hydrogen peroxide or other oxidative agents.

# Chapter 5: Characterization of a Myosin VII MyTH/FERM domain

Reprinted with permission from:

Rebecca J. Moen, Daniel O. Johnsrud, David D. Thomas, and Margaret A. Titus. Characterization of a Myosin VII MyTH/FERM domain. *J Mol Biol.* 2011;413(1):17-23.

**Copyright © 2011 Elsevier Limited**

Contributions of Authors:

Rebecca J. Moen: Assisted with experiment design. Established expression and purification protocol for MF1 protein. Performed mass spectrometry and data analysis shown in Figure 29C. Performed cosedimentation assays shown in Figures 30 and 31 and circular dichroism and thermal denaturation experiments shown in 32B and 32C, respectively and analyzed associated data. Made all figures and wrote the manuscript.

Daniel O. Johnsrud: Expression and purification of MF1 protein. Performed cosedimentation assays shown in Figures 30 and 31 and gel filtration experiment shown in Figure 32A and analyzed associated data. Edited the manuscript.

David. D. Thomas: Assisted with experiment design and edited figures and manuscript.

Margaret A. Titus: Designed all experiments. Edited all figures and wrote the manuscript.

## 5.1 Chapter Summary

A group of closely related myosins are characterized by the presence of at least one MyTH/FERM (myosin talin homology 4; band 4.1, ezrin, radixin, moesin) domain in their C-terminal tails. This domain interacts with a variety of binding partners, and mutations in either the MyTH4 or FERM domains of myosin VII and XV result in deafness, highlighting the functional importance of each domain. The N-terminal MyTH/FERM region of *Dictyostelium* myosin VII (M7) has been isolated as a first step toward gaining insight into the function of this domain and its interaction with binding partners. The M7 MyTH4/FERM domain (MF1) binds to both actin and microtubules *in vitro*, with dissociation constants of 13.76 and 1.71  $\mu\text{M}$ , respectively. Gel filtration and UV spectroscopy reveal that MF1 exists as a monomer in solution and forms a well-folded, compact conformation with a high degree of secondary structure. These results indicate that MF1 forms an integrated structural domain that serves to couple actin filaments and microtubules in specific regions of the cytoskeleton.

## 5.2 Introduction

Unconventional myosins have diverse cellular roles that are dictated, in large part, by class-specific tail domains that target each motor to specific cargo or subcellular locations. A subgroup of these motors, myosin VII (M7), myosin X (M10) and myosin XV (M15), is referred to as MyTH/FERM myosins because of the presence of one or two MyTH/FERM domains (myosin talin homology 4; band 4.1, ezrin, radixin, moesin) in their C-termini. The MyTH/FERM myosins are closely related both phylogenetically and functionally - for example, all MyTH/FERM myosins are localized to the tips of actin-

rich projections such as filopodia or stereocilia and play a role in the extension of these structures [10, 182-184]. MyTH/FERM domains are also found in other motors and proteins with roles in cytoskeletal function, including a plant kinesin and MAX-1 [185, 186]. While solo FERM domains are found in a large number of proteins, including talin and focal adhesion kinase, MyTH4 domains are frequently N-terminal to a FERM domain, suggesting a functional integration of the two domains. The importance of the myosin MyTH/FERM domain is highlighted by the finding that mutations in either the MyTH4 or FERM domains of M7a and M15a result in deafness in human patients [2-4, 6].

The MyTH/FERM domains of M7, M10 and M15 interact with a variety of proteins, including both microtubules and actin. A plant kinesin MyTH4 domain cosediments with microtubules [186], and the combined MyTH/FERM domains of human and *Xenopus* M10 interact with microtubules [12, 187]. M10 colocalizes with microtubules in the meiotic spindle of *Xenopus* oocytes, is found at mitotic spindle poles in embryos [187, 188] and is required for correct mitotic spindle orientation [188, 189]. The isolated C-terminal FERM domain of *Drosophila* M7a binds actin with moderate affinity ( $\sim 30 \mu\text{M}$ ) [190] and the FERM domain of a *Tetrahymena* MyTH/FERM myosin is found in actin immunoprecipitates [191]. The tails of these myosins can thus bind to either actin or microtubules, enabling them to slide actin against either microtubules or another actin filament or even tether actin or microtubules to actin.

Detailed characterization of the biophysical and structural properties of the MyTH/FERM domain, along with the ability to determine the nature of its interaction with partner proteins that serve to anchor or regulate myosin activity, is necessary to fully

understand MyTH/FERM myosin function, as well as the role of other proteins that have this domain. The social amoeba *Dictyostelium* expresses a class 7 myosin (DdM7) that contains two MyTH/FERM domains separated by an SH3 domain [192]. This myosin is required for filopod extension and cell-substrate adhesion, roles quite similar to those described for M10 [10, 183, 192, 193]. The tail domain of DdM7 interacts specifically with another FERM domain protein required for adhesion, talinA, [9] which modulates the dynamic membrane association of DdM7 [194]. The contribution of the MyTH/FERM domains to DdM7 function is not yet known. In the present study, the ability to readily express protein domains fused to the motor domain of myosin II [195] was exploited to purify and characterize the N-terminal MyTH/FERM domain of DdM7 as a first step toward a more detailed understanding of this combined domain and its interaction with both actin and microtubules.

### **5.3 Methods**

*Construction of myosin-fusion plasmid* - The region of the Dd M7 gene encompassing the N-terminal MyTH/FERM (amino acids 1085-1620) domain was amplified from genomic DNA using standard PCR techniques. The 5' oligo included an Nhe I restriction site and the 3' oligo included an extension that encoded an 8x His tag followed by an Xho I site. The PCR product was TA cloned using the Strataclone system (Stratagene) and the sequence verified (BioMedical Genomics Center). A modified pDXA-mako 4b expression plasmid [195] that encoded the TEV cleavage sequence ENLYFQG to optimize cleavage of MF1 from the myosin fusion, pDXA-mako4B-TEV\*,

was generated by PCR and the Nhe I/Xho I MF1 insert was cloned into this plasmid between the NheI and XhoI restriction sites. The resulting plasmid, pDTi225, encoded the myosin II motor domain (S1) followed by the TEV cleavage site then the MF1 region of Dd M7.

*Cell growth and transformation* - *Dictyostelium discoideum* cells were grown in suspension (at 150 rpm) or on bacteriological plastic in HL5 [196]. Plasmid DNA encoding the MF1 was electrotransformed into log phase *Dictyostelium* as previously described [197]. Single clones were picked and then screened for the S1-MF1 fusion by performing a small-scale rigor cytoskeleton prep [195, 198].

*MF1 Purification* - The S1-MF1 fusion was first isolated using a modified version of a standard *Dictyostelium* myosin motor domain prep [198, 199]. Cells were grown to a density of  $6 \times 10^6$  to  $1 \times 10^7$  cells/ml and then harvested by centrifugation at  $1500 \times g$  for 15 min then washed once with cold Sorenson's phosphate buffer pH 6.4 (16.6 mM K/Na phosphate) and the wet cell pellet weight determined. Cells were either then drop frozen in liquid nitrogen for storage or used fresh. Cells were resuspended in lysis buffer (4 ml/g of wet cell paste) containing 50 mM Tris-HCl pH 8.0, 0.1 mM EGTA, 5 mM  $\beta$ -mercaptoethanol, 5  $\mu$ g/ml Leupeptin, 1 mM AEBSF, 0.1 mM TLCK, and 1X EDTA-free Complete protease inhibitor cocktail (Roche). Cells were lysed at room temperature for 15 minutes by adding lysis buffer (2 ml/g cells) containing 1% Triton-X100 (Anatrace), 15  $\mu$ g/ml RNAase A, and 5 U/ml of alkaline phosphatase. The lysate was then centrifuged at  $15,000 \times g$  for 30 minutes. The resulting pellets containing the rigor cytoskeletal fraction (actin, myosin, MF1-myosin motor fusion), were washed with 10 mM HEPES pH 7.2, 20 mM NaCl, 5 mM  $\beta$ -ME (6 ml/g starting material) and the rinsed

pellets homogenized with the same buffer with protease inhibitors, then a total of 1 mg purified TEV protease added per X volume (1 ml/g starting material) and the sample allowed to incubate for 2 -3 hr at room temperature with gentle mixing to cleave the MF1 domain from the myosin motor affinity tag. After cleavage, the suspension was centrifuged at 15,000×g for 30 minutes, yielding the MF1 domain in supernatant. The supernatant was applied to DEAE CL-6B Sepharose resin (Pharmacia), incubated with gentle agitation for 30 minutes to allow binding, and then centrifuged at 700×g for 5 minutes. The unbound fraction, containing the MF1 domain that has a relatively high calculated pI of 7.9, was then applied directly to Talon metal affinity resin (Clontech), incubated with gentle agitation at 4° C overnight to allow binding of MF1 domain. The resin was collected and washed batchwise twice with 10 bed volumes of high salt buffer (10 mM HEPES pH 7.5, 300 mM KAc, 5 mM imidazole, 5 mM β-mercaptoethanol) and then poured into an empty glass column. The column was washed with 5 bed volumes of high salt buffer, then 5 bed volumes low imidazole wash buffer (30 mM KAc, 10 mM imidazole pH 7.5 and 5 mM β-mercaptoethanol) and eluted with a 5 bed volumes of elution buffer (250 mM imidazole pH 7.5, 30 mM KAc, 5 mM β-mercaptoethanol). Eluates containing purified MF1 were dialyzed against buffer containing 20 mM HEPES pH 7.5, 50 mM NaCl and then concentrated.

The pMHTdelta286 plasmid (provided by Dr. B.G. Fox, U. Wisconsin, to the Protein Structure Initiative Material Repository at Harvard Institute of Proteomics; available as clone TvCD00084286) was transformed into BL21(pLysS) bacteria, MBP-TEV expression induced and TEV protease purified as described [200].

*ESI (electrospray ionization) mass spectrometry* - MF1 was desalted using Millipore C4 ZipTips according to the manufacturer's protocol prior to mass spectrometry. The molecular mass of MF1 was determined using a QSTAR quadrupole-TOF mass spectrometer (ABI) with an electrospray ionization source (Center for Mass Spectroscopy and Proteomics). Data was acquired continuously during load buffer infusion and protein infusions over the range 500 – 2000 m/z. ESI spectra were analyzed with BioAnalyst QS (ABI) software v 1.1.5.

*Actin Cosedimentation* - Cosedimentation actin binding assays were performed by mixing increasing concentrations of actin with 2.5  $\mu$ M MF1 in 10 mM imidazole, 2 mM  $MgCl_2$ , 1 mM ATP, 0.1 mM DTT pH 7.5 buffer followed by centrifugation at 340,000 x g using a TLA100.3 rotor (Beckman Coulter) to pellet the actoMF1 complex. Supernatant and pellet samples were run on 10% SDS-PAGE gels that were stained with Coomassie G and band intensity analyzed by densitometry using Image J. Actin used in these experiments was extracted from rabbit skeletal muscle acetone powder, purified as described previously [104].

*Microtubule Cosedimentation* - Cosedimentation microtubule binding assays [201] were performed by mixing increasing  $\mu$ M concentrations of tubulin (Cytoskeleton or gift from Dr. Holly Davidson, Notre Dame) with 2.5  $\mu$ M MF1 in 10 mM PIPES, 5 mM  $MgCl_2$ , 1 mM EGTA, pH 7.0 buffer, incubated for 30 min at room temperature, followed by centrifugation at 90,000 x g for 10 min at 25°C to pellet the tubulin-MF1 complex. The pellet was resuspended in 10 mM PIPES, 5 mM  $MgCl_2$ , 1 mM EGTA, 5 mM  $CaCl_2$  pH 7.0 allowing MTs to depolymerize. Supernatant and pellet samples were run on 10%



SDS-PAGE gels, then stained with Coomassie G and band intensities analyzed by densitometry using Image J.

*Gel Filtration* - Gel filtration was performed on a ToyoPearl HW-55F (Tosoh Biosciences LLC) packed column with a diameter of 2.2 cm and height of 78 cm using 25 mM HEPES (pH 7.4), 50 mM NaCl, and 0.1 mM EGTA. A total of 1 mL of 0.5 - 1 mg/mL MF1 was loaded on the column with a flow rate of 1.5 mL/minute and 4 mL fractions were collected. The fractions were analyzed by 10% SDS-PAGE and Coomassie G staining. The Stokes radius of MF1 was determined by comparison with the following standards: aldolase (4.81 nm), ovalbumin (3.05 nm), and RNase A (1.64 nm).

*Circular Dichroism* - CD spectra were recorded in the far- (190–250 nm) UV region using a JASCO J-815 spectrophotometer and a temperature-jacketed spectral cell. A path length of 0.1 mm was used with spectra recorded at 1 nm intervals for 10  $\mu$ M MF1 in phosphate buffer pH 7.0 at 25°C. Baseline scans were obtained using the same acquisition parameters with buffer alone; which were subtracted from the respective CD data scans of MF1. The raw CD signal  $\theta_\lambda$  (millidegrees of ellipticity) was converted to mean residue molar ellipticity  $\theta$  using Eq. 2 where MRE = 110, C=protein concentration, and l = path length. Far- UV CD spectra were analyzed using CDPro Analysis Software [158]. Average secondary structure percentage for FERM domains was calculated using the software STRIDE [202] and PDB structures: 1GC7, 1E5W, 1ISN, 2HE7, 1H4R, 1EF1, 1GG3, and 1NI2.

*Temperature-Induced Denaturation* - Thermal denaturation of MF1 was monitored by CD at 222 nm using a JASCO J-815 spectrophotometer with an automated temperature controller. The temperature was increased from 10 to 70°C with a step size

of 1°C with the CD in millidegrees of ellipticity measured at each temperature after incubation for 2 min. At the end of each thermal denaturation experiment, the sample was rapidly cooled to 25°C to determine the extent of refolding.

## 5.4 Results

Isolation of the DdM7 N-terminal MyTH4/FERM domain - The N-terminal MyTH4/FERM domain of DdM7 (MF1 - residues 1085-1620) (FIGURE 29A) was fused

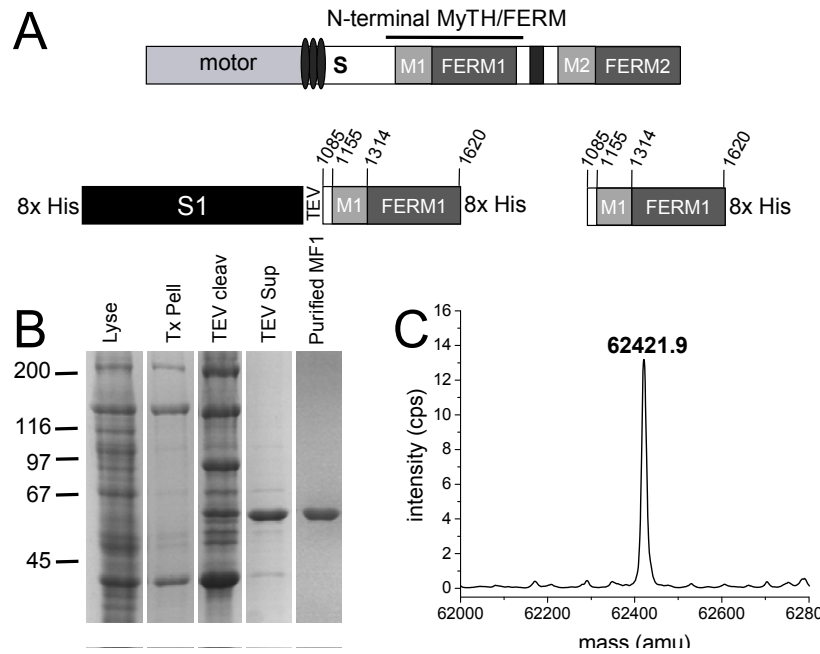


**FIGURE 29. Isolation of the N-terminal MyTH/FERM domain of DdM7.** A, Schematic illustration of the full-length DdM7 highlighting the major domains, including the IQ motifs (ovals), single alpha-helix (S), N-terminal MyTH/FERM (M1, FERM1), SH3 (black rectangle) and C-terminal MyTH/FERM (M2, FERM2). The S1-MF1 fusion is also shown, with the myosin II motor domain (S1) and the locations of the TEV cleavage site and His tag indicated. B, Purification of MF1 as monitored by SDS-PAGE. Samples from key steps of the purification were run on a 10% gel that was stained with Coomassie G. Shown are the total cell lysate (Lyse), rigor cytoskeleton (Tx Pell), cytoskeleton following TEV cleavage (TEV cleav), soluble fraction following centrifugation of the cleaved cytoskeleton pellet (TEV sup) and purified MF1. C, ESI MS of MF1.

to the C-terminal end of the myosin II motor domain (S1) 21 and after lysis under rigor conditions, the fusion was highly enriched in the cytoskeleton fraction (FIGURE 29B). Following release from the cytoskeleton with MgATP, cleavage from S1 with TEV and metal affinity chromatography, purified MF1 was obtained (FIGURE 29B) and its identity confirmed by mass spectrometry (FIGURE 29C).

*MF1 binding to F-actin* - FERM domains are considered to interact primarily with the cytoplasmic tails of membrane receptors. It has only recently been appreciated that they can also bind directly to F-actin [190, 203]. The talin FERM domain interacts directly with actin and while the affinity is not known, it has been suggested that it is sufficient to account for the interaction of talin to actin [203]. The affinity of MF1 for

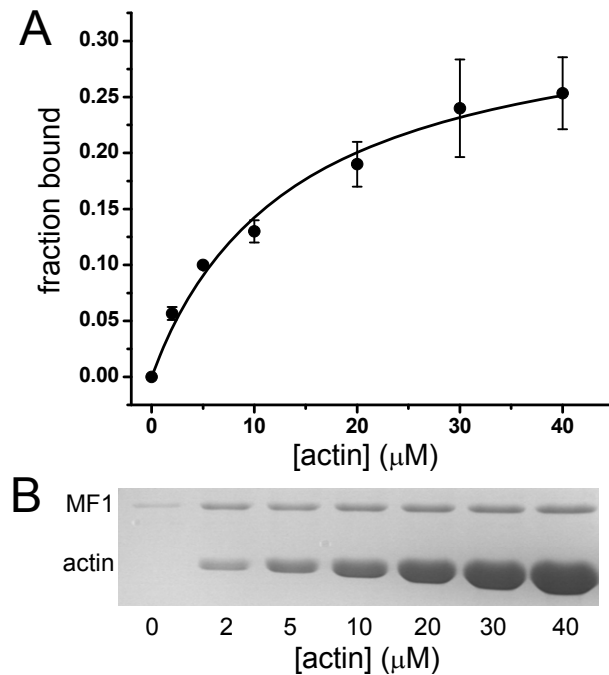


**FIGURE 30. Binding of MF1 to actin.** A, Fraction bound MF1 with increasing actin concentration. Data was fit to a hyperbola yielding  $K_d = 13.67 \pm 2.57 \mu\text{M}$ . Data shown represents three independent experiments. B, SDS-PAGE bands of pellets from cosedimentation illustrating MF1 pellets with actin.

actin was measured by cosedimentation [99] and the binding curve reveals a single  $K_d$  of  $13.767 \pm 2.657 \mu\text{M}$  (FIGURE 30). The finding that MF1 has a nearly 2-fold greater  $K_d$  for actin binding, in comparison to the fly M7a C-terminal FERM domain ( $\sim 30 \mu\text{M}$ ) [190], suggests that the MyTH4 domain could increase the binding affinity, possibly by causing the actin-binding sequence to be more exposed and accessible. These results indicate that the FERM-actin interaction is conserved but generally of low affinity. However, the existence of two domains within the M7 molecule that interact weakly with F-actin would result in stronger overall actin binding.

*MF1 binding to Microtubules* - The interaction of myosin MyTH4 domains with microtubules is known, but the binding strength has not been measured. The interaction of MF1 with microtubules was assayed by cosedimentation [201] and the resulting binding curve yields a single  $K_d$  of  $1.71 \pm 0.53 \mu\text{M}$  (FIGURE 31), indicating a stronger affinity for microtubules than for actin. The curve unexpectedly showed saturation at 0.25 fraction bound, initially suggesting that a significant portion of the MF1 preparation was unable to interact with microtubules. A similar low binding saturation was observed for the actoMF1 interaction (FIGURE 30). The supernatant from the highest tubulin concentration ( $10 \mu\text{M}$ ) was recovered, additional microtubules added ( $10 \mu\text{M}$  tubulin, final concentration) and the sample re-centrifuged (FIGURE 31). Approximately 25% of MF1 from the supernatant cosedimented with the microtubules, as observed in the initial binding assay (FIGURE 31B), indicating that the low overall saturation binding was not due to a large fraction of the preparation being denatured. These results show clearly that the isolated MF1 domain is in equilibrium between two conformational states, one of which does not bind to microtubules or actin and one that does.

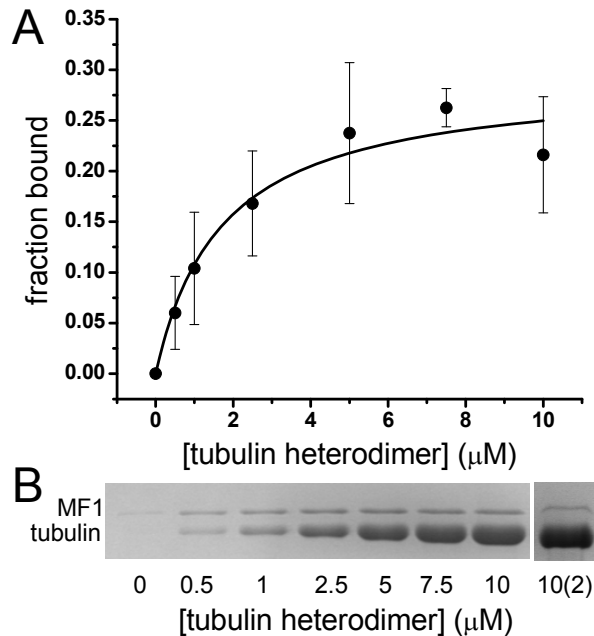


**FIGURE 31: Binding of MF1 to tubulin.** A, Fraction bound MF1 with increasing tubulin heterodimer concentrations. Data was fit to a hyperbola, yielding  $K_d = 1.71 \pm 0.53$   $\mu\text{M}$ . Data represents five independent experiments. B, SDS-PAGE bands of pellets from cosedimentation illustrating MF1 pellets with microtubules. 10(2) illustrates cosedimentation of additional MF1 with microtubules after initial binding.

*Overall MF1 Structure and Stability* - The crystal structures of two myosin MyTH/FERM domains in association with known binding partner peptides have recently been solved [12, 204, 205]. The MyTH4 domain is a bundle of helices, 6 of which are highly conserved. The FERM domain, consistent with previously published x-ray and NMR studies of FERM domains from talin, radixin, moesin, merlin, and protein 4.1R [206-208], adopts the canonical three-lobe cloverleaf structure, with the three subdomains denoted F1, F2, and F3. In both the M7a and M10 MyTH/FERM structures, the MyTH4 and FERM domains interact with one another, forming a functional and structural supramodule. Consistent with these findings, gel filtration analysis of the purified MF1 reveals that it is a tightly folded monomer with a calculated Stokes radius of  $2.74 \pm 0.34$  nm (FIGURE 32A). The far-UV circular dichroism (CD) spectrum of MF1 also confirms

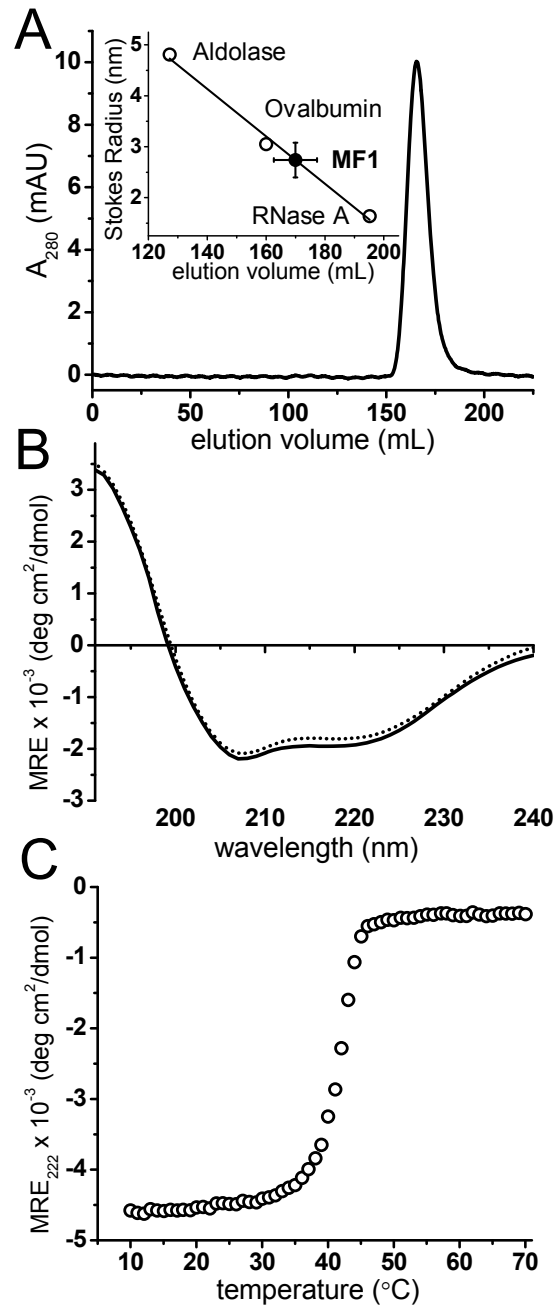


**FIGURE 32. Structure and stability of MF1.** A, Gel Filtration elution profile of MF1. B, Far-UV CD spectrum indicating a highly helical MF1 structure. Experimental CD spectrum (solid line) and best fit spectrum from CDPro Analysis (dotted line). C, Thermal denaturation curve of MF1 measured by changes in mean residue ellipticity. The temperature was increased from 10 to 70°C with a step size of 1°C with the CD in millidegrees of ellipticity measured at each temperature after incubation for 2 min.

that it is a highly helical protein with intense CD bands at both 208 nm and 222 nm (FIGURE 32B). Analysis of the CD spectrum, using CDPro Analysis [158], yielded an estimated secondary structure of  $55\% \pm 3\%$  alpha-helix and  $21\% \pm 4\%$  beta-sheet. The thermal unfolding of MF1 secondary structure occurred in one transition, with an onset of unfolding at  $\sim 35^\circ\text{C}$  and a transition midpoint ( $T_m$ ) at  $42^\circ\text{C}$  (FIGURE 32C).

The secondary structure of the mammalian M7a and M10 MyTH/FERM domains are 46% alpha-helix/15% beta-sheet and 49% alpha-helix/14% beta-sheet, respectively (determined using STRIDE [202] and Protein Data Bank files 3PVL and 3PZD). The alpha-helix and beta-sheet content of DdM7 MF1 are predicted to be slightly higher than calculated for mammalian M7a and M10, with  $55\% \pm 3\%$  alpha-helix and  $21\% \pm 4\%$  beta-sheet based on fitting of the far-UV CD spectrum (FIGURE 32B). The differences in secondary structure may be attributed to the sequence divergence between amoeba and vertebrate MyTH/FERM domains and/or that MF1 exists in the apo state.

## 5.5 Discussion

The amoeba *Dictyostelium discoideum* is evolutionary quite distant from vertebrates [209]. A comparison of the MyTH-FERM domain sequences from mouse M7a (residues 993-1567, GenBank AAB40708.1) and human M10 (residues 1503-2047, GenBank AAF68025.2) to DdM7 MF1 reveals a low sequence identity of 20% for both and sequence homology of 36% and 39%, respectively. Sequence alignment reveals the DdM7 N-terminal MyTH4 sequence is substantially shorter than both the M7a and M10 MyTH4 sequences. The missing sequence of DdM7 encompasses helices 3 and 4 of the mammalian M7a MyTH domain, suggesting that the DdM7 MF1 MyTH4 structure

differs slightly from that of M7a, although the 6-helix core is predicted to remain intact [205].

A positively charged patch on the MyTH4 domain of human M10 consisting of eight positively charged residues is thought to be required for binding to MTs [204]. Consistent with this possibility, mutation of two of these (K1647 and K1650) is sufficient to abolish all binding to tubulin acidic tails [12]. Three of these eight positively charged residues are conserved between the human M10 and DdM7 MF1 MyTH4 domains (R1643, K1647, K1654 in M10; R1257, K1261, and K1268 in DdM7), suggesting that MF1 may also bind to MTs by a similar electrostatic interaction.

## 5.6 Conclusion

MyTH/FERM domains are present in numerous cytoskeletal signaling and motor proteins and much remains to be learned about their combined structure and function. The structure of MyTH/FERM domains is predicted to be conserved throughout evolution despite a high degree of sequence divergence of these domains. The ability of MF1 to bind both actin and microtubules suggests an important role for this domain in linking cytoskeletal elements. M7 and M10 are localized to regions of the cell where actin and microtubules are both present [187, 210]. M10 and M15 can link microtubule-based structures to actin [187-189, 211] but the contribution of microtubule binding to M7 activity is not yet clear. Fly M7a is monomeric *in vitro* and most likely exists in a folded conformation, with the FERM domain interacting with and inhibiting the motor domain [190]. The MyTH/FERM regions might be partially or fully blocked from



binding to microtubules or actin in this configuration. Consistent with this possibility is the observation that DdM7 is largely cytosolic [9, 10]. Activation of the folded myosin, either by as yet unknown regulatory factors that dimerize M7 [212] or the presence of high local concentrations of either actin or microtubules, might expose these sites. Our data also suggests an alternative mechanism, in which there exist two conformations of the MyTH/FERM domain itself, only one of which is available for actin or microtubule binding. This poised equilibrium is an obvious target for regulatory control, as shown recently for the myosin regulatory light chain [213]. Once the binding sites are available, the tail could interact with both actin and microtubules, enabling cortical DdM7 to actively stabilize the leading edge of the cells by strengthening cell-substrate adhesions.

## Chapter 6: Future Direction

The ability of the molecular motor myosin to produce movement is an intensely studied biophysical process. However, many of the mechanistic and structural details remain elusive. Although the work presented here provides insights into the structural transitions associated with the actomyosin ATPase mechanism and the effects of oxidative modification on the actomyosin complex, continued work is needed to provide a more detailed understanding of this complex system.

*Cleft Crosslinked Myosin* – The myosin cleft mutant 416.583 crosslinked with BSL has complete inhibition of actin-activated ATPase activity and a weakened actin affinity. This suggests that the interaction of actin with crosslinked S1dC produces a dead-end complex, trapping myosin in an intermediate cleft conformation where product release is prohibited in the presence of actin. Crosslinking traps actomyosin in a unique statically disordered, novel W state that may represent a possible missing link in the ATPase cycle mechanism, at the threshold of force generation (FIGURE 14). It will be interesting to study the spectroscopic properties of crosslinked myosin in combination with other regions of myosin. For example, it would be possible to study the nucleotide-binding pocket structural dynamics of the crosslinked myosin using spin-labeled nucleotides. In addition, the crosslinked myosin may also affect actin dynamics, which can be tested by time-resolved phosphorescence anisotropy [67]. It would also be interesting to test other crosslinking sites across the actin-binding cleft, such as 413.583, to see if different crosslinking sites in the cleft produce the same intermediate W state with similar functional and structural characteristics.

*The bifunctional spin-label* - In addition to crosslinking specific regions of the myosin catalytic domain to capture dynamic intermediates, the bifunctional spin-label can crosslink two Cys residues at  $i$  and  $i+4$  on a helix producing an EPR probe rigidly and stereospecifically coupled to the peptide backbone, enabling extremely accurate measurements of correlation time, orientation, and distance by EPR [46, 47, 111]. As the exact coupling of cleft structural transitions to biochemical states remains elusive, it would be feasible to use the highly oriented bifunctional spin label and attach it to helices in the L50 and U50 (FIGURE 4) domains to detect nucleotide-dependent changes in the structure and orientation of the cleft both free and when bound to oriented actin.

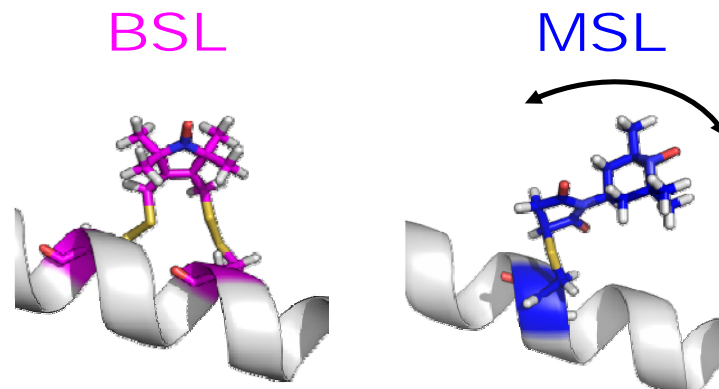


**FIGURE 33. Bifunctional spin label** binds rigidly and stereospecifically thus improving resolution compared with monofunctional MSL to measure interprobe distance and helix orientation.

*Methionine Oxidation* - Methionine oxidation affects the structural dynamics of the actin-binding cleft of myosin (FIGURE 20 & FIGURE 21), but it remains unknown whether other regions of the myosin catalytic domain are susceptible to structural changes induced by methionine oxidation. Only one labeling site within the force-generating domain of myosin has been tested (FIGURE 22) at T688C in the SH1 helix. This particular site was insensitive to oxidation in every biochemical state tested,

including when actin was present (FIGURE 22). This is a surprising result as M486 of *Dicty* myosin II is chemically sensitive to oxidation (FIGURE 17) and is situated directly in the bend of the relay helix. It would be interesting to test whether relay helix dynamics are sensitive to oxidation, as structural transitions (i.e. bending of the relay helix) are readily observed in various biochemical states for this helix [89]. Additional spin probe labeling sites should be investigated in both in the force-generating domain and near the nucleotide binding pocket to further explore the structural changes in the myosin catalytic domain with Met oxidation. Also, the effects of Met oxidation are most evident in the actin-bound state of myosin (FIGURE 20B & FIGURE 21B). It would be interesting to investigate the orientation and rotational motion of oxidized myosin by EPR as in Chapter 2 for crosslinked myosin (FIGURE 13).

To study the effects of methionine oxidation site-specifically, we have utilized a mutagenesis scheme that introduces M-to-L mutations to protect from oxidation. Leucine mutants are used as the leucine side-chain is of similar size and hydrophobicity as methionine. In addition, it was well established in numerous biological systems that M-to-L mutants do confer protection from oxidation with little perturbation of structure and function [75, 76, 172, 177, 214-216]. It has been suggested that methionine to glutamine (M-to-Q) mutations can be used to mimic oxidation site-specifically as this mutation introduces an oxygen atom at a similar position in the amino acid side chain as MetO [74, 75, 217]. Several M-to-Q mutations should be made at critical Met residues (such as M394, M486, and M642) within *Dicty* myosin II to see if M-to-Q mutants show similar functional and structural perturbations as *in vitro* oxidation with hydrogen peroxide (FIGURE 17). More rigorous testing of M-to-Q mutations needs to be done to confirm

that this mutagenesis scheme can be used universally to mimic oxidation. Although the results from Chapter 3 strongly suggest the oxidation of at least three residues with the *Dicty* myosin II catalytic domain, additional mass spectrometry should also be used to confirm sites of Met oxidation, as previously done for muscle isolated from rabbit psoas fibers [66].

*Redox sensitivity of myosin catalytic domain* - Preliminary data in Chapter 4 illustrates that myosin Met modifications are chemically (FIGURE 25) and functionally (FIGURE 26) reversible by the antioxidant enzyme Msr. It remains to be known if the structural perturbations induced by Met oxidation in the actin-binding cleft (FIGURE 20 & FIGURE 21) are also reversible. In addition, the *Dicty* myosin II catalytic domain appears to be susceptible to glutathionylation causing changes in actomyosin functional interaction (FIGURE 28). Although the glutathionylation of myosin causes a 5-fold decrease in actin-activated ATPase activity, it has not been investigated if this reaction is reversible and whether it may protect cysteine thiols against irreversible oxidation. As well, possible structural changes associated with glutathionylation have yet to be determined.

*MyTH/FERM domain of Myosin VII* – Chapter 5 reveals that the *Dicty* myosin VII N-terminal MyTH/FERM domain is a folded, stable supramodule that can interact with both actin and microtubules. The ability of MF1 to bind actin and microtubules simultaneously needs to be determined. The exact location of actin and microtubule binding sites in the MF1 domain is also unknown. Hirano et al. show a positively charged-patch on the solvent-exposed surface of the MyTH domain is responsible for binding microtubules in myosin X [12], and it appears this patch is conserved to the

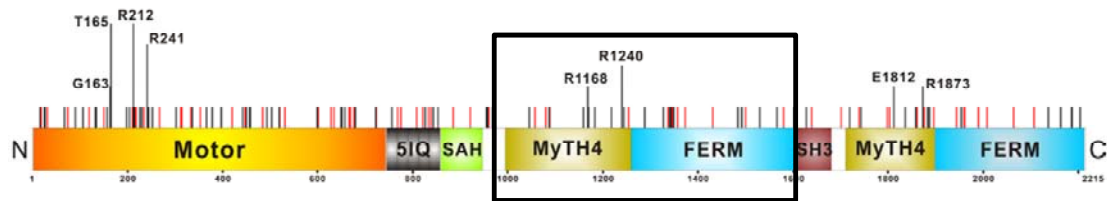


**FIGURE 34. Schematic representation of full-length myosin VII** summarizing frequency of mutations of MYO7a in Usher syndrome patients. The height of the vertical lines represents the frequency of a given mutation found in human patients with missense mutations colored black and deletion or truncation mutations in red. Figure modified from [205]. Reprinted with permission from AAAS.

DdM7 N-terminal MyTH domain. Charge-reversal mutagenesis of this patch would reveal its role in binding microtubules. Numerous Usher syndrome disease-causing mutations are located in the C-terminal tail of myosin VII (FIGURE 34) [205]. Many of these mutations are conserved between human and *Dictyostelium* suggesting a highly important role in domain stability or interaction with binding partners. Some interesting, conserved mutations to investigate include R1240Q/W and E1327K, proposed to disrupt the MyTH/FERM interface, and R1168P/W and E1170K, predicted to disrupt proper folding of the MyTH domain [205]. Introducing these mutations in the DdM7 MF1 domain and investigating effects on domain structure and stability and ability to bind actin and microtubules would provide insight into the Usher disease mechanism.

## Bibliography

1. Hartman, M.A. and Spudich, J.A., *The myosin superfamily at a glance*. J Cell Sci, 2012. **125**(Pt 7): p. 1627-32.
2. Jaijo, T., et al., *MYO7A mutation screening in Usher syndrome type I patients from diverse origins*. J Med Genet, 2007. **44**(3): p. e71.
3. Liburd, N., et al., *Novel mutations of MYO15A associated with profound deafness in consanguineous families and moderately severe hearing loss in a patient with Smith-Magenis syndrome*. Hum Genet, 2001. **109**(5): p. 535-41.
4. Riazuddin, S., et al., *Mutation spectrum of MYO7A and evaluation of a novel nonsyndromic deafness DFNB2 allele with residual function*. Hum Mutat, 2008. **29**(4): p. 502-11.
5. Sellers, J.R., *Myosins: a diverse superfamily*. Biochim Biophys Acta, 2000. **1496**(1): p. 3-22.
6. Wang, A., et al., *Association of unconventional myosin MYO15 mutations with human nonsyndromic deafness DFNB3*. Science, 1998. **280**(5368): p. 1447-51.
7. Thompson, R.F. and Langford, G.M., *Myosin superfamily evolutionary history*. Anat Rec, 2002. **268**(3): p. 276-89.
8. Akhmanova, A. and Hammer, J.A., 3rd, *Linking molecular motors to membrane cargo*. Curr Opin Cell Biol, 2010. **22**(4): p. 479-87.
9. Tuxworth, R.I., et al., *Identification of a myosin VII-talin complex*. J Biol Chem, 2005. **280**(28): p. 26557-64.
10. Tuxworth, R.I., et al., *A role for myosin VII in dynamic cell adhesion*. Curr Biol, 2001. **11**(5): p. 318-29.
11. Berg, J.S., et al., *Myosin-X, a novel myosin with pleckstrin homology domains, associates with regions of dynamic actin*. J Cell Sci, 2000. **113 Pt 19**: p. 3439-51.
12. Hirano, Y., et al., *Structural basis of cargo recognition by the myosin-X MyTH4-FERM domain*. EMBO J, 2011. **30**(13): p. 2734-47.
13. Huxley, A.F. and Niedergerke, R., *Structural changes in muscle during contraction; interference microscopy of living muscle fibres*. Nature, 1954. **173**(4412): p. 971-3.
14. Huxley, H. and Hanson, J., *Changes in the cross-striations of muscle during contraction and stretch and their structural interpretation*. Nature, 1954. **173**(4412): p. 973-6.
15. Lymn, R.W. and Taylor, E.W., *Mechanism of adenosine triphosphate hydrolysis by actomyosin*. Biochemistry, 1971. **10**(25): p. 4617-24.
16. Thomas, D.D., Kast, D., and Korman, V.L., *Site-directed spectroscopic probes of actomyosin structural dynamics*. Annu Rev Biophys, 2009. **38**: p. 347-69.
17. Holmes, K.C., *The swinging lever-arm hypothesis of muscle contraction*. Curr Biol, 1997. **7**(2): p. R112-8.
18. Cooke, R., *The mechanism of muscle contraction*. CRC Crit Rev Biochem, 1986. **21**(1): p. 53-118.
19. Huxley, A.F. and Simmons, R.M., *Proposed mechanism of force generation in striated muscle*. Nature, 1971. **233**(5321): p. 533-8.

20. Rayment, I., et al., *Three-dimensional structure of myosin subfragment-1: a molecular motor*. Science, 1993. **261**(5117): p. 50-8.
21. Asukagawa, H. and Sutoh, K., *The alanine-scanning mutagenesis of Dictyostelium myosin II at the ionic interface with actin*. Results Probl Cell Differ, 2002. **36**: p. 65-74.
22. Furch, M., Geeves, M.A., and Manstein, D.J., *Modulation of actin affinity and actomyosin adenosine triphosphatase by charge changes in the myosin motor domain*. Biochemistry, 1998. **37**(18): p. 6317-26.
23. Hirayama, Y., Sutoh, K., and Watabe, S., *Structure-function relationships of the two surface loops of myosin heavy chain isoforms from thermally acclimated carp*. Biochem Biophys Res Commun, 2000. **269**(1): p. 237-41.
24. Sasaki, N., et al., *Deletion of the myopathy loop of Dictyostelium myosin II and its impact on motor functions*. J Biol Chem, 1999. **274**(53): p. 37840-4.
25. Sasaki, N., Ohkura, R., and Sutoh, K., *Insertion or deletion of a single residue in the strut sequence of Dictyostelium myosin II abolishes strong binding to actin*. J Biol Chem, 2000. **275**(49): p. 38705-9.
26. Sasaki, N., Ohkura, R., and Sutoh, K., *Dictyostelium myosin II as a model to study the actin-myosin interactions during force generation*. J Muscle Res Cell Motil, 2002. **23**(7-8): p. 697-702.
27. Uyeda, T.Q., Ruppel, K.M., and Spudich, J.A., *Enzymatic activities correlate with chimaeric substitutions at the actin-binding face of myosin*. Nature, 1994. **368**(6471): p. 567-9.
28. Coureux, P.D., et al., *A structural state of the myosin V motor without bound nucleotide*. Nature, 2003. **425**(6956): p. 419-23.
29. Malnasi-Csizmadia, A. and Kovacs, M., *Emerging complex pathways of the actomyosin powerstroke*. Trends Biochem Sci, 2010. **35**(12): p. 684-90.
30. Sweeney, H.L. and Houdusse, A., *Structural and functional insights into the Myosin motor mechanism*. Annu Rev Biophys, 2010. **39**: p. 539-57.
31. Zeng, W., et al., *Dynamics of actomyosin interactions in relation to the cross-bridge cycle*. Philos Trans R Soc Lond B Biol Sci, 2004. **359**(1452): p. 1843-55.
32. Behrmann, E., et al., *Structure of the rigor actin-tropomyosin-Myosin complex*. Cell, 2012. **150**(2): p. 327-38.
33. Sun, M., et al., *Characterization of the pre-force-generation state in the actomyosin cross-bridge cycle*. Proc Natl Acad Sci U S A, 2008. **105**(25): p. 8631-6.
34. Dausse, E. and Schwartz, K., *Genetic heterogeneity of familial hypertrophic cardiomyopathy*. Neuromuscul Disord, 1993. **3**(5-6): p. 483-6.
35. Erdmann, J., et al., *Mutation spectrum in a large cohort of unrelated consecutive patients with hypertrophic cardiomyopathy*. Clin Genet, 2003. **64**(4): p. 339-49.
36. Geisterfer-Lowrance, A.A., et al., *A molecular basis for familial hypertrophic cardiomyopathy: a beta cardiac myosin heavy chain gene missense mutation*. Cell, 1990. **62**(5): p. 999-1006.
37. Mohiddin, S.A., et al., *Utility of genetic screening in hypertrophic cardiomyopathy: prevalence and significance of novel and double (homozygous and heterozygous) beta-myosin mutations*. Genet Test, 2003. **7**(1): p. 21-7.



38. Dellefave, L.M., et al., *Sarcomere mutations in cardiomyopathy with left ventricular hypertrabeculation*. *Circ Cardiovasc Genet*, 2009. **2**(5): p. 442-9.
39. Hoedemaekers, Y.M., et al., *Cardiac beta-myosin heavy chain defects in two families with non-compaction cardiomyopathy: linking non-compaction to hypertrophic, restrictive, and dilated cardiomyopathies*. *Eur Heart J*, 2007. **28**(22): p. 2732-7.
40. Iascone, M.R., Marchetti, D., and Ferrazzi, P., *Gene symbol: MYH7*. *Hum Genet*, 2007. **120**(6): p. 916.
41. Kamisago, M., et al., *Mutations in sarcomere protein genes as a cause of dilated cardiomyopathy*. *N Engl J Med*, 2000. **343**(23): p. 1688-96.
42. Fujita, H., et al., *Characterization of mutant myosins of Dictyostelium discoideum equivalent to human familial hypertrophic cardiomyopathy mutants. Molecular force level of mutant myosins may have a prognostic implication*. *J Clin Invest*, 1997. **99**(5): p. 1010-5.
43. Sweeney, H.L., et al., *Heterologous expression of a cardiomyopathic myosin that is defective in its actin interaction*. *J Biol Chem*, 1994. **269**(3): p. 1603-5.
44. Bobkov, A. and Reisler, E., *Is SH1-SH2-cross-linked myosin subfragment 1 a structural analog of the weakly-bound state of myosin?* *Biophys J*, 2000. **79**(1): p. 460-7.
45. Chalovich, J., Greene, L., and Eisenberg, E., *Crosslinked myosin subfragment 1: a stable analogue of the subfragment-1.ATP complex*. *Proc Natl Acad Sci USA*, 1983. **80**(16): p. 4909-13.
46. Mello, R.N. and Thomas, D.D., *Three distinct actin-attached structural states of myosin in muscle fibers*. *Biophys J*, 2012. **102**(5): p. 1088-96.
47. Thompson, A.R., et al., *Structural dynamics of the actomyosin complex probed by a bifunctional spin label that cross-links SH1 and SH2*. *Biophys J*, 2008. **95**(11): p. 5238-46.
48. Nitao, L.K. and Reisler, E., *Probing the conformational states of the SH1-SH2 helix in myosin: a cross-linking approach*. *Biochemistry*, 1998. **37**(47): p. 16704-10.
49. Shih, W.M. and Spudich, J.A., *The myosin relay helix to converter interface remains intact throughout the actomyosin ATPase cycle*. *J Biol Chem*, 2001. **276**(22): p. 19491-4.
50. Coirault, C., et al., *Oxidative stress of myosin contributes to skeletal muscle dysfunction in rats with chronic heart failure*. *Am J Physiol Heart Circ Physiol*, 2007. **292**(2): p. H1009-17.
51. Oh-Ishi, M., Ueno, T., and Maeda, T., *Proteomic method detects oxidatively induced protein carbonyls in muscles of a diabetes model Otsuka Long-Evans Tokushima Fatty (OLETF) rat*. *Free Radic Biol Med*, 2003. **34**(1): p. 11-22.
52. Ramamurthy, B., et al., *Changes in myosin structure and function in response to glycation*. *Faseb J*, 2001. **15**(13): p. 2415-22.
53. Syrový, I. and Hodný, Z., *Non-enzymatic glycosylation of myosin: effects of diabetes and ageing*. *Gen Physiol Biophys*, 1992. **11**(3): p. 301-7.
54. Thompson, L.V., et al., *Myosin and actin expression and oxidation in aging muscle*. *J Appl Physiol*, 2006. **101**(6): p. 1581-7.

55. Prochniewicz, E., Thomas, D.D., and Thompson, L.V., *Age-related decline in actomyosin function*. J Gerontol A Biol Sci Med Sci, 2005. **60**(4): p. 425-31.
56. Passarelli, C., et al., *Myosin as a potential redox-sensor: an in vitro study*. J Muscle Res Cell Motil, 2008. **29**(2-5): p. 119-26.
57. Delbono, O., *Molecular mechanisms and therapeutics of the deficit in specific force in ageing skeletal muscle*. Biogerontology, 2002. **3**(5): p. 265-70.
58. Prochniewicz, E., Thompson, L.V., and Thomas, D.D., *Age-related decline in actomyosin structure and function*. Exp Gerontol, 2007. **42**(10): p. 931-8.
59. Moylan, J.S. and Reid, M.B., *Oxidative stress, chronic disease, and muscle wasting*. Muscle Nerve, 2007. **35**(4): p. 411-29.
60. Stadtman, E.R., *Protein oxidation and aging*. Free Radic Res, 2006. **40**(12): p. 1250-8.
61. Avner, B.S., et al., *Hydrogen Peroxide Alters Rat Cardiac Sarcomere Function And Protein Phosphorylation Through Redox Signaling*. Am J Physiol Heart Circ Physiol, 2010.
62. Baltgalvis, K.A., et al., *Estrogen regulates estrogen receptors and antioxidant gene expression in mouse skeletal muscle*. PLoS One, 2010. **5**(4): p. e10164.
63. Jackson, M.J., *Redox regulation of skeletal muscle*. IUBMB Life, 2008. **60**(8): p. 497-501.
64. Jackson, M.J., *Redox regulation of adaptive responses in skeletal muscle to contractile activity*. Free Radic Biol Med, 2009. **47**(9): p. 1267-75.
65. Lowe, D.A., et al., *Electron paramagnetic resonance reveals age-related myosin structural changes in rat skeletal muscle fibers*. Am J Physiol Cell Physiol, 2001. **280**(3): p. C540-7.
66. Prochniewicz, E., et al., *Functional, structural, and chemical changes in myosin associated with hydrogen peroxide treatment of skeletal muscle fibers*. Am J Physiol Cell Physiol, 2008. **294**(2): p. C613-26.
67. Prochniewicz, E., Spakowicz, D., and Thomas, D.D., *Changes in actin structural transitions associated with oxidative inhibition of muscle contraction*. Biochemistry, 2008. **47**(45): p. 11811-7.
68. Stadtman, E.R., et al., *Methionine oxidation and aging*. Biochim Biophys Acta, 2005. **1703**(2): p. 135-40.
69. Gao, J., et al., *Progressive decline in the ability of calmodulin isolated from aged brain to activate the plasma membrane Ca-ATPase*. Biochemistry, 1998. **37**(26): p. 9536-48.
70. Michaelis, M.L., et al., *Decreased plasma membrane calcium transport activity in aging brain*. Life Sci, 1996. **59**(5-6): p. 405-12.
71. Minniti, A.N., et al., *Methionine sulfoxide reductase A expression is regulated by the DAF-16/FOXO pathway in Caenorhabditis elegans*. Aging Cell, 2009. **8**(6): p. 690-705.
72. Moskovitz, J., et al., *Methionine sulfoxide reductase (MsrA) is a regulator of antioxidant defense and lifespan in mammals*. Proc Natl Acad Sci U S A, 2001. **98**(23): p. 12920-5.
73. Herndon, L.A., et al., *Stochastic and genetic factors influence tissue-specific decline in ageing C. elegans*. Nature, 2002. **419**(6909): p. 808-14.

74. Balog, E.M., et al., *Calmodulin oxidation and methionine to glutamine substitutions reveal methionine residues critical for functional interaction with ryanodine receptor-1*. J Biol Chem, 2003. **278**(18): p. 15615-21.
75. Balog, E.M., et al., *Role of calmodulin methionine residues in mediating productive association with cardiac ryanodine receptors*. Am J Physiol Heart Circ Physiol, 2006. **290**(2): p. H794-9.
76. Balog, E.M., et al., *Site-Specific Methionine Oxidation Initiates Calmodulin Degradation by the 20S Proteasome (dagger)*. Biochemistry, 2009. **48**(13): p. 3005-16.
77. Erickson, J.R., et al., *A dynamic pathway for calcium-independent activation of CaMKII by methionine oxidation*. Cell, 2008. **133**(3): p. 462-74.
78. Boschek, C.B., et al., *Loss of the calmodulin-dependent inhibition of the RyR1 calcium release channel upon oxidation of methionines in calmodulin*. Biochemistry, 2008. **47**(1): p. 131-42.
79. Anbanandam, A., et al., *Mediating molecular recognition by methionine oxidation: conformational switching by oxidation of methionine in the carboxyl-terminal domain of calmodulin*. Biochemistry, 2005. **44**(27): p. 9486-96.
80. Bartlett, R.K., et al., *Oxidation of Met144 and Met145 in calmodulin blocks calmodulin dependent activation of the plasma membrane Ca-ATPase*. Biochemistry, 2003. **42**(11): p. 3231-8.
81. Sun, H., et al., *Repair of oxidized calmodulin by methionine sulfoxide reductase restores ability to activate the plasma membrane Ca-ATPase*. Biochemistry, 1999. **38**(1): p. 105-12.
82. Theis, J.L., et al., *Expression patterns of cardiac myofilament proteins: genomic and protein analysis of surgical myectomy tissue from patients with obstructive hypertrophic cardiomyopathy*. Circ Heart Fail, 2009. **2**(4): p. 325-33.
83. Lowe, D.A., et al., *Molecular and cellular contractile dysfunction of dystrophic muscle from young mice*. Muscle Nerve, 2006. **34**(1): p. 92-100.
84. Klein, J.C., et al., *Actin-binding cleft closure in myosin II probed by site-directed spin labeling and pulsed EPR*. Proc Natl Acad Sci U S A, 2008. **105**(35): p. 12867-72.
85. Baker, J.E., et al., *A large and distinct rotation of the myosin light chain domain occurs upon muscle contraction*. Proc Natl Acad Sci U S A, 1998. **95**(6): p. 2944-9.
86. LaConte, L.E., Baker, J.E., and Thomas, D.D., *Transient kinetics and mechanics of myosin's force-generating rotation in muscle: resolution of millisecond rotational transitions in the spin-labeled myosin light-chain domain*. Biochemistry, 2003. **42**(32): p. 9797-803.
87. Taylor, K., et al., *Tomographic 3D reconstruction of quick-frozen, Ca<sup>2+</sup>-activated contracting insect flight muscle*. Cell, 1999. **99**(4): p. 421-31.
88. Thomas, D.D., et al., *The mechanism of force generation in myosin: a disorder-to-order transition, coupled to internal structural changes*. Biophys J, 1995. **68**(4 Suppl): p. 135S-141S.
89. Agafonov, R.V., et al., *Structural dynamics of the myosin relay helix by time-resolved EPR and FRET*. Proc Natl Acad Sci U S A, 2009. **106**(51): p. 21625-30.

90. Agafonov, R.V., et al., *Muscle and nonmuscle myosins probed by a spin label at equivalent sites in the force-generating domain*. Proc Natl Acad Sci U S A, 2008. **105**(36): p. 13397-402.
91. Nesmelov, Y.E., et al., *Structural kinetics of myosin by transient time-resolved FRET*. Proc Natl Acad Sci U S A, 2011. **108**(5): p. 1891-6.
92. Holmes, K.C., et al., *Electron cryo-microscopy shows how strong binding of myosin to actin releases nucleotide*. Nature, 2003. **425**(6956): p. 423-7.
93. Volkman, N., et al., *Evidence for cleft closure in actomyosin upon ADP release*. Nat Struct Biol, 2000. **7**(12): p. 1147-55.
94. Volkman, N., et al., *The structural basis of myosin V processive movement as revealed by electron cryomicroscopy*. Mol Cell, 2005. **19**(5): p. 595-605.
95. Yengo, C.M., et al., *Actin-induced closure of the actin-binding cleft of smooth muscle myosin*. J Biol Chem, 2002. **277**(27): p. 24114-9.
96. Fajer, P.G., Gyimesi, M., Málnási-Csizmadia, A., Bagshaw, C. R., Sen, K. I. & Song, L., *Myosin cleft closure by double electron-electron resonance and dipolar EPR*. Journal of Physics: Condensed Matter, 2007. **19**: p. 285208.
97. Conibear, P.B., et al., *Myosin cleft movement and its coupling to actomyosin dissociation*. Nat Struct Biol, 2003. **10**(10): p. 831-5.
98. Yang, Y., et al., *Rigor-like structures from muscle myosins reveal key mechanical elements in the transduction pathways of this allosteric motor*. Structure, 2007. **15**(5): p. 553-64.
99. Prochniewicz, E. and Thomas, D.D., *Site-specific mutations in the myosin binding sites of actin affect structural transitions that control myosin binding*. Biochemistry, 2001. **40**(46): p. 13933-40.
100. Rasband, W.S., *Image J*. 1997-2012, U.S. National Institutes of Health: Bethesda, Maryland, USA.
101. Lanzetta, P.A., et al., *An improved assay for nanomole amounts of inorganic phosphate*. Anal Biochem, 1979. **100**(1): p. 95-7.
102. De La Cruz, E.M. and Ostap, E.M., *Kinetic and equilibrium analysis of the myosin ATPase*. Methods Enzymol, 2009. **455**: p. 157-92.
103. Geeves, M.A. and Halsall, D.J., *The dynamics of the interaction between myosin subfragment 1 and pyrene- labelled thin filaments, from rabbit skeletal muscle*. Proc R Soc Lond B Biol Sci, 1986. **229**(1254): p. 85-95.
104. Prochniewicz, E., Walseth, T.F., and Thomas, D.D., *Structural dynamics of actin during active interaction with myosin: different effects of weakly and strongly bound myosin heads*. Biochemistry, 2004. **43**(33): p. 10642-52.
105. Goldman, S.A., Bruno, G.V., and Freed, J.H., *Estimating slow-motional rotational correlation times for nitroxides by electron spin resonance*. J Phys Chem, 1972. **76**: p. 1858-1860.
106. Thomas, D.D. and Cooke, R., *Orientation of spin-labeled myosin heads in glycerinated muscle fibers*. Biophys J, 1980. **32**(3): p. 891-906.
107. Fajer, P.G., et al., *General method for multiparameter fitting of high-resolution EPR spectra using a simplex algorithm*. J Magn Res, 1990. **88**: p. 111-25.

108. Squier, T.C. and Thomas, D.D., *Applications of new saturation transfer electron paramagnetic resonance methodology to the rotational dynamics of the Ca-ATPase in sarcoplasmic reticulum membranes*. Biophys J, 1986. **49**(4): p. 937-42.
109. Squier, T.C. and Thomas, D.D., *Methodology for increased precision in saturation transfer electron paramagnetic resonance studies of rotational dynamics*. Biophys J, 1986. **49**(4): p. 921-35.
110. Kirby, T.L., Karim, C.B., and Thomas, D.D., *Electron paramagnetic resonance reveals a large-scale conformational change in the cytoplasmic domain of phospholamban upon binding to the sarcoplasmic reticulum Ca-ATPase*. Biochemistry, 2004. **43**(19): p. 5842-52.
111. Fleissner, M.R., et al., *Structure and dynamics of a conformationally constrained nitroxide side chain and applications in EPR spectroscopy*. Proc Natl Acad Sci U S A, 2011. **108**(39): p. 16241-6.
112. Batra, R., Geeves, M.A., and Manstein, D.J., *Kinetic analysis of Dictyostelium discoideum myosin motor domains with glycine-to-alanine mutations in the reactive thiol region*. Biochemistry, 1999. **38**(19): p. 6126-34.
113. Klein, J.C., et al., *Structural and Functional Impact of Site-Directed Methionine Oxidation in Myosin*. Biochemistry, 2011.
114. Thomas, D.D., et al., *Spectroscopic probes of muscle proteins*, in *Comprehensive Biophysics*. 2012, Elsevier: Amsterdam. p. 226-250.
115. Thomas, D.D., et al., *The quantitative measurement of rotational motion of the subfragment-1 region of myosin by saturation transfer epr spectroscopy*. J Supramol Struct, 1975. **3**(4): p. 376-90.
116. Thomas, D.D., *Rotational dynamics in spin-labeled biomacromolecular assemblies: saturation transfer electron paramagnetic resonance*. Ph. D. Thesis. Stanford University., 1976.
117. Berger, C.L., Svensson, E.C., and Thomas, D.D., *Photolysis of a photolabile precursor of ATP (caged ATP) induces microsecond rotational motions of myosin heads bound to actin*. Proc Natl Acad Sci U S A, 1989. **86**(22): p. 8753-7.
118. Berger, C.L. and Thomas, D.D., *Rotational dynamics of actin-bound intermediates in the myosin ATPase cycle*. Biochemistry, 1991. **30**(46): p. 11036-45.
119. Berger, C.L. and Thomas, D.D., *Rotational dynamics of actin-bound myosin heads in active myofibrils*. Biochemistry, 1993. **32**(14): p. 3812-21.
120. Berger, C.L. and Thomas, D.D., *Rotational dynamics of actin-bound intermediates of the myosin adenosine triphosphatase cycle in myofibrils*. Biophys J, 1994. **67**(1): p. 250-61.
121. Thomas, D.D., et al., *Sub-millisecond rotational dynamics of spin-labeled myosin heads in myofibrils*. Biophys J, 1980. **32**(3): p. 873-89.
122. Thompson, A.R., *The structural dynamics of force generation in muscle, probed by electron paramagnetic resonance of bifunctionally labeled myosin.*, in *PhD Thesis, Physics Department*. 2009, University of Minnesota: Minneapolis.
123. Bagshaw, C.R., *Muscle Contraction*. 2nd ed. 1993, New York: Chapman & Hall. 155.

124. Joel, P.B., Trybus, K.M., and Sweeney, H.L., *Two conserved lysines at the 50/20-kDa junction of myosin are necessary for triggering actin activation*. J Biol Chem, 2001. **276**(5): p. 2998-3003.
125. Onishi, H., Mikhailenko, S.V., and Morales, M.F., *Toward understanding actin activation of myosin ATPase: the role of myosin surface loops*. Proc Natl Acad Sci U S A, 2006. **103**(16): p. 6136-41.
126. Gyimesi, M., et al., *The mechanism of the reverse recovery step, phosphate release, and actin activation of Dictyostelium myosin II*. J Biol Chem, 2008. **283**(13): p. 8153-63.
127. Cooke, R., Crowder, M.S., and Thomas, D.D., *Orientation of spin labels attached to cross-bridges in contracting muscle fibres*. Nature, 1982. **300**(5894): p. 776-8.
128. Fajer, P.G., et al., *Orientational disorder and motion of weakly attached cross-bridges*. Biophys J, 1991. **60**(3): p. 642-9.
129. Roopnarine, O. and Thomas, D.D., *Orientational dynamics of indane dione spin-labeled myosin heads in relaxed and contracting skeletal muscle fibers*. Biophys J, 1995. **68**(4): p. 1461-71.
130. Roopnarine, O. and Thomas, D.D., *A spin label that binds to myosin heads in muscle fibers with its principal axis parallel to the fiber axis*. Biophys J, 1994. **67**(4): p. 1634-45.
131. Stein, R.A., et al., *Time-resolved rotational dynamics of phosphorescent-labeled myosin heads in contracting muscle fibers*. Biochemistry, 1990. **29**(43): p. 10023-31.
132. Svensson, E.C. and Thomas, D.D., *ATP induces microsecond rotational motions of myosin heads crosslinked to actin*. Biophys J, 1986. **50**(5): p. 999-1002.
133. Kuhner, S. and Fischer, S., *Structural mechanism of the ATP-induced dissociation of rigor myosin from actin*. Proc Natl Acad Sci U S A, 2011. **108**(19): p. 7793-8.
134. Kintses, B., et al., *Reversible movement of switch 1 loop of myosin determines actin interaction*. Embo J, 2007. **26**(1): p. 265-74.
135. Trivedi, D.V., et al., *Switch II mutants reveal coupling between the nucleotide- and actin-binding regions in myosin V*. Biophys J, 2012. **102**(11): p. 2545-55.
136. Holmes, K.C. and Geeves, M.A., *The structural basis of muscle contraction*. Philos Trans R Soc Lond B Biol Sci, 2000. **355**(1396): p. 419-31.
137. Geeves, M.A. and Holmes, K.C., *Structural mechanism of muscle contraction*. Annu Rev Biochem, 1999. **68**: p. 687-728.
138. Varkuti, B.H., et al., *A novel actin binding site of myosin required for effective muscle contraction*. Nat Struct Mol Biol, 2012. **19**(3): p. 299-306.
139. Hoshi, T. and Heinemann, S., *Regulation of cell function by methionine oxidation and reduction*. J Physiol, 2001. **531**(Pt 1): p. 1-11.
140. Davies, K.J., *Oxidative stress, antioxidant defenses, and damage removal, repair, and replacement systems*. IUBMB Life, 2000. **50**(4-5): p. 279-89.
141. Bigelow, D.J. and Squier, T.C., *Redox modulation of cellular signaling and metabolism through reversible oxidation of methionine sensors in calcium regulatory proteins*. Biochim Biophys Acta, 2005. **1703**(2): p. 121-34.
142. Emes, M.J., *Oxidation of methionine residues: the missing link between stress and signalling responses in plants*. Biochem J, 2009. **422**(2): p. e1-2.

143. Prentice, H.M., et al., *MsrA protects cardiac myocytes against hypoxia/reoxygenation induced cell death*. Biochem Biophys Res Commun, 2008. **366**(3): p. 775-8.
144. Palomero, J. and Jackson, M.J., *Redox regulation in skeletal muscle during contractile activity and aging*. J Anim Sci, 2010. **88**(4): p. 1307-13.
145. Kinugawa, S., et al., *Treatment with dimethylthiourea prevents left ventricular remodeling and failure after experimental myocardial infarction in mice: role of oxidative stress*. Circ Res, 2000. **87**(5): p. 392-8.
146. Maack, C., et al., *Oxygen free radical release in human failing myocardium is associated with increased activity of rac1-GTPase and represents a target for statin treatment*. Circulation, 2003. **108**(13): p. 1567-74.
147. Reid, M.B. and Durham, W.J., *Generation of reactive oxygen and nitrogen species in contracting skeletal muscle: potential impact on aging*. Ann N Y Acad Sci, 2002. **959**: p. 108-16.
148. Reid, M.B., *Invited Review: redox modulation of skeletal muscle contraction: what we know and what we don't*. J Appl Physiol, 2001. **90**(2): p. 724-31.
149. Tidball, J.G. and Wehling-Henricks, M., *The role of free radicals in the pathophysiology of muscular dystrophy*. J Appl Physiol, 2007. **102**(4): p. 1677-86.
150. Stadtman, E.R. and Berlett, B.S., *Reactive oxygen-mediated protein oxidation in aging and disease*. Chem Res Toxicol, 1997. **10**(5): p. 485-94.
151. Lowe, D.A., et al., *Muscle activity and aging affect myosin structural distribution and force generation in rat fibers*. J Appl Physiol, 2004. **96**(2): p. 498-506.
152. Ghesquiere, B., et al., *Redox proteomics of protein-bound methionine oxidation*. Mol Cell Proteomics, 2011. **10**(5).
153. Hardin, S.C., et al., *Coupling oxidative signals to protein phosphorylation via methionine oxidation in Arabidopsis*. Biochem J, 2009. **422**(2): p. 305-12.
154. Agbas, A. and Moskovitz, J., *The Role of Methionine Oxidation/Reduction in the Regulation of Immune Response*. Curr Signal Transduct Ther, 2009. **4**(1): p. 46-50.
155. Carruthers, N.J. and Stemmer, P.M., *Methionine oxidation in the calmodulin-binding domain of calcineurin disrupts calmodulin binding and calcineurin activation*. Biochemistry, 2008. **47**(10): p. 3085-95.
156. Prochniewicz, E., et al., *Microsecond rotational dynamics of actin: spectroscopic detection and theoretical simulation*. J Mol Biol, 1996. **255**(3): p. 446-57.
157. Fiske, C.H. and Subbarow, Y., *The colorimetric Determination of Phosphorus*. The Journal of Biological Chemistry, 1925. **26**(2): p. 375-400.
158. Sreerama, N. and Woody, R.W., *Estimation of protein secondary structure from circular dichroism spectra: comparison of CONTIN, SELCON, and CDSSTR methods with an expanded reference set*. Anal Biochem, 2000. **287**(2): p. 252-60.
159. Budil, D.E., et al., *Nonlinear-least-squares analysis of slow-motion EPR spectra in one and two dimensions using a modified Levenberg-Marquardt algorithm*. J. Magn. Reson., 1996. **A 120**: p. 155 - 189.
160. Nsmelov, Y.E., et al., *Structure and dynamics of the force-generating domain of myosin probed by multifrequency electron paramagnetic resonance*. Biophys J, 2008. **95**(1): p. 247-56.

161. Nesmelov, Y.E., et al., *Rotational dynamics of phospholamban determined by multifrequency electron paramagnetic resonance*. Biophys J, 2007. **93**(8): p. 2805-12.
162. Pannier, M., et al., *Dead-time free measurement of dipole-dipole interactions between electron spins*. J Magn Reson, 2000. **142**(2): p. 331-40.
163. Pake, G.E., *Nuclear Resonance Absorption in Hydrated Crystals: Fine Structure of the Proton Line*. Journal of Chemical Physics, 1948. **16**: p. 327-336.
164. Rabenstein, M. and Shin, Y.K., *A peptide from the heptad repeat of human immunodeficiency virus gp41 shows both membrane binding and coiled-coil formation*. Biochemistry, 1995. **34**(41): p. 13390-7.
165. Steinhoff, H.J., et al., *Determination of interspin distances between spin labels attached to insulin: comparison of electron paramagnetic resonance data with the X-ray structure*. Biophys J, 1997. **73**(6): p. 3287-98.
166. Altenbach, C., et al., *Structure and function in rhodopsin: mapping light-dependent changes in distance between residue 65 in helix TM1 and residues in the sequence 306-319 at the cytoplasmic end of helix TM7 and in helix H8*. Biochemistry, 2001. **40**(51): p. 15483-92.
167. Jeschke, G., *Distance measurements in the nanometer range by pulse EPR*. Chemphyschem, 2002. **3**(11): p. 927-32.
168. Schroder, R.R., et al., *Three-dimensional atomic model of F-actin decorated with Dictyostelium myosin SI*. Nature, 1993. **364**(6433): p. 171-4.
169. Bauer, C.B., et al., *X-ray structures of the apo and MgATP-bound states of Dictyostelium discoideum myosin motor domain*. J Biol Chem, 2000. **275**(49): p. 38494-9.
170. Fraczekiewicz, R. and Braun, W., *Exact and Efficient Analytical Calculation of the Accessible Surface Areas and Their Gradients for Macromolecules*. J. Comp. Chem, 1998. **19**: p. 319-333.
171. Humphrey, W., Dalke, A., and Schulten, K., *VMD: visual molecular dynamics*. J Mol Graph, 1996. **14**(1): p. 33-8, 27-8.
172. Kim, Y.H., et al., *Comparing the effect on protein stability of methionine oxidation versus mutagenesis: steps toward engineering oxidative resistance in proteins*. Protein Eng, 2001. **14**(5): p. 343-7.
173. Yergey, J., et al., *Isotopic distributions in mass spectra of large molecules*. Analytical Chemistry, 1983. **55**(2): p. 353-356.
174. Zolkiewski, M., et al., *Thermal unfolding of Acanthamoeba myosin II and skeletal muscle myosin*. Biophys Chem, 1996. **59**(3): p. 365-71.
175. Rasmussen, H.H., et al., *Reversible oxidative modification: implications for cardiovascular physiology and pathophysiology*. Trends Cardiovasc Med, 2010. **20**(3): p. 85-90.
176. Passarelli, C., et al., *Susceptibility of isolated myofibrils to in vitro glutathionylation: Potential relevance to muscle functions*. Cytoskeleton (Hoboken), 2010. **67**(2): p. 81-9.
177. Hung, R.J., Pak, C.W., and Terman, J.R., *Direct redox regulation of F-actin assembly and disassembly by Mical*. Science, 2011. **334**(6063): p. 1710-3.



178. Burgoyne, J.R., et al., *Cysteine redox sensor in PKGI $\alpha$  enables oxidant-induced activation*. *Science*, 2007. **317**(5843): p. 1393-7.
179. Humphries, K.M., Juliano, C., and Taylor, S.S., *Regulation of cAMP-dependent protein kinase activity by glutathionylation*. *J Biol Chem*, 2002. **277**(45): p. 43505-11.
180. Ward, N.E., et al., *Oxidant-induced S-glutathiolation inactivates protein kinase C- $\alpha$  (PKC- $\alpha$ ): a potential mechanism of PKC isozyme regulation*. *Biochemistry*, 2000. **39**(33): p. 10319-29.
181. Prochniewicz, E., et al., *Myosin isoform determines the conformational dynamics and cooperativity of actin filaments in the strongly bound actomyosin complex*. *J Mol Biol*, 2010. **396**(3): p. 501-9.
182. Belyantseva, I.A., et al., *Myosin-XVa is required for tip localization of whirlin and differential elongation of hair-cell stereocilia*. *Nat Cell Biol*, 2005. **7**(2): p. 148-56.
183. Bohil, A.B., Robertson, B.W., and Cheney, R.E., *Myosin-X is a molecular motor that functions in filopodia formation*. *Proc Natl Acad Sci U S A*, 2006. **103**(33): p. 12411-6.
184. Prosser, H.M., et al., *Mosaic complementation demonstrates a regulatory role for myosin VIIa in actin dynamics of stereocilia*. *Mol Cell Biol*, 2008. **28**(5): p. 1702-12.
185. Huang, X., et al., *MAX-1, a novel PH/MyTH4/FERM domain cytoplasmic protein implicated in netrin-mediated axon repulsion*. *Neuron*, 2002. **34**(4): p. 563-76.
186. Narasimhulu, S.B. and Reddy, A.S., *Characterization of microtubule binding domains in the Arabidopsis kinesin-like calmodulin binding protein*. *Plant Cell*, 1998. **10**(6): p. 957-65.
187. Weber, K.L., et al., *A microtubule-binding myosin required for nuclear anchoring and spindle assembly*. *Nature*, 2004. **431**(7006): p. 325-9.
188. Woolner, S., et al., *Myosin-10 and actin filaments are essential for mitotic spindle function*. *J Cell Biol*, 2008. **182**(1): p. 77-88.
189. Toyoshima, F. and Nishida, E., *Integrin-mediated adhesion orients the spindle parallel to the substratum in an EBI- and myosin X-dependent manner*. *Embo J*, 2007. **26**(6): p. 1487-98.
190. Yang, Y., et al., *A FERM domain autoregulates Drosophila myosin 7a activity*. *Proc Natl Acad Sci U S A*, 2009. **106**(11): p. 4189-94.
191. Gotesman, M., Hosein, R.E., and Gavin, R.H., *A FERM domain in a class XIV myosin interacts with actin and tubulin and localizes to the cytoskeleton, phagosomes, and nucleus in Tetrahymena thermophila*. *Cytoskeleton (Hoboken)*, 2010. **67**(2): p. 90-101.
192. Titus, M.A., *A class VII unconventional myosin is required for phagocytosis*. *Curr Biol*, 1999. **9**(22): p. 1297-303.
193. Zhang, H., et al., *Myosin-X provides a motor-based link between integrins and the cytoskeleton*. *Nat Cell Biol*, 2004. **6**(6): p. 523-31.
194. Galdeen, S.A., et al., *Talin influences the dynamics of the myosin VII-membrane interaction*. *Mol Biol Cell*, 2007. **18**(10): p. 4074-84.

195. Kollmar, M., *Use of the myosin motor domain as large-affinity tag for the expression and purification of proteins in Dictyostelium discoideum*. Int J Biol Macromol, 2006. **39**(1-3): p. 37-44.
196. Fey, P., et al., *Protocols for growth and development of Dictyostelium discoideum*. Nat Protoc, 2007. **2**(6): p. 1307-16.
197. Gaudet, P., et al., *Transformation of Dictyostelium discoideum with plasmid DNA*. Nat Protoc, 2007. **2**(6): p. 1317-24.
198. Manstein, D.J. and Hunt, D.M., *Overexpression of myosin motor domains in Dictyostelium: screening of transformants and purification of the affinity tagged protein*. J Muscle Res Cell Motil, 1995. **16**(3): p. 325-32.
199. Korman, V.L., et al., *Structural dynamics of the actin-myosin interface by site-directed spectroscopy*. J Mol Biol, 2006. **356**(5): p. 1107-17.
200. Blommel, P.G. and Fox, B.G., *A combined approach to improving large-scale production of tobacco etch virus protease*. Protein Expr Purif, 2007. **55**(1): p. 53-68.
201. Allingham, J.S., et al., *Vik1 modulates microtubule-Kar3 interactions through a motor domain that lacks an active site*. Cell, 2007. **128**(6): p. 1161-72.
202. Heinig, M. and Frishman, D., *STRIDE: a web server for secondary structure assignment from known atomic coordinates of proteins*. Nucleic Acids Res, 2004. **32**(Web Server issue): p. W500-2.
203. Lee, H.S., et al., *Characterization of an actin-binding site within the talin FERM domain*. J Mol Biol, 2004. **343**(3): p. 771-84.
204. Wei, Z., et al., *Cargo recognition mechanism of myosin X revealed by the structure of its tail MyTH4-FERM tandem in complex with the DCC P3 domain*. Proc Natl Acad Sci U S A, 2011. **108**(9): p. 3572-7.
205. Wu, L., et al., *Structure of MyTH4-FERM domains in myosin VIIa tail bound to cargo*. Science, 2011. **331**(6018): p. 757-60.
206. Hamada, K., et al., *Structural basis of the membrane-targeting and unmasking mechanisms of the radixin FERM domain*. Embo J, 2000. **19**(17): p. 4449-62.
207. Han, B.G., et al., *Protein 4.1R core domain structure and insights into regulation of cytoskeletal organization*. Nat Struct Biol, 2000. **7**(10): p. 871-5.
208. Pearson, M.A., et al., *Structure of the ERM protein moesin reveals the FERM domain fold masked by an extended actin binding tail domain*. Cell, 2000. **101**(3): p. 259-70.
209. Schaap, P., et al., *Molecular phylogeny and evolution of morphology in the social amoebas*. Science, 2006. **314**(5799): p. 661-3.
210. Wolfrum, U., et al., *Myosin VIIa as a common component of cilia and microvilli*. Cell Motil Cytoskeleton, 1998. **40**(3): p. 261-71.
211. Kwon, M., et al., *Mechanisms to suppress multipolar divisions in cancer cells with extra centrosomes*. Genes Dev, 2008. **22**(16): p. 2189-203.
212. Sakai, T., et al., *Cargo binding activates myosin VIIA motor function in cells*. Proc Natl Acad Sci U S A, 2011. **108**(17): p. 7028-33.
213. Kast, D., et al., *Phosphorylation-induced structural changes in smooth muscle myosin regulatory light chain*. Proc Natl Acad Sci U S A, 2010. **107**(18): p. 8207-12.

214. Estell, D.A., Graycar, T.P., and Wells, J.A., *Engineering an enzyme by site-directed mutagenesis to be resistant to chemical oxidation*. J Biol Chem, 1985. **260**(11): p. 6518-21.
215. Ju, S.S., et al., *Substitution of the critical methionine residues in *trigonopsis variabilis* D-amino acid oxidase with leucine enhances its resistance to hydrogen peroxide*. FEMS Microbiol Lett, 2000. **186**(2): p. 215-9.
216. Santarelli, L.C., et al., *Three methionine residues located within the regulator of conductance for K<sup>+</sup> (RCK) domains confer oxidative sensitivity to large-conductance Ca<sup>2+</sup>-activated K<sup>+</sup> channels*. J Physiol, 2006. **571**(Pt 2): p. 329-48.
217. Chin, D. and Means, A.R., *Methionine to glutamine substitutions in the C-terminal domain of calmodulin impair the activation of three protein kinases*. J Biol Chem, 1996. **271**(48): p. 30465-71.

## **Appendix**

Rights and Permissions for reprint of copyrighted material.

Chapter 2 reprinted with permission from:

Rebecca J. Moen, David D. Thomas, and Jennifer C. Klein. Conformationally trapping the actin-binding cleft of myosin with a bifunctional spin label. *J Biol Chem.* 2013;288(5):3016-3024.

Copyright © 2013 The American Society for Biochemistry and Molecular Biology, Inc.



11200 Rockville Pike  
Suite 302  
Rockville, Maryland 20852

August 19, 2011

American Society for Biochemistry and Molecular Biology

---

To whom it may concern,

It is the policy of the American Society for Biochemistry and Molecular Biology to allow reuse of any material published in its journals (the Journal of Biological Chemistry, Molecular & Cellular Proteomics and the Journal of Lipid Research) in a thesis or dissertation at no cost and with no explicit permission needed. Please see our copyright permissions page on the journal site for more information.

Best wishes,

Sarah Crespi

[American Society for Biochemistry and Molecular Biology](#)

11200 Rockville Pike, Rockville, MD

Suite 302

240-283-6616

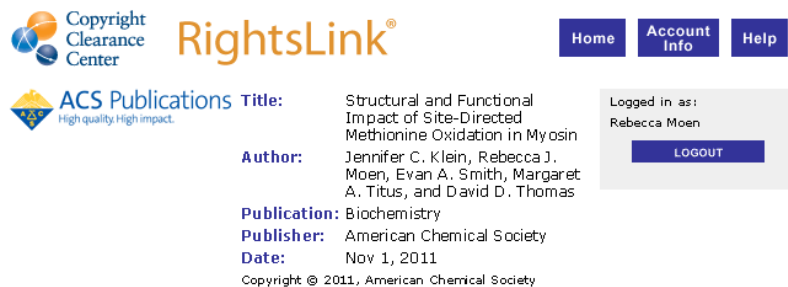
[JBC](#) | [MCP](#) | [JLR](#)

## Chapter 3 reprinted with permission from:

Jennifer C. Klein, Rebecca J. Moen, Evan A. Smith, Margaret A. Titus, and David D. Thomas. Structural and functional impact of site-directed methionine oxidation in myosin. *Biochemistry*. 2011;50(47):10318-10327.

### Copyright © 2011 American Chemical Society

Rightslink® by Copyright Clearance Center



The image shows a screenshot of the RightsLink interface. On the left, there are logos for Copyright Clearance Center and ACS Publications. The main content area displays the following metadata:

- Title:** Structural and Functional Impact of Site-Directed Methionine Oxidation in Myosin
- Author:** Jennifer C. Klein, Rebecca J. Moen, Evan A. Smith, Margaret A. Titus, and David D. Thomas
- Publication:** Biochemistry
- Publisher:** American Chemical Society
- Date:** Nov 1, 2011
- Copyright:** © 2011, American Chemical Society

On the right side, there is a navigation menu with buttons for Home, Account Info, and Help. Below that, a user is logged in as Rebecca Moen, with a LOGOUT button.

#### PERMISSION/LICENSE IS GRANTED FOR YOUR ORDER AT NO CHARGE

This type of permission/license, instead of the standard Terms & Conditions, is sent to you because no fee is being charged for your order. Please note the following:

- Permission is granted for your request in both print and electronic formats, and translations.
- If figures and/or tables were requested, they may be adapted or used in part.
- Please print this page for your records and send a copy of it to your publisher/graduate school.
- Appropriate credit for the requested material should be given as follows: "Reprinted (adapted) with permission from (COMPLETE REFERENCE CITATION). Copyright (YEAR) American Chemical Society." Insert appropriate information in place of the capitalized words.
- One-time permission is granted only for the use specified in your request. No additional uses are granted (such as derivative works or other editions). For any other uses, please submit a new request.

BACK

CLOSE WINDOW

Copyright © 2013 Copyright Clearance Center, Inc. All Rights Reserved. [Privacy statement](#).  
Comments? We would like to hear from you. E-mail us at [customer-care@copyright.com](mailto:customer-care@copyright.com)

<https://s100.copyright.com/AppDispatchServlet>[6/19/2013 10:25:58 AM]

Chapter 5 reprinted with permission from:

Rebecca J. Moen, Daniel O. Johnsrud, David D. Thomas, and Margaret A. Titus. Characterization of a Myosin VII MyTH/FERM domain. *J Mol Biol.* 2011;413(1):17-23.

Copyright © 2011 Elsevier Limited

Rightslink® by Copyright Clearance Center



RightsLink®

Home Account Info Help



**Title:** Characterization of a Myosin VII MyTH/FERM Domain  
**Author:** Rebecca J. Moen, Daniel O. Johnsrud, David D. Thomas, Margaret A. Titus  
**Publication:** Journal of Molecular Biology  
**Publisher:** Elsevier  
**Date:** 14 October 2011  
Copyright © 2011, Elsevier

Logged in as:  
Rebecca Moen

LOGOUT

### Order Completed

Thank you very much for your order.

This is a License Agreement between Rebecca J Moen ("You") and Elsevier ("Elsevier"). The license consists of your order details, the terms and conditions provided by Elsevier, and the [payment terms and conditions](#).

[Get the printable license.](#)

License Number	3172550705390
License date	Jun 19, 2013
Licensed content publisher	Elsevier
Licensed content publication	Journal of Molecular Biology
Licensed content title	Characterization of a Myosin VII MyTH/FERM Domain
Licensed content author	Rebecca J. Moen, Daniel O. Johnsrud, David D. Thomas, Margaret A. Titus
Licensed content date	14 October 2011
Licensed content volume number	413
Licensed content issue number	1
Number of pages	7
Type of Use	reuse in a thesis/dissertation
Portion	full article
Format	both print and electronic
Are you the author of this Elsevier article?	Yes
Will you be translating?	No
Order reference number	
Title of your thesis/dissertation	Site-directed Modifications of Myosin
Expected completion date	Jun 2013
Elsevier VAT number	GB 494 6272 12
Permissions price	0.00 USD
VAT/Local Sales Tax	0.00 USD
Total	0.00 USD

ORDER MORE...

CLOSE WINDOW

Copyright © 2013 Copyright Clearance Center, Inc. All Rights Reserved. [Privacy statement](#).  
Comments? We would like to hear from you. E-mail us at [customercare@copyright.com](mailto:customercare@copyright.com)

Figure 34 in Chapter 6 reprinted with permission from:

Lin Wu, Lifeng Pan, Zhiyi Wei, and Mingjie Zhang. Structure of MyTH4-FERM Domains in Myosin VIIa Tail Bound to Cargo. *Science*. 2011;331(6018):757-760:Supplementary Information.

Copyright © 2011 The American Association for the Advancement of Science

Rightslink Printable License

<https://s100.copyright.com/App/PrintableLicenseFrame.jsp?publisherID=...>

**THE AMERICAN ASSOCIATION FOR THE ADVANCEMENT OF SCIENCE LICENSE  
TERMS AND CONDITIONS**

Jun 25, 2013

This is a License Agreement between Rebecca J Moen ("You") and The American Association for the Advancement of Science ("The American Association for the Advancement of Science") provided by Copyright Clearance Center ("CCC"). The license consists of your order details, the terms and conditions provided by The American Association for the Advancement of Science, and the payment terms and conditions.

**All payments must be made in full to CCC. For payment instructions, please see information listed at the bottom of this form.**

License Number	3175990124306
License date	Jun 25, 2013
Licensed content publisher	The American Association for the Advancement of Science
Licensed content publication	Science
Licensed content title	Structure of MyTH4-FERM Domains in Myosin VIIa Tail Bound to Cargo
Licensed content author	Lin Wu, Lifeng Pan, Zhiyi Wei, Mingjie Zhang
Licensed content date	Feb 11, 2011
Volume number	331
Issue number	6018
Type of Use	Thesis / Dissertation
Requestor type	Scientist/individual at a research institution
Format	Print and electronic
Portion	Figure
Number of figures/tables	1
Order reference number	
Title of your thesis / dissertation	Site-directed Modifications of Myosin
Expected completion date	Jun 2013
Estimated size(pages)	140
Total	0.00 USD
Terms and Conditions	

American Association for the Advancement of Science TERMS AND CONDITIONS

Regarding your request, we are pleased to grant you non-exclusive, non-transferable permission, to republish the AAAS material identified above in your work identified above, subject to the terms and conditions herein. We must be contacted for permission for any uses other than those specifically identified in your request above.

The following credit line must be printed along with the AAAS material: "From [Full Reference Citation]. Reprinted with permission from AAAS."